Crop Assessment and Monitoring Using Optical Sensors

by

Huan Wang

B.S., China Agricultural University, 2012

AN ABSTRACT OF A DISSERTATION

submitted in partial fulfillment of the requirements for the degree

DOCTOR OF PHILOSOPHY

Department of Agronomy
College of Agriculture

KANSAS STATE UNIVERSITY
Manhattan, Kansas

2017

Abstract

Crop assessment and monitoring is important to crop management both at crop production level and research plot level, such as high-throughput phenotyping in breeding programs. Optical sensors based agricultural applications have been around for decades and have soared over the past ten years because of the potential of some new technologies to be low-cost, accessible, and high resolution for crop remote sensing which can help to improve crop management to maintain producers' income and diminish environmental degradation. The overall objective of this study was to develop methods and compare the different optical sensors in crop assessment and monitoring at different scales and perspectives.

At crop production level, we reviewed the current status of different optical sensors used in precision crop production including satellite-based, manned aerial vehicle (MAV)-based, unmanned aircraft system (UAS)-based, and vehicle-based active or passive optical sensors. These types of sensors were compared thoroughly on their specification, data collection efficiency, data availability, applications and limitation, economics, and adoption.

At research plot level, four winter wheat experiments were conducted to compare three optical sensors (a Canon T4i® modified color infrared (CIR) camera, a MicaSense RedEdge® multispectral imager and a Holland Scientific® RapidScan CS-45® hand-held active optical sensor (AOS)) based high-throughput phenotyping for in-season biomass estimation, canopy estimation, and grain yield prediction in winter wheat across eleven Feekes stages from 3 through 11.3. The results showed that the vegetation indices (VIs) derived from the Canon T4i CIR camera and the RedEdge multispectral camera were highly correlated and can equally estimate winter wheat in-season biomass between Feekes 3 and 11.1 with the optimum point at booting stage and can predict grain yield as early as Feekes 7. Compared to passive sensors, the

RapidScan AOS was less powerful and less temporally stable for biomass estimation and yield prediction. Precise canopy height maps were generated from a CMOS sensor camera and a multispectral imager although the accuracy could still be improved. Besides, an image processing workflow and a radiometric calibration method were developed for UAS based imagery data as bi-products in this project.

At temporal dimension, a wheat phenology model based on weather data and field contextual information was developed to predict the starting date of three key growth stages (Feekes 4, 7, and 9), which are critical for N management. The model could be applied to new data within the state of Kansas to optimize the date for optical sensor (such as UAS) data collection and save random or unnecessary field trips. Sensor data collected at these stages could then be plugged into pre-built biomass estimation models (mentioned in the last paragraph) to estimate the productivity variability within 20% relative error.

Crop Assessment and Monitoring Using Optical Sensors

by

Huan Wang

B.S., China Agricultural University, 2012

A DISSERTATION

submitted in partial fulfillment of the requirements for the degree

DOCTOR OF PHILOSOPHY

Department of Agronomy
College of Agriculture

KANSAS STATE UNIVERSITY
Manhattan, Kansas

2017

Approved by:

Major Professor
P.V. Vara Prasad

Copyright

Abstract

Crop assessment and monitoring is important to crop management both at crop production level and research plot level, such as high-throughput phenotyping in breeding programs. Optical sensors based agricultural applications have been around for decades and have soared over the past ten years because of the potential of some new technologies to be low-cost, accessible, and high resolution for crop remote sensing which can help to improve crop management to maintain producers' income and diminish environmental degradation. The overall objective for this study was to develop methods and compare the different optical sensors in crop assessment and monitoring at different scales and perspectives.

At crop production level, we reviewed the current status of different optical sensors used in precision crop production including satellite-based, manned aerial vehicle (MAV)-based, unmanned aircraft system (UAS)-based, and vehicle-based active or passive optical sensors. These types of sensors were compared thoroughly on their specification, data collection efficiency, data availability, applications and limitation, economics, and adoption.

At research plot level, four winter wheat experiments were conducted to compare three optical sensors (a Canon T4i® modified color infrared (CIR) camera, a MicaSense RedEdge® multispectral imager and a Holland Scientific® RapidScan CS-45® hand-held active optical sensor (AOS)) based high-throughput phenotyping for in-season biomass estimation, canopy estimation, and grain yield prediction in winter wheat across eleven Feekes stages from 3 through 11.3. The results showed that the vegetation indices (VIs) derived from the Canon T4i CIR camera and the RedEdge multispectral camera were highly correlated and can equally estimate winter wheat in-season biomass between Feekes 3 and 11.1 with the optimum point at booting stage and can predict grain yield as early as Feekes 7. Compared to passive sensors, the

RapidScan AOS was less powerful and less temporally stable for biomass estimation and yield prediction. Precise canopy height maps were generated from a CMOS sensor camera and a multispectral imager although the accuracy could still be improved. Besides, an image processing workflow and a radiometric calibration method were developed for UAS based imagery data as bi-products in this project.

At temporal dimension, a wheat phenology model based on weather data and field contextual information was developed to predict the starting date of three key growth stages (Feekes 4, 7, and 9), which are critical for N management. The model could be applied to new data within the state of Kansas to optimize the date for optical sensor (such as UAS) data collection and save random or unnecessary field trips. Sensor data collected at these stages could then be plugged into pre-built biomass estimation models (mentioned in the last paragraph) to estimate the productivity variability within 20% relative error.

Table of Contents

List of Figures

List of Tables

Acknowledgements

I would like to take this opportunity to thank all the people who helped me over the years during my pursuit for a Ph.D. in Agronomy at Kansas State University.

I thank my major professor, Dr. Vara Prasad, for his support on letting me decide my research topics that really interested me and providing all the resources needed to do my research. Every time I walked out from your office, I felt comfortable and had clearer goals. Thank you for guiding my career path instrumentally and emotionally. It was my honor to be your last graduate student.

I am grateful to Dr. Antonio “Ray” Asebedo. Ray was originally my classmate and then became my committee member. He actively involved in my projects and provided me valuable guidance. He is not only my mentor on research but also a friend I can consult for career advices. We had many conversations discussing the problems in precision agriculture and what are the product the farmers really need, which formulated my research goals in the future.

I greatly appreciate Dr. Steve Welch for his help with the crop modeling. He uses his wisdom not only to obtain broad and deep knowledge but also convey those to us in his own style which is easy and fun to follow. His teaching philosophy had such an impact on me.

I would like to thank Dr. Deon van der Merwe for teaching me how to fly fixed wings and getting me interested in the UAV applications back in 2012. Thank you for showing me the perfect combination of interest and work. I want to be cool like that.

I also owe a great amount of appreciation to my former major advisor, Dr. Kevin Price, without whom, I wouldn’t have the opportunity to pursue my degree in the US. Thank you for training my remote sensing skills from scratch and trying your best to help me in any way.

I greatly appreciate the data collection support of Andrew Newsum, Ashley Lorence, Victor Tomei, Austin Hughes, Black Bergkamp, and Scott Cain; the field preparation and planting of Dr. Kraig Roozeboom and Russel Dille; the coding assistantship of Abhishes Lamsal, Nan An, and Wen Fung Leong, and the vehicle and facility usage of Dr. Krishna Jagadish.

Dedication

This is dedicated to my parents, Wang and Zhu. Without your numerous sacrifices, support, respect, and belief in me, I would not be able to get better education at the very beginning and to get this Ph.D. finally. It's been a long journey and more than twenty moves since we left the small town, Chongxin. It is you, my Dad, taught me how to change your life and pursue your dream by doing it. I will definitely pass it to Ryder.

This is also dedicated to my wife, Pan and our boy, Ryder. Thank you, Pan, for taking care of our baby while I locked myself in the library to write dissertation at late nights and for helping me with the field works and even my research problems. It was your courage, wisdom, and encouragement that made me a better man. Our boy, Ryder, would always say "Ba Ba Jia You!" ("Work hard! Daddy!") with a serious face before I went to school and give me a big hug and smile when I got back.

It is my name on the diploma but this achievement belongs to all of us.

Chapter 1 - Introduction

Precision farm management

Crop production strategies have changed dramatically over the past decades to meet the challenge of increasing agricultural productivity while reducing inputs, maximizing profits, and mitigating environmental degradation (Zhang et al., 2002). This requires the agriculture systems to be resource-efficient by integrating tools, technologies, and information management systems that come under the precision agriculture (PA) concept (Whelan et al., 1997), which is a farming management concept based on observing, measuring, and responding to inter and intra-field variability in soil and crops to optimize profitability and protect the environment.

The general components of PA practice are data collection, field variability mapping, decision making, and finally management practice (Zhang et al., 2002). To get accurate and consistent data during the growing season over matching spatial scale and to understand intra-field variability in assessing potential productivity are the foundations of decision making and final field practice in real world PA. Along with the advances in global position system (GPS), geographic information system (GIS), and variable rate technology (VRT), remote sensing data has provided powerful analysis tools for PA, which has changed the traditional way of farming (Mulla, 2013).

High-throughput phenotyping in breeding program

Perhaps the greatest challenge of plant science and crop improvement in the 21st century is predicting how a plant's appearance (phenotype) is dictated by its genetic make-up (genotype) (Davey et al., 2011). Spectacular advances in "next generation" DNA sequencing are rapidly

reducing the costs of genotyping (Furbank et al.,2011). In contrast, methods for rapid characterization of plant traits (phenotypes) have evolved little over the past 30 years (White et al., 2012), In the area of phenotyping, two major challenges are 1) breeding programs spend tremendous effort manually collecting routine phenotypic data (Araus et al., 2014). 2) the repeated measurements of dynamic traits can be invalid. As a result, accurate measurement of biophysical variables at large scale remains problematic, even though such measurements are critical for assessing optimal plant characteristics for screening germplasm for tolerances.

Recognition of the phenotyping constraint has stimulated development of high-throughput phenotyping (HTP) that seeks to accurately characterize large numbers of individuals or populations using a fraction of time and labor of manual phenotyping methods. An increasing number of scientists are turning to the use of remotely sensed measurements for characterizing plant phenotypes (Montes et al., 2007; Seiffert et al., 2010; Munns et al., 2010).

Agronomic information

To link remote sensing data with agronomic information, first we need to understand what are the agronomic information. As reviewed by Moran et al. (1997), the three basic categories of agronomic information required by PA are:

Seasonally stable conditions

Seasonally stable conditions are those that are relatively constant through the growing season and only need to be determined preseason and simply updated, when and if necessary. These conditions include but are not limited to, field boundaries, historical yield, crop residue, crop type, soil properties (e.g., type, texture, water holding capacity, organic matter), water

availability (rain-fed or irrigated field), terrain, etc. These seasonal stable conditions provide detailed information about the current state of the field and are great indicator of yield potentials (the yield of an adapted crop variety or hybrid when grown under favorable conditions without growth limitations from abiotic and biotic stresses).

Seasonally variable conditions

Seasonally variable conditions are those that change continually within the season and need to be determine these conditions numerous times during the season for proper management. These conditions include crop status (e.g. development, growth, nutrient, canopy temperature, water content, disease, weed, pests), and soil conditions (e.g. soil moisture, soil temperature).

Cause of yield variability

This type of information requires to diagnose the cause of the crop yield variability and normally encompass both seasonally stable and seasonally variable conditions. With this information, people can develop models and algorithms to assist the final management decision by answering the “4R” principle questions (or part of them) --What is the right product to apply? When is the right time to apply? Where is the right place to apply? And what is the right rate to apply?

Linking Remote Sensing with Agronomic Information

Reflectance of crop and soil

The basic underlying premise of remote sensing applications in PA is that the variations within the spectral reflectance and absorption collected by remote sensing tools can be used to

detect the agronomic information mentioned above (Warren and Metternicht, 2005). There is fairly good amount of evidence showing that they can. For example, Figure 1.1, 1.2, 1.3, and 1.4 show the example of reflectance of crop and soil at different conditions.

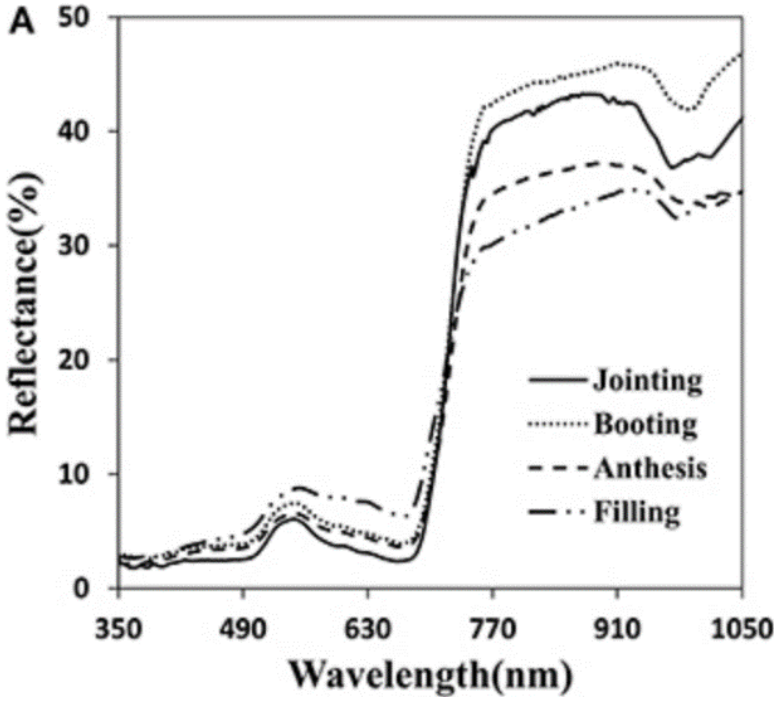

Figure 1.1 Comparison of the spectral reflectance curve of plant samples at different growth stages.

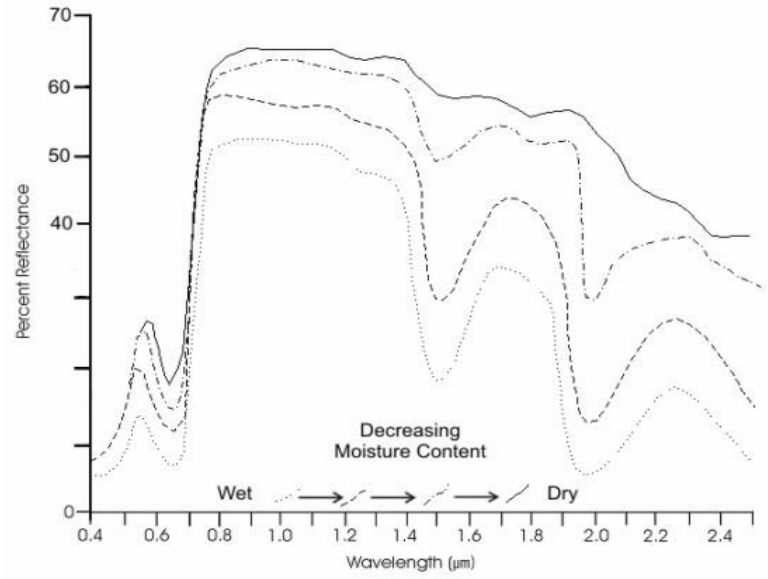

Figure 1.2 Comparison of the spectral reflectance curve of plant samples with different water content.

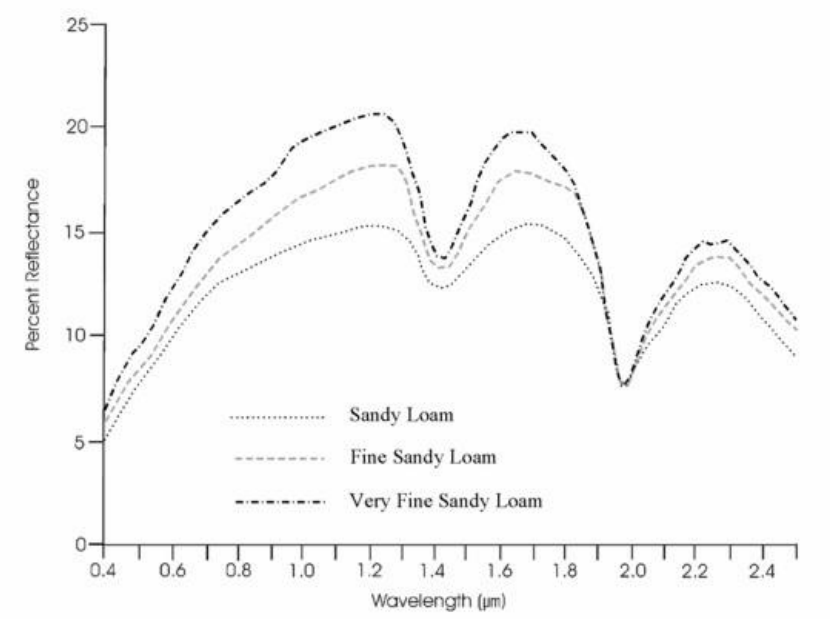

Figure 1.3 Comparison of the spectral reflectance curve of soil samples with different soil texture.

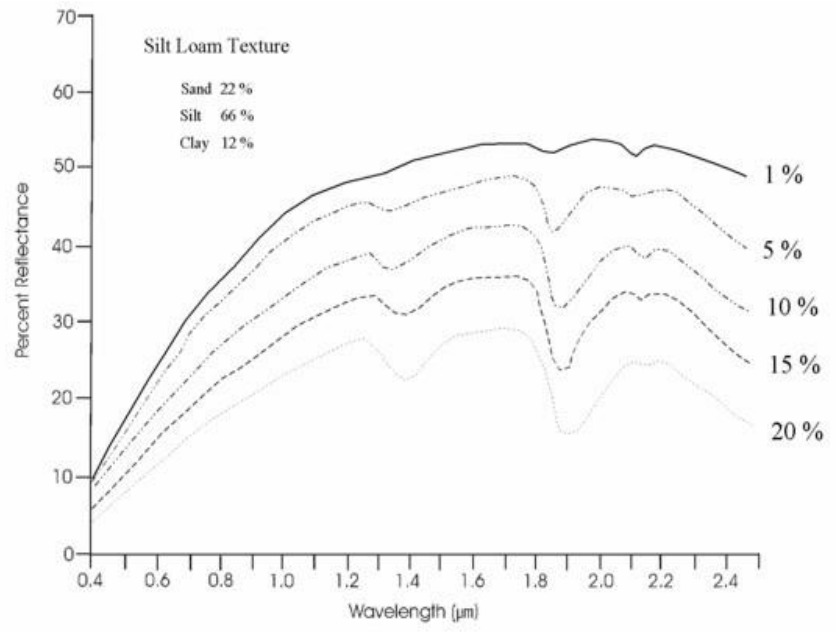

Figure 1.4 Comparison of the spectral reflectance curve of soil samples with different moisture content.

For crop, the blue and red wavelengths are absorbed for photosynthesis while the green is reflected by chlorophyll content. NIR wavelength, on the other hand, passes through the surface of the leaf (the palisade tissue) and scatters in both upward (reflected) and downward (transmitted) direction as a function of LAI, cell turgor, leaf thickness, internal air, and water content. The transmitted NIR can then be reflected back by the layers of leaves along the passage and the soil background. Therefore, the reflectance is lower in visible spectrum and higher in the NIR spectrum. As a result, healthy crops will show higher reflectance in NIR and lower reflectance in visible spectrum while stressed crops will have a lower reflectance in NIR and a broadening reflectance peak in the whole visible spectrum (by carotenoid and xanthophyll) due to the lower chlorophyll content (Pinter et al., 2003).

For soil, the reflectance increases monotonically from visible to NIR with varying slopes depending on the soil properties such as soil texture (Figure 1.3) and soil moisture (Figure 1.4). It is higher than crop in visible spectrum and lower than crop in NIR, which can be used to differentiate soil from crops.

Vegetation indices (VIs)

To make these signal even stronger, people developed different vegetation indices (VIs) through the past few decades. For example, the most widely used vegetation index, Normalized Difference Vegetation Index (NDVI), was designed based on this feature (Rouse Jr et al., 1974). The advantage and limitation of different vegetation indices have been reviewed by many researchers (Viña et al., 2011; Elvidge et al., 1995; Hansen & Schjoerring, 2003) and will not be covered in this study. With the help of vegetation indices and ground truth measurements in the field, we already can build empirical models to estimate crop biophysical parameters such as leaf

area index (LAI) (Haboudane et al., 2004), fraction of canopy cover (fCOVER) (Baret et al., 2007; Bacour et al., 2006), chlorophyll content (Haboudane et al., 2002; Wu et al., 2002), and above ground biomass (AGB) (Hansen & Schjoerring, 2003; Mutanga & Skidmore, 2004), which have big impact on the final grain yield. These biophysical parameters can be furtherly utilized as canopy state variables and integrated into the more sophisticated crop simulation models (CSMs) to make more robust estimations and predictions on the crop growth processes at a large scale (Patel et al., 2001; Reynolds et al., 2000).

Remote Sensing Data Quality

In order to get to this point, we need to quality control each process along the way. The first and the most critical thing is the quality of the data. Remote sensing data quality are evaluated by four resolutions. Each of them is highly correlated with one component of the "4R" principle mentioned earlier.

Spatial Resolution: (coupled with Right place)

Spatial resolution is a measure of the area or size of the smallest dimension on the Earth's surface (check with RS bible). Figure 1.5 shows the examples of a coarse resolution image and a fine resolution image. If one wants to make nitrogen recommendation for the different plots shown on Figure 1.5.b, the resolution of Figure 1.5.a will not be fine enough and use of it will result in placing the nitrogen fertilizer at the wrong location and degrade the crop performance.

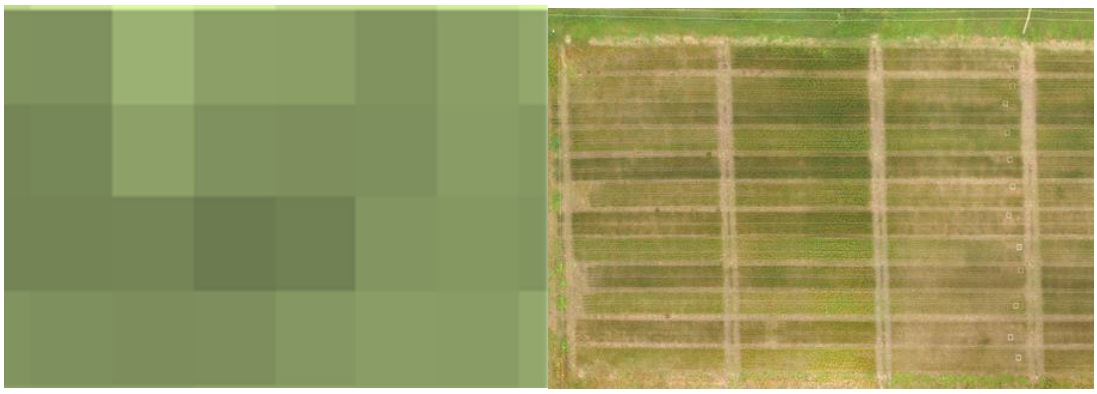

a b

Figure 1.5 Examples of a coarse resolution and a fine resolution image taken at the same field. a. 2 cm resolution RGB image taken at 60 m above ground level (AGL); b. 10 m resolution RGB image taken by Sentinel-2.

Temporal Resolution: (Coupled with Right time)

Temporal resolution is a measure of revisit period or how often does a sensor collect data for the same area. For example, the temporal resolution for Landsat 8 satellite is 16 days (USGS, 2017), which means, you can get one Landsat 8 image for the same area every 16 days. In PA, this is not frequent enough because most of the field practice is growth stage sensitive such as herbicides application---some herbicides can only be applied before or after a certain growth stage without causing any trouble to the crop. If you miss the time, you miss the yield potential. In addition, it is always better to respond to a field issue as soon as possible before the situation get worse.

Radiometric Resolution: (Coupled with Right rate)

Radiometric resolution is a measure of the sensitivity of a sensor to the magnitude of the electromagnetic energy or the number of intensity levels that a sensor can use to record a given signal. Basically, this is answering the question, how many levels of green of corn leaves a sensor can detect. For the passive optical sensors, the radiometric resolution often refers to the number of divisions of bit depth (for example, 255 for 8-bit, 65536 for 16-bit, and so on that n-

bit = n^{th}-1) in data collected by a sensor. The Figure 1.6 shows the example of a satellite image with two different radiometric resolutions. The 8-bit image on the left delivers more shades in each band with 256 in total while the 2-bit image on the right lost a lot of details or sub differences.

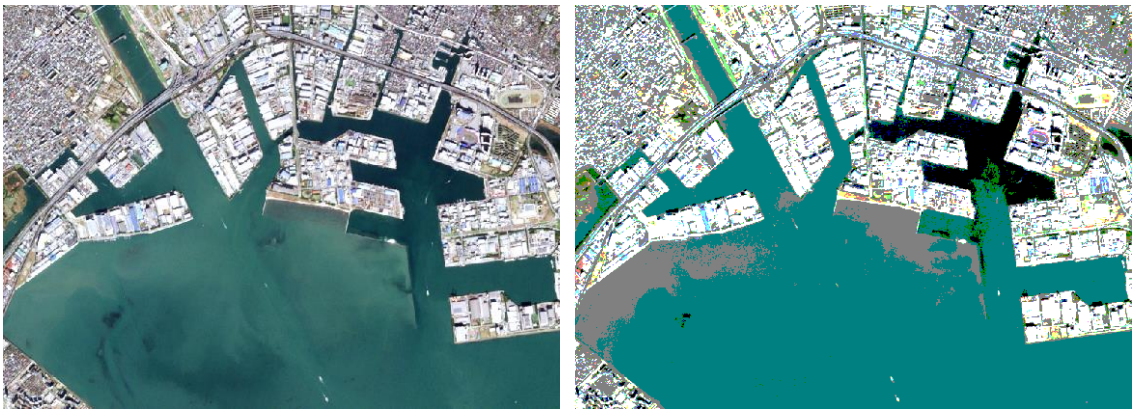

a b

Figure 1.6 Different radiometric resolution. a. 8-bit Sentinel-2 image; b. 2-bit Sentinel-2 image.

Another terminology, dynamic range, has been used frequently in sensor comparison, which is the ratio between the maximum output signal level and the noise floor at minimum signal amplification (noise floor is the root mean square noise level in a black image.) Dynamic range is not equal to the radiometric resolution such that a 12-bit sensor does not necessarily have 12 bits of dynamic range because this does not consider the noise. The causality is reversed; if a camera has 12-bit of dynamic range that the A/D converters need to be at least 12 bits as well and preferably higher. DR represents the camera's ability to display/reproduce the brightest and darkest portions of the image and how many variations in between which is critical in variability mapping for both soil and crop.

Spectral Resolution: (Coupled with Right product)

Spectral resolution is the number of the spectral bands and the range of each band. Different waveband has different applications. Red and NIR bands are useful for detecting the nitrogen deficiency while thermal band is useful for detecting water stress. Until we figure out what is the core problem of the crop can we determine what product to use.

In PA, spatial resolution and temporal resolution have the higher priority because farm management is time sensitive and space sensitive. Also, the other two resolutions, spectral resolution and radiometric resolution, are determined by the sensor design thus cannot be adjusted while spatial and temporal resolution may be adjusted by flying the sensor at different altitudes with different frequencies. For example, aerial images taken at 500 m and 1000 m AGL have different spatial resolution and the temporal resolution can be either one day or one week, which only depend on how often you want to collect data with a certain budget.

Outlines

Chapter 2 reviewed the current status of different optical sensors used in precision crop production including satellite-based, manned aerial vehicle (MAV)-based, unmanned aircraft system (UAS)-based, and vehicle-based active or passive optical sensors. These types of sensors were compared thoroughly on their specification, data collection efficiency, data availability, applications and limitation, economics, and adoption.

Chapter 3 focused on one of the components from Chapter 2, “application”, and dived deeper. This chapter concentrated on the research plot level, developed methods to do winter

wheat high-throughput phenotyping including in-season biomass estimation, canopy estimation, and grain yield prediction for three different optical sensors, and compared their performance.

Chapter 4 focused on one of the components from Chapter 3, “biomass estimation”, and dived deeper. A wheat phenology was developed to predict the starting dates of certain growth stages to optimize the date for sensor data collection, which could be integrated to biomass models developed in Chapter 3 to estimate the productivity variability at Feekes 4, 7, and 9.

Chapter 5 is a summary chapter.

References

Araus, J. L., & Cairns, J. E. (2014). Field high-throughput phenotyping: the new crop breeding frontier. *Trends in plant science*, 19(1), 52-61.

Bacour, C., Baret, F., Béal, D., Weiss, M., & Pavageau, K. (2006). Neural network estimation of LAI, fAPAR, fCover and LAI× C ab, from top of canopy MERIS reflectance data: Principles and validation. *Remote sensing of environment*, *105*(4), 313-325.

Baret, F., Hagolle, O., Geiger, B., Bicheron, P., Miras, B., Huc, M., ... & Roujean, J. L. (2007). LAI, fAPAR and fCover CYCLOPES global products derived from VEGETATION: Part 1: Principles of the algorithm. *Remote sensing of environment*, *110*(3), 275-286.

Davey, J. W., Hohenlohe, P. A., Etter, P. D., Boone, J. Q., Catchen, J. M., & Blaxter, M. L. (2011). Genome-wide genetic marker discovery and genotyping using next-generation sequencing. *Nature Reviews Genetics*, 12(7), 499-510.

Elvidge, C. D., & Chen, Z. (1995). Comparison of broad-band and narrow-band red and near-infrared vegetation indices. *Remote sensing of environment*, 54(1), 38-48.

Furbank, R. T., & Tester, M. (2011). Phenomics–technologies to relieve the phenotyping bottleneck. Trends in plant science, 16(12), 635-644.

Haboudane, D., Miller, J. R., Tremblay, N., Zarco-Tejada, P. J., & Dextraze, L. (2002). Integrated narrow-band vegetation indices for prediction of crop chlorophyll content for application to precision agriculture. *Remote sensing of environment*, *81*(2), 416-426.

Haboudane, D., Miller, J. R., Pattey, E., Zarco-Tejada, P. J., & Strachan, I. B. (2004). Hyperspectral vegetation indices and novel algorithms for predicting green LAI of crop canopies: Modeling and validation in the context of precision agriculture. *Remote sensing of environment*, *90*(3), 337-352.

Hansen, P. M., & Schjoerring, J. K. (2003). Reflectance measurement of canopy biomass and nitrogen status in wheat crops using normalized difference vegetation indices and partial least squares regression. *Remote sensing of environment*, 86(4), 542-553.

https://landsat.usgs.gov

Montes, J. M., Melchinger, A. E., & Reif, J. C. (2007). Novel throughput phenotyping platforms in plant genetic studies. *Trends in plant science*, 12(10), 433-436.

Moran, M. S., Inoue, Y., & Barnes, E. M. (1997). Opportunities and limitations for image-based remote sensing in precision crop management. *Remote sensing of Environment*, 61(3), 319-346.

Mulla, D. J. (2013). Twenty-five years of remote sensing in precision agriculture: Key advances and remaining knowledge gaps. *Biosystems engineering*, 114(4), 358-371.

Munns, R., James, R. A., Sirault, X. R., Furbank, R. T., & Jones, H. G. (2010). New phenotyping methods for screening wheat and barley for beneficial responses to water deficit. *Journal of Experimental Botany*, erq199.

Mutanga, O., & Skidmore, A. K. (2004). Narrow band vegetation indices overcome the saturation problem in biomass estimation. *International Journal of Remote Sensing*, *25*(19), 3999-4014.

Pinter Jr, P. J., Hatfield, J. L., Schepers, J. S., Barnes, E. M., Moran, M. S., Daughtry, C. S., & Upchurch, D. R. (2003). Remote sensing for crop management. *Photogrammetric Engineering & Remote Sensing*, 69(6), 647-664.

Ray, T. W. (1994). A FAQ on vegetation in remote sensing. California: Div. of Geological and Planetary Sciences California Institute of Technology.

Rouse Jr, J., Haas, R. H., Schell, J. A., & Deering, D. W. (1974). Monitoring vegetation systems in the Great Plains with ERTS.

Seiffert, U., Bollenbeck, F., Mock, H. P., & Matros, A. (2010, June). Clustering of crop phenotypes by means of hyperspectral signatures using artificial neural networks. In 2010 2nd

Workshop on Hyperspectral Image and Signal Processing: Evolution in Remote Sensing (pp. 1-4). IEEE.

Viña, A., Gitelson, A. A., Nguy-Robertson, A. L., & Peng, Y. (2011). Comparison of different vegetation indices for the remote assessment of green leaf area index of crops. *Remote Sensing of Environment*, 115(12), 3468-3478.

Warren, G., & Metternicht, G. (2005). Agricultural Applications of High-Resolution Digital Multispectral Imagery. *Photogrammetric Engineering & Remote Sensing*, 71(5), 595-602.

Whelan, B. M., McBratney, A. B., & Boydell, B. C. (1997). The impact of precision agriculture. proceedings of the ABARE outlook conference. The Future of Cropping in NW NSW, Moree, UK, 5.

White, J. W., Andrade-Sanchez, P., Gore, M. A., Bronson, K. F., Coffelt, T. A., Conley, M. M., ... & Jenks, M. A. (2012). Field-based phenomics for plant genetics research. *Field Crops Research*, 133, 101-112.

Zhang, N., Wang, M., & Wang, N. (2002). Precision agriculture—a worldwide overview. *Computers and electronics in agriculture*, 36(2), 113-132.

Wu, C., Niu, Z., Tang, Q., & Huang, W. (2008). Estimating chlorophyll content from hyperspectral vegetation indices: Modeling and validation. *Agricultural and forest meteorology*, *148*(8), 1230-1241.

Chapter 2 - Comparison of Different Remote Sensing Tools for Site-specific Crop Management: A Review

Introduction

Crop production strategies have changed dramatically over the past decades to meet the challenge of increasing agricultural productivity while reducing inputs, maximizing profits, and mitigating environmental degradation (Zhang et al., 2002). This requires the agriculture systems to be resource-efficient by integrating tools, technologies, and information management systems that come under the precision agriculture (PA) concept (Whelan et al., 1997), which is a farming management concept based on observing, measuring, and responding to inter and intra-field variability in soil and crops to optimize profitability and protect the environment.

The general components of PA practice are data collection, field variability mapping, decision making, and finally management practice (Zhang et al., 2002). To get accurate and consistent data during the growing season over matching spatial scale and to understand intra-field variability in assessing potential productivity are the foundations of decision making and final field practice in real world PA. Along with the advances in global position system (GPS), geographic information system (GIS), and variable rate technology (VRT), remote sensing data has provided powerful analysis tools for PA, which has changed the traditional way of farming (Mulla, 2013).

PA requires accurate mapping of seasonally stable crop management units, such as field boundary, soil type, historical yield; monitoring of seasonally variable information, such as soil moisture and nutrients, crop growth and development, crop stress caused by nutrient deficiency, disease, weeds, pests, and extreme weather conditions; as well as incorporating and interpreting

of these information to optimize the management practice and promote the final grain yield. For this wide range of applications, the first and foremost task is to select and combine remote sensing data, which comes from an abundant variety of platforms and sensors, that best suits the specific application in the farm. As showed in this section, remote sensing has been providing valuable insights to PA. These remote sensing data can be collected from an abundant series of sensors. Here we categorized the sensors through the platforms they are mounted on as shown in Figure 2.1.

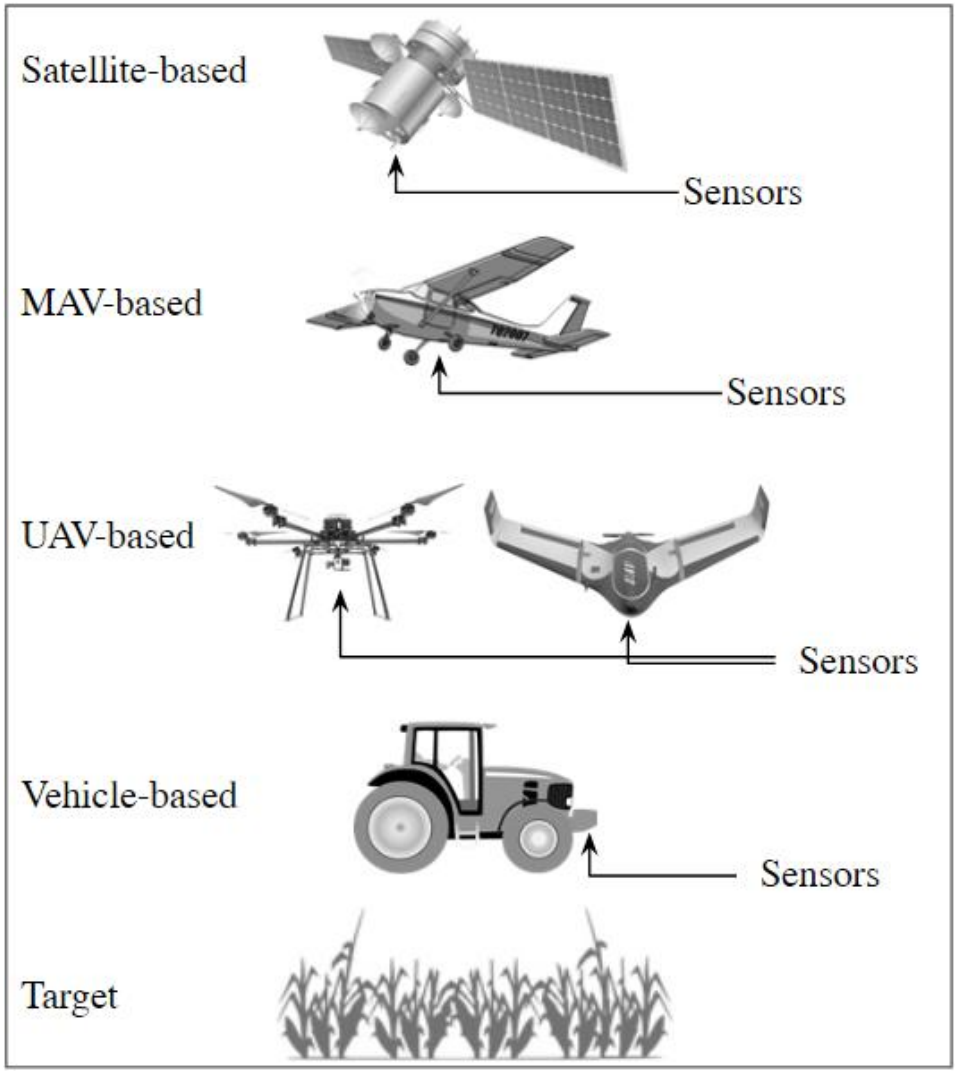

Figure 2.1 Satellite-based, MAV (manned aerial vehicle)-based, UAV (unmanned aerial vehicle)-based, and vehicle-based remote sensing platforms for precision agriculture.

The objective of this chapter is to provide a thorough survey on the different remote sensing tools for site-specific crop management in real world crop production, and show their advantages, limitations, and tradeoffs.

Sensors/Vendors to be used in comparisons

To compare remote sensors mounted on different platforms, we selected the most widely used sensors or sensor representatives for each category.

For vehicle-based remote sensing, there are two types of sensors. One is for sensing crops and the other is for sensing soil. We selected RapidScan CS-45 (Holland Scientific, Inc., Lincoln, NE), GreenSeeker Model 505 (NTech Industries, Inc., Ukiah, CA), Hand-held Greenseeker (Trimble Inc., Sunnyvale, CA) and Crop Circle ACS-430 (Holland Scientific, Inc., Lincoln, NE) as the representative for crop sensors while selected Veris MSP3 (Veris technologies, Inc, Salina, KS) as representative for soil sensors. These sensors were intensively used and were accepted by the researchers (Aranguren et al., 2016; Cordero et al., 2016; Raper et al., 2013; Osborne, 2007; Deery et al., 2014; Arora et al., 2013; Tremblay et al., 2011; Amaral et al., 2015; Fulton et al., 2011; Grisso et al., 2005).

For UAV-based remote sensing, we are only interest in the UAVs that normally fly under 400 ft (122 m) above ground level (AGL). In terms of the sensors, we selected three multispectral imagers: a RedEdge (MicaSense Inc., Seattle, WA), a Parrot Sequoia (Parrot SA Inc., Paris, France), a Tetracam Micro-MCA (Tetracam Inc., Chatsworth, CA), and a thermal camera--a FLIR VUE Pro (640 x 512, 30 hz, 13 mm, FLIR System Inc., Wilsonville, OR). All of these sensors are specifically designed for UAV power support. We also included an example of modified digital cameras--a Canon T4i digital single-lens reflex (DSLR) camera (Canon Inc,

Tokyo, Japan) modified by LDP LLC., Carlstadt, NJ to allowing the record of NIR light. Most modified cameras are done on Canon and Sony Point-Shot cameras and some lightweight DSLR cameras (Torres-Rua, 2017).

For MAV-based sensing, we did not select the sensors since it is normally cheaper to outsource the imagery data from imaging service companies instead of customizing the sensor and flying the mission him or herself. These companies normally have their own planes, sensors, and customized image processing workflow. We picked three of the leading MAV imaging companies in the industries for the comparisons. They are Cornerstone Mapping Inc., Roca, NE, Ceres Imaging Inc., Oakland, CA, and TerrAvion Inc., San Leandro, CA.

For satellite-based remote sensing, we only include the satellite with high spatial resolution (less than 10 m) which is suitable for PA and currently available (Table 2.1). There are some other high resolution satellites out there that were excluded from the comparisons due to different reasons. i.e. IKONOS (4 m) ceased new collections in January 2015; SPOT-5 (6 m) has been decommissioned as of March 2015.

There are some other sensors that are really useful for agriculture such as LiDAR (Light Detection and Ranging), hyperspectral cameras, synthetic aperture radar (SAR), and laser scanner. But they are not readily available to PA due to high expenses, complex of operation and data process, or huge payload that won't fit an UAV or a MAV. Also, their application in PA are still in the development phase or proof-of-concept phase (Whitehead et al., 2014), therefore, they will not be reviewed in this paper.

In the sections followed, we further compared different platforms on multiple dimensions including specification, data collection efficiency and data availability, applications, limitations, economics, and adoption.

Comparisons

Section 1: Specification

The specifications of sensors mounted on different remote sensing platforms were summarized in Table 2.1. Vehicle-based sensors normally have three bands or less, including a visible band (mainly Red), a NIR band, and sometimes a Red edge band on some newly developed sensors. Literature suggested that suggested VIs using red edge wavelengths, such as NDRE, are more efficient than NDVI in identifying N variability in crops (Shiratsuchi et al., 2011; Feng et al. 2016; Rosa et al. 2016) and can be used for vegetation stress studies (Hruska et al. 2012). This band combination is sufficient for applications such as assessing the crop nitrogen status but will have limitations on other applications that requires other bands. e.g. water stress detection requires a thermal band which cover the water absorption band in the spectrum; crop residue detection requires wavelengths (around 2100 nm) that are sensitive to cellulose and lignin in the residue (Daughtry, 2001). UAV, MAV, and Satellite-based sensors normally are capable to collect data at multiples bands (4+), which provide possibilities to unlock more applications. A detailed evaluation of optimal wavebands for different PA application is provided by Thenkabail et al. (2002), which is recommended to read.

Table 2.1 Comparisons of sensor specifications mounted on different remote sensing platforms for precision agriculture.

	Swatch Width	Spatial Resolution	Band No.	Wavelength (nm)	Bit Depth
Vehicle-based Active Sensor	**At 0.6 m above canopy**				
Holland Scitifics RapidScan CS-45	67 cm	n/a	3	670, 730, 780	n/a
Ntech GreenSeeker Model 505	60 cm	n/a	2	530 (or 650), 770	n/a
Trimble Hand-held Greenseeker	60 cm	n/a	2	660, 770	n/a
Holland Scientifics Crop Circle ACS-430	32 cm	n/a	3	670, 730, 780	n/a
UAV-based Passive Sensors	**At 122 m AGL**				
Micasense RedEdge Multispectral Imager	106 m	8.32 cm	5	475, 560, 668, 717, 840	12
Parrot Sequoia Multispectral Imager	189 m	14.8 cm	4	550, 660, 735, 790	10
Tetracam mini-MCA-6 Multispectral Imager	86 m	6.6 cm	6	450, 530, 670, 700, 740, 780	8
FLIR VUE PRO (640 x 512, 30 hz, 13 mm)	101 m	15.8 cm	1	750-1350	14
Modified DSLR camera (Canon T4i)	63 m	3.3 cm	3	552, 638, 833	14
MAV-based Passive Sensors	**At 610 m AGL**				
Vendor 1: Cornerstone Mapping	n/a	20, 100 (Thermal)	4	Blue, Green, Red, NIR, Thermal	n/a
Vendor 2: Ceres Imaging	n/a	20, 100 (Thermal)	4	Blue, Green, Red, NIR, Thermal	n/a
Vendor 3: TerrAvion	n/a	9-18, 200 (Thermal)	4	Blue, Green, Red, NIR, Thermal	n/a
Satellite-based Passive Sensors	**At corresponding orbit**				
Quickbird	18 km	2.4 m	4	485, 560, 660, 830	11
SPOT-6	60 km	6 m	4	490, 560, 660, 825	11
SPOT-7	60 km	6 m	4	490, 560, 660, 825	11
RapidEye	77 km	5 m	5	475, 555, 657, 710, 805	12
GeoEye-1	15.2 km	2 m	4	480, 545, 672, 850	11
WorldView-2	17.2 km	2 m	8	425, 480, 545, 605, 660, 725, 832, 950	11
Pleiades 1	20 km	2 m	4	490, 550, 660, 850	12
Sentinel 2	290 km	10 m	4	490, 560, 665, 842	12
Landsat 7	185 km	30 m	6	485, 560, 660, 835, 1650, 2220	8
Landsat 8	185 km	30 m	7	443, 482, 561, 654, 865, 1608, 2220	12

The spatial resolution is negatively correlated with the distance between the sensor position and the target or the flying altitude (except vehicle-based active sensors since they collect point samples with a certain frequency instead of taking image). Finer resolution from UAV based sensors has the privilege to better detect the sub details in the field such as weed detection (weed or not weed) and even weed classification (which type/species of weed). The spatial resolution of MAV-based sensor is not as fine as UAV-based sensor but still very fine (20 cm for multispectral, 100-200 cm for thermal band). This is the sweet point for MAV-based sensors, they can collect data much more efficiently and keep the data quality as high as UAV-based ones or very close to it. A detailed comparison process of data collection efficiency is provided below.

Section 2: Data collection efficiency and data availability

The technology users or decision makers needs to know the area that PA tool can cover per unit time or effective rate (Griffin et al., 2005). Working rate was defined as below and used to measure the **data collection efficiency**:

$$WR = Speed\ (mph)\ x\ Width\ (ft)\ x\ FE\ (\%)\ /\ 8.25 \qquad Eq.\ 2.1$$

Where,

WR = Working rate

Speed = Ground speed of the equipment

Width = Swath width that a sensor can capture

FE = the field efficiency

The field efficiency is the ratio of the amount of time that the equipment is actively conducting the role to the time that the equipment was devoted to the task including but not limited by warming up, changing batteries, set-up. When speed is expressed as mpg and width in feet, the product of all their parameters are divided by the constant 8.25 (assuming the units are in mpg and feet). The following table shows the working rate for Vehicle-based, UAV-based, and MAV-based optical sensors.

Table 2.2 Comparisons of data collection efficiency for vehicle-based, UAV-based, and MAV-based optical sensor. FE: field efficiency, WR: working rate.

Optical Sensor	Speed (mpg)	Width(ft)	FE(%)	WR (ac/hour)
Vehicle-based	20	40	90	87
UAV-based	20	130	70	221
MAV-based	90	2000	30	6545

Data availability of different sensors are depending on their temporal resolutions. For vehicle, UAV, and MAV-based sensor, the temporal resolution is flexible. Data can be collected daily (extreme situation), weekly (key crop growth stages), or biweekly (less important growth stages). For satellite based sensors, the temporal resolution ranges from 3 days (RapidEye) to 6 months (WorldView-2). Also the cloud coverage condition has a big impact on the data quality thus the data availability. An example of data availability comparison between a UAV-based sensor and the Sentinel-2 is provided below by Wang et al., 2017 (Table 2.3). The Sentinel-2 data was selected because it is the best quality satellite data (spatially and temporally) for free by far.

Table 2.3 Comparisons of a UAV-based sensor and the Sentinel-2 data availability on a wheat experiment at Manhattan, Kansas for 2015-2016 season.

	Total No. of images	Total No. of useful images	Total No. of dicarded images	Reason for discard
UAV-based	15	14	1	bad exposure
Sentinel-2	30	4	13	target field was completely blocked by cloud
			11	target field was excluded from the tile
			2	redundant image (same day but different scene)

Section 3: Application and limitation

Table 2.4 Comparison of capability of UAV, MAV, Satellite, and Vehicle-based remote sensing on different site-specific precision agriculture applications.

Applications	UAV-based	MAV-based	Satellite-based	Vehicle-based
Field boundary mapping	yes	yes	yes	
Crop biomass estimation	yes	yes	potential	yes
Crop yield prediction	yes	yes	potential	yes
Crop chlorophyll content	yes	yes	potential	yes
Crop nutrient status (N)	yes	yes	potential	yes
Crop nutrient status (Other nutrients)	yes	yes		
Crop water status	yes	yes		
Crop canopy height estimation	yes			
Crop disease	potential			
Residue detection	potential			
Weed detection	potential			
Insects infestation detection	potential			

UAV-based remote sensing application for various agriculture applications has soared over the last decade because of their potential to be a low-cost, accessible, and practical substitute for satellite and MAV for high resolution remote sense data. A variety of platforms have been developed: Fixed-wing, helicopter, multirotor, powered glider, powered parachute, assembled units from off-the-shelf parts, and commercial ready-to-fly UAVs (Myers et al., 2015). A variety of sensors can be mounted on the UAVs for PA: regular off-the-shelf RGB digital cameras, custom-converted digital cameras that can sense NIR by simply removing an infrared filter, consumer grade multispectral imager, hyperspectral imaging systems, thermal cameras (Myers et al., 2015). The cost of each type of sensors has been declining as manufacturing processes are improved and new technologies are developed. Due to the high maneuverability, UAV-based remote sensing has been applied to lots of application including but are not limited to: crop disease detection (Garcia-Ruiz et al., 2013; Franke & Menz, 2007), assessment of crop nitrogen status (Stafford 2000; Berni et al. 2009a, b; Hunt 2005) and water stress (Zarco-Tejada et al. 2012; Berni et al. 2009a; Gago et al., 2015), weed detection (Gomez-Casero et al. 2010), in-season biomass estimation and final grain yield prediction (Hunt 2005; Swain et al. 2010; Wang et al., 2017), estimation of soil properties such as soil organic matter,

soil surface moisture, and soil temperature (Chaves et al., 2015; Sona et al., 2016), determination of the relative density, canopy height estimation with the digital surface model (DSM) generated with ultra-high resolution imagery (Bendig et al., 2013, Bendig et al., 2014). In general, UAV-based remote sensing have been used extensively in PA, for much higher spatial resolution (down to cm), flexible data acquisition time, and flexible choice of sensors specific application.

While the UAV-based PA applications have seen tremendous growth in recent years, there are still some shortcomings that need to be aware of. Chief among these are the fact that most sensors they carry for PA applications are passive optical sensors such as multispectral cameras, converted digital cameras. They lack of direct measurement of reflectance which is the remotes sensing base for PA, and their measurements, brightness values, are influenced by the camera setting and ambient light condition. To be able to get consistent measurements and compared them across time, space, and different sensors. Effective radiometric calibration should be performed. Some calibration methods were developed for multispectral cameras and modified digital cameras (Wang et al., 2017; Wang et al., 2015). These calibration processes work under the assumption that the light condition does not change during a single flight, which is quite possible for a UAV mission since it does not take too long to cover a field (data collection efficiency was provided in Table 2) and the battery will run out of juice at a certain point (for multirotor, it is about 39 minutes max). However, there are still some circumstances this assumption does not hold true. For example, the flight mission is using a fixed-wing to cover a gigantic area at once which will last over one hour and during which the light condition is changing rapidly, or the mission is just happening at a place where the light condition is changing so rapidly. For multispectral cameras, there is trend to integrating a downwelling light sensor (DLS) to the multispectral imagers such as Micasense Rededge and Parrot Sequoia

(www.micasense.com; www.parrot.com) to improve reflectance calibration in situations where ambient light conditions are changing in the middle of a flight . The evaluation of the reliability or efficiency of this type of DLS has not been seen on any science publication. Compared to MAV, UAV usually has much less payload capacity which limits the selection of bulky sensors such as LiDAR and SAR, but newly developed high end sensor systems are getting lighter, more compact, and more user-friendly, which provides more opportunities in UAV-based applications. The trade-off between spatial resolution and processing time should be noted as the image processing time increases dramatically with spatial resolution, but too low of a resolution limits the ability to differentiate sub-detail in the field. It is important to optimize the path planning and sensing strategies to minimize data redundancy and processing time when using UAV-based sensing.

Another thing people are interested is the Federal Aviation Administration (FAA) regulations on UAV use. On August 29, 2016, the awaited FAA regulation for civil unmanned aircraft, 14 CFR Part 107, took effect. While newsgathering drones are severely restricted, as well as food or package delivery via drones are effectively prohibited, agriculture and environmental uses have the least restriction under Part 107. They include crop dusting, livestock or wildlife tracking, and the inspection of crops, forests, or foliage. Environmental or agricultural drones are unlikely to encounter non-participating people. The line of sight restriction is not so burdensome. Nor should the 55-pound weight limit restrict operation. In sum, agricultural and environmental drone uses are generally permitted by Part 107 (Olsen 2017).

Satellite-based remote sensing has been applied to agriculture for decades at larger scale (regional, national). At sub-field level, because of the coarser spatial resolution compared to UAV and MAV based aerial imagery, only a few applications are feasible such as field mapping (Immitzer et al., 2016), phenology modeling (Duncan et al., 2015), biomass estimation (Kross et al., 2015), chlorophyll content and N status assessment (Clevers & Gitelson, 2013), and yield forecasting (Kolotii et al., 2015).

Most of the high-resolution satellites are not equipped with the thermal band and the spatial resolution of the thermal band on available satellites are usually too coarse (e.g. 60 m for Landsat &, 100 m for Landsat 8, and 90 for ASTER) to assess crop water stress at field scale. Therefore, MAV-based and UAV-based are the more practical choice in thermal irrigation management applications (Moran et al., 1994). Nutrient deficiencies are hard to be detected with satellite imagery because they rarely occur uniformly across a field and often need to be distinguished against background variation in canopy density using advanced analysis tools such as partial least-squares regression and spectral mixing techniques (Pinter Jr et al., 2003). Related studies are usually carried out with MAV-based and UAV-based platforms (Maresma et al., 2016).

The crop diseases and insect infestation detection normally require high spatial resolution and high spectral resolution such as hyperspectral imaging is preferred (Singh et al., 2009), which can provide assistance on differentiating crop diseases from other causes of plant stress such as nutrient deficiency and water stress. Weed detection requires high spatial resolution and it is time sensitive--they can only be detected at some stages and during when weeds have unique

growth patterns different from surrounding vegetation. Low spatial resolution from satellites and MAVs cannot detect small infestation and weeds mixed with crops (Lass et al., 2009).

Generally speaking, Satellite-based remotes sensing in PA are still limited by the coarse spatial resolution, cloud interference during image acquisition, and slow turnaround. The sub-field variability oriented applications challenged the effective use of satellite-based remote sensing in PA. The sensitivity of high resolution imagery to canopy variations needs to be further tested (Wu et al., 2007) before they can be more widely used in making timely management decisions.

MAV-based remote sensing application in PA are rarely seen in publications because it is more expensive and difficult to do so. For researchers who want to do MAV related project, they have to face multiple challenges: 1) To get good sensors that can collect quality data at a medium altitude (500 m to 1500 m AGL), 2) To find a MAV that is suitable to carry the sensors and willing to do the modification to fit the sensors (such as cutting a hole on the bottom of the plane or removing the back seats to spare rooms for the sensors), 3) to find someone who can operate the sensor and do troubleshooting in the air, and 4) to be able to afford all the above things and labor.

The number of publications of MAV-based PA applications are minimal does not mean that MAV cannot be used and widely used in PA. In fact, MAV-based remote sensing meet most of the requirement for PA applications and share some advantages with both UAV and satellite-based remote sensing. The spatial resolution is very high (< 20 cm for multispectral and < 2 m for thermal), which is much higher than satellite-based sensors and very close to UAV (<10 cm). The data collection time is flexible (weekly or biweekly in growing seasons, www.terravion.com) just like UAV, but can collect data much more efficiently than UAV (Table 2). The sensor

selection is also flexible due to the great payload capacity. You can have multispectral, thermal, LiDAR, and hyperspectral sensors all together mounted on the MAV and collecting data simultaneously, which UAV are not able to. We admit that it is neither feasible nor necessary to buy or pay everything in the 4-challenge-list mentioned earlier. However, with the blossom of PA, more and more companies started to provide MAV-based sensor data specifically for PA applications and the cost are reasonably low. Detailed cost analysis of different platforms will be provided in next section. Since the imagery products from third party companies are normally orthomosaics which is the final product after a series of image processing such as color correction, distortion correction, stitching, and geometric correction. It saves the labor and cost for image processing that usually involved in UAV imagery data.

Since MAV-based multispectral cameras are passive sensors just like UAV-based ones. Radiometric calibration need to be performed before quantitative analysis. Residue detection, crop disease detection, weed detection, and insect infestation detection are still challenging to MAV-based remote sensing since the spatial resolution is not high enough to differentiate the sub difference in small area in the field. The ability of estimating canopy height will decrease as the flying altitude increase. DSM generated from MAV based multispectral imagery has very minimum sensitivity to canopy height since the imagery is collected at 500 m AGL or above. MAV-remote sensing does not have cloud block issue like satellite does, but the cloud shadow projected on part of the target field may pose a challenge when comparing the area in the shadow with the area not in the shadow. Compared to UAV and vehicle-based data collection, MAV flights mission are more difficult to coordinate.

Generally speaking, MAV-based remote sensing has huge potential in PA application due to its high spatial, temporal, and spectral resolutions and has some limitations in applications that targeting the sub difference in small areas within a field.

Vehicle-based remote sensing are acceptable for lots of researchers and have been used to determine management zones and nitrogen status, estimate leaf area, detect green biomass in cereal crops, and estimate the soil organic matter (Tremblay et al., 2009; Shaver et al., 2010; Trotter et al., 2008; Fitzgerald, 2010; Wang et al., 2017; Erdle et al., 2011; Bricklemyer & Brown, 2010). Vehicle-based remote sensing normally are equipped with active sensors that use the internal light source and take reflectance measurements directly. No additional calibration is needed and can be used under any weather condition and anytime of a day while passive sensor data derived from UAV and MAV need to be collected within two hours of the solar noon for optimum performance. Also, the image processing is not required since vehicle-based active sensors output spectral reflectance (and VIs) directly and usually can be exported to a spreadsheet for immediate analysis.

While the vehicle-based sensors are so easy to use, there are still some shortcomings that need to be aware of. The first and foremost is the low efficiency on data collection compared to aerial platforms (Table 2.2). Secondly, vehicle-based sensors take point samples at a certain frequency instead of taking images so the area did not get sampled need to be interpolated by some techniques such as inverse distance weighting (IDW) and Kriging. This interpolation can be unreliable when the distance between paths are too large because the variability between two data point is not linear but generic. At early growth stage, the values from active sensors are less reliable since the crop has not reached adequate coverage, soil is the main reflector and the noise source for crop assessment. Also, spectral resolution for vehicle-based sensors are normally low

(2 or 3 bands). As a results, the usage is limited to the applications only require these bands. Another drawback the vehicle-based remote sensing cannot avoid is that they will are destructive to the field and can cause soil compaction if data were collected on a regular basis.

Generally speaking, vehicle-based remote sensing can be used in a few applications such as N assessment and biomass estimation that require minimum spectral resolution. They are not efficient to be used at larger scale.

Section 4: Economics

This section compared the economics of different PA remote sensing tools at whole-farm level. In this comparison we used, 500 ac, the averaged Kansas farm size, as the farm size, 10 as the total number of optical sensor data collections in one growing season, and 4 years as the economic life of the PA remote sensing tool since this is the average use life for most cameras and sensors.

From an economic perspective, all cost and benefits from PA technology use should be captured and analyzed to determine profitability. Understanding the cost and benefits of different PA tool is essential to determine the return on investment (ROI) as calculated in Eq.2.2:

$$ROI = II + PVC + PVB \qquad Eq.2.2$$

where,

$ROI = Return\ on\ Investment$

$II = Initial\ investment\ in\ the\ precision\ technology$

$PVC = Present\ Value\ of\ Costs$

$PVB = Present\ Value\ of\ Benefits$

The cost including the initial investment and the additional cost. The additional cost includes, but are not limited to, the data acquisition, travel, annual subscription(s) for image processing, information analysis, and the repairing and maintenance. The data acquisition cost of MAV and satellite-based data are included in the data purchase while UAV and vehicle-based data require separate data acquisition which involves labor cost. The labor cost not only occur during the data collections but also occur on the way to the targeted fields. Let us assume it will take about 1.5 hours to travel for a 500 ac farm for one data collection in the season. The following table shows the labor cost during data collection for UAV-based and Vehicle-based optical sensors where the rates were estimated by www.glassdoor.com using "UAV Operator" and "Field Data Collector" as the searching terms.

Table 2.5 Labor cost during data collection for UAV-based and vehicle-based remote sensing for a 500 ac farm.

Job Type	Rate/hr ($)	hours: Collection+Travel	Total # of Data Collections	Total Cost ($)
UAV Operator	75	2.3 + 1.5	10	3000
Field Data Collector	38	5.7 + 1.5	10	2850

Once the additional costs are determined, this information were then organized to do cost cash flow analysis. In terms of the ROI analysis for a PA tool, we used Present Value of Costs (PVC) to sum the yearly cost cash flow because this measurement does take into account the time value. Time value of money is the concept that $1 today is not worth the same to an individual as $1 at some time in the future. To calculate the PVC, the following formula was used:

$$PVC = \frac{CCF_1}{(1+i)^1} + \frac{CCF_2}{(1+i)^2} + \cdots + \frac{CCF_n}{(1+i)^n} \qquad Eq.\ 2.3$$

where,

$CCFt = Cost\ Cash\ Flow\ at\ time\ t$

$i = interest\ rate$

Benefits that can occur with precision technologies include a reduction in inputs such as N fertilizer, yield and quality increases, improvements in production and machine efficiency, and enhanced marketing decisions (Schimmelpfennig, 2016). For the four PA tools we are interested, their benefits mainly fall into the category of input reduction such as N saving. It is not appropriate to assume that the benefits for all the PA tools are the same since they depend on the performance of each sensor and the way the sensor been used. Thus, we calculated and compared the total cost ($II + PVC$) of each PA tool as below, unit: USD:

Vehicle-based optical sensor:

Representative: RapidScan CS-45

Table 2.6 Total Costs on using vehicle-based remote sensing in PA.

Initial Investment	Year 0			
Sensor: Holland Scientific RapidScan CS-45 x 1	4325			
Total Initial investment	4325			
Additional Costs	Year 1	Year 2	Year 3	Year 4
Data Acquisition	2850	2850	2850	2850
Travel	300	300	300	300
Image to Application Translation	6574	6574	6574	6574
Total Additional costs	9724	9724	9724	9724
Present Values of Additional Costs	8840	8036.364	7305.785	6641.623
Total Costs		**35148.7**		

Note: The sources for the cost estimations are: RapidScan CS-45: a quote provided by Holland Scientific, Inc.; Data Acquisition: Table 2.5; Travel: estimated using $30 per data collection x 10 times = $300; Image to Application Translation: estimated by www.glassdoor.com using “Quantitative Researcher” as the searching term.

UAV-based optical sensor:

Representative: MicaSense RedEdge + DJI Matrice 100

Table 2.7 Total Costs on using UAV-based remote sensing in PA.

Initial Investment	Year 0			
UAV: DJI Matrice 100 x 1	3299			
Sensor: MicaSense RedEdge x 1	5195			
Batteries: DJI Matrice TB48D x 6	1194			
Total Initial investment	9688			
Additional Costs	Year 1	Year 2	Year 3	Year 4
Data Acquisition	3000	3000	3000	3000
Travel	300	300	300	300
Battery	1194	1194	1194	1194
Repair & Maintenance	500	500	500	500
Image Processing (subscription)	474	474	474	474
Image to Application Translation	6574	6574	6574	6574
Total Additional costs	12042	12042	12042	12042
Present Values of Additional Costs	10947.27	9952.066	9047.333	8224.848
Total Costs		**47859.5**		

Note: The sources for the cost estimations are: DJI Matrice 100: www.dji.com; MicaSense RedEdge: www.micasense.com; DJI Matrice TB48D: www.dji.com; Data Acquisition: Table 2.5; Travel: same as the Vehicle-based sensors; Battery: same as the DJI Matrice TB48D; Repair & Maintenance: estimated based on personal experience; Image Processing: www.agribotix.com; Image to Application Translation: same as the Vehicle-based sensors.

MAV-based optical sensor:

Representative: TerrAvion Inc.

Table 2.8 Total Costs on using MAV-based remote sensing in PA.

Initial Investment	Year 0			
Total Initial investment	0			
Additional Costs	Year 1	Year 2	Year 3	Year 4
Data (including image processing)	2000	2000	2000	2000
Image to Application Translation	6574	6574	6574	6574
Total Additional costs	8574	8574	8574	8574
Present Values of Additional Costs	7794.545	7085.95	6441.773	5856.157
Total Costs	**27178.4**			

Note: The sources for the cost estimations are: Data: based on the private conversation with the sales personnel from TerrAvion Inc. This cost includes 12 data collections per season; Image to Application Translation: same as the UAV-based sensors.

Satellite-based optical sensor:

There is no initial investment for satellite-based remote sensing. For each satellite, there are different product options. Normally satellite will have panchromatic band and multispectral bands. Panchromatic band imagery has higher resolution, higher price, but single band. For precision agriculture use, multispectral part is more useful which include Red, Green, Blue and Near-Infrared. All the prices below are based on a 4-band multispectral bundle, which gives us enough bands to work with and keeps the price to a minimum.

Table 2.2.9 Price of high resolution satellite data. Data source: www.landinfo.com

Satellite	Spatial Resolution (m)	Price ($/sq. km)
Quickbird	2.4	25
SPOT-6	6	1.75
SPOT-7	6	1.75
RapidEye	5	1.28
GeoEye-1	2	27.5
WorldView-2	2	29
Pleiades 1	2	23
Sentinel 2	10	Free

Representative: RapidEye

Table 2.10 Cash flow analysis on using Satellite-based remote sensing in PA (Representative: RapidEye).

Initial Investment	Year 0			
Total Initial investment	0			
Additional Costs	Year 1	Year 2	Year 3	Year 4
Satellite Imagery Data (RapidEye)	5760	5760	5760	5760
Image processing (subscription)	474	474	474	474
Image to Application Translation	6574	6574	6574	6574
Total Additional costs	12808	12808	12808	12808
Present Values of Additional Costs	11643.64	10585.12	9622.84	8748.036
Total Costs		**40599.6**		

Note: The sources for the cost estimations are: Satellite Imagery Data: Table 2.9; Image processing: same as the UAV-based sensors; Image to Application Translation: same as the UAV-base sensors.

The total costs comparison of different remote sensing types is summarized in Table 11 below. MAV-based remote sensing is the cheapest tool to use in precision agriculture while UAV-based is the most expensive. This result is under the baseline of 500 ac farm size and 10 data collections for a growing season.

Table 2.11 Total costs of four types of remote sensors used in PA.

Sensor Type	Satellite-based	MAV-based	UAV-based	Vehicle-based
Sensor Representative	RapidEye	Ceres Imaging Inc.	MicaSense RedEdge DJI Matrice 100	RapidScan CS-45
Total Costs ($)	40600	27178	47860	35149

To better interpret the total costs comparison, we also calculated the minimum benefit required to make the ROI positive using Eq. 2.4,2.5.

$$PVB = -(II + PVC) \qquad Eq.2.4$$

$$Benefit = \frac{-(II + PVC)}{(1+i)^1 + (1+i)^2 + \cdots + (1+i)^n} \qquad Eq.\,2.5$$

where,

Benefit = Constant benefit per year.

As shown in Figure 2.2, to get a positive ROI, MAV-based sensors only need to provide a benefit of $11/ac while UAV-based sensors have to provide the most benefit per acre, $19/ac.

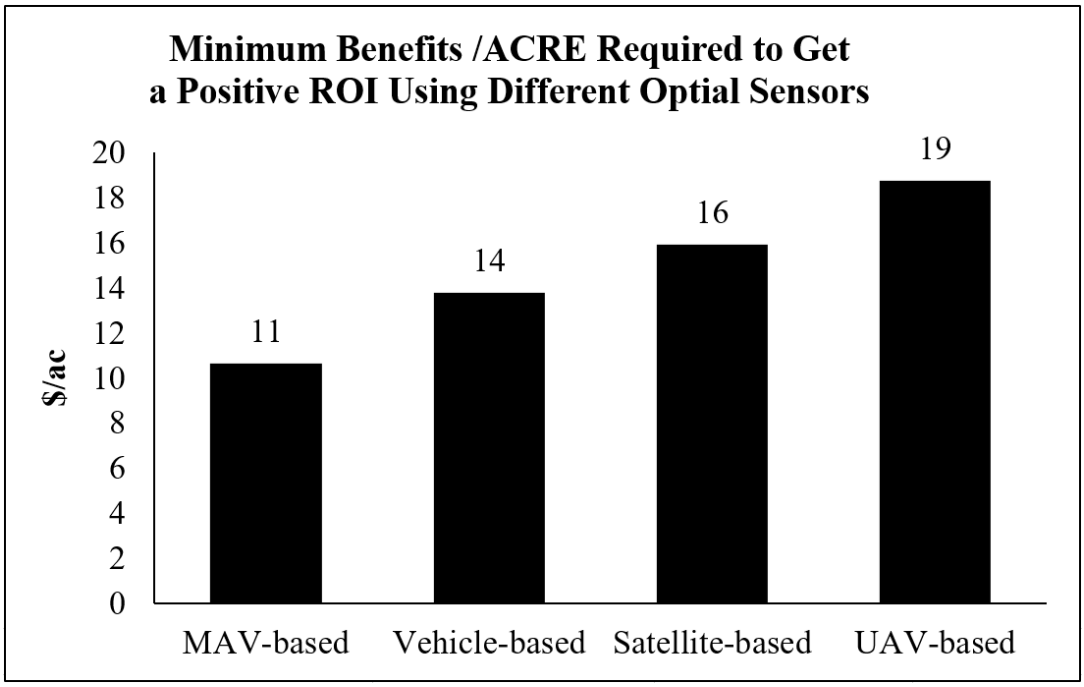

Figure 2.2 Minimum Benefits per Acre Required to Get a Positive ROI Using Different Optical Sensors.

For example, if the benefit is coming from the N saving, MAV and UAV-based sensors have to save at least 32 and 57 lb/ac N, respectively, to make the ROI positive. This is under the assumption that the price of Urea is $305/ton and the N concentrate in Urea is 46%.

One thing should be noted is that the number one cost of the additional cost for all platforms is “Image to Application Translation”, which is the process to convert sensor values or colorful maps to practical management plans. This part need to be done by experienced quantitative researchers who are familiar with crop physiology, remote sensing, and

mathematical modeling, which can be time consuming and expensive to provide reliable recommendations for decision making. With more and more applications developed for PA, this part, hopefully, can be accelerated, and eventually automated. Therefore, the total additional cost will reduce dramatically and make the remote sensing tools more profitable.

Another thing should be recognized is the learning cost associated with the new technology, especially for the farmers who want to fly UAVs and do the imagery interpretation or VIs-based recommendations by themselves. This requires specialized skills and an additional time investment by the farmers (Miller et al., 2017). Since it is very difficult to quantify and varies from one farmer to another, the learning costs were not included in the cost analysis.

Section 5: Adoption of remote sensing in PA

Applications of remote sensing in PA have shown to be beneficial and profitable, but current adoption in real world crop production are still low (Miller et al., 2017). According to the survey conducted by Purdue University in the USA 2015 (Figure 2.3). The most popular technology used was Satellite-based and MAV-based remote sensing (51%, values were the same because they were merged into one category in the survey as “Satellite/aerial”). UAV-based sensors were less popular (16%) and Vehicle-based crop or soil sensing was the least popular technology.

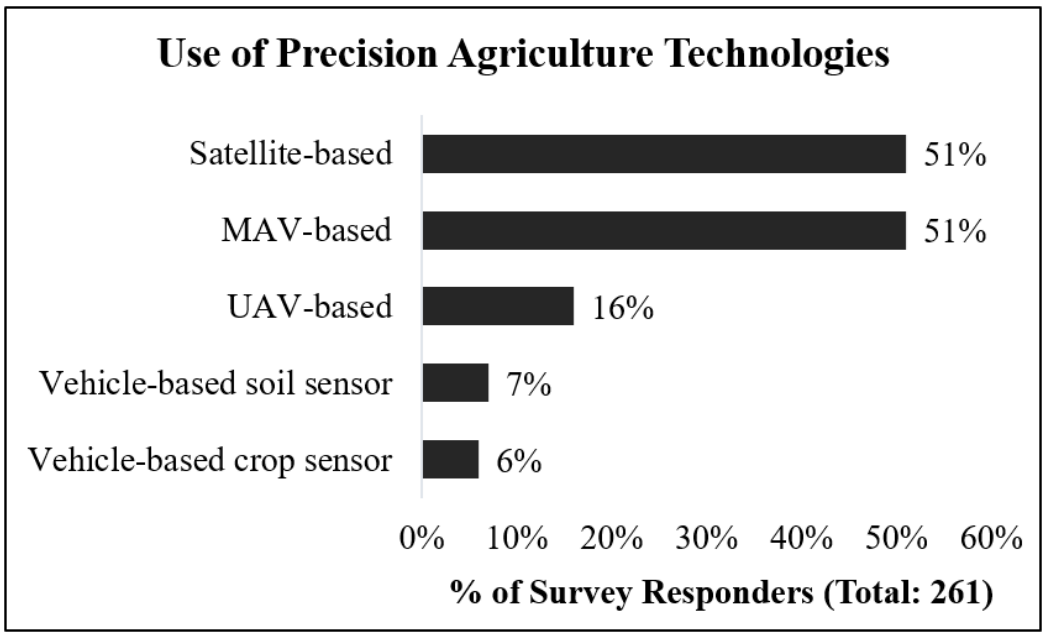

Figure 2.3 Use of precision agriculture technologies in 2015 (Adapted from Erickson & Widmar, 2015)

Overall, the adoption rate is increasing over time as shown in Figure 2.4. In recent years, satellite-based and MAV-based imagery have shown strong gains in adoption from 30 to 51% between 2011 and 2015. UAV adoption was firstly recorded in 2015 as 16% which was high considering that this technology was fairly new to the producers. The adoption rates of vehicle-base crop and soil sensing were increasing but still less than 10%.

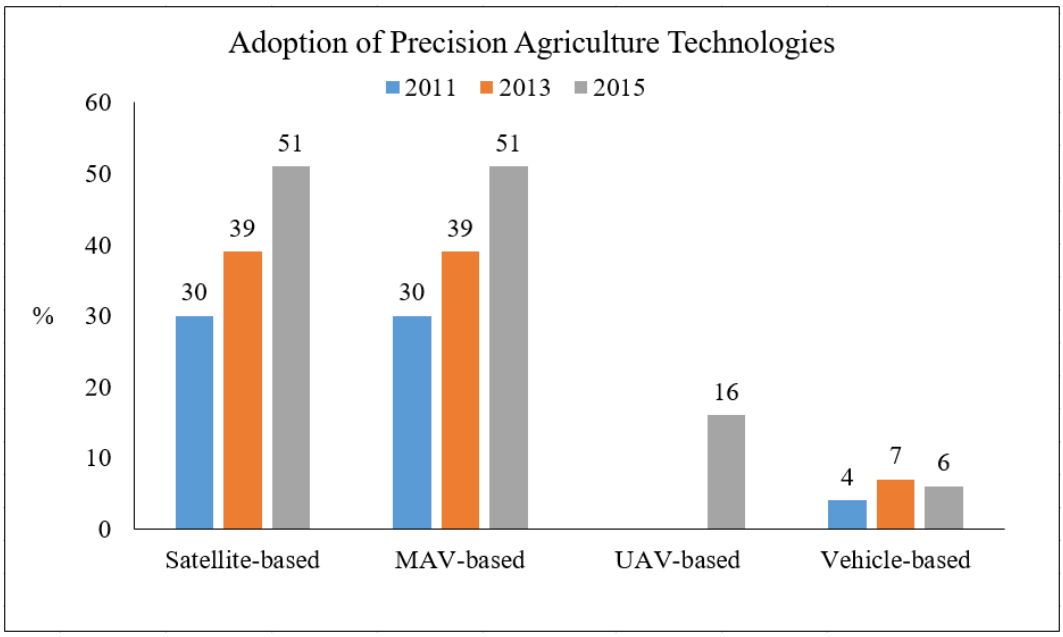

Figure 2.4 Adoption of precision agriculture technologies in 2015 (Adapted from Erickson & Widmar, 2015)

The farms who use precision technologies do not necessarily use them on all their acre. Figure 2.5 shows the estimated percentage of acres using various PA technologies over time and the prediction for 2018. Overall, all remote sensing platforms have been and will be used on more farmland acres.

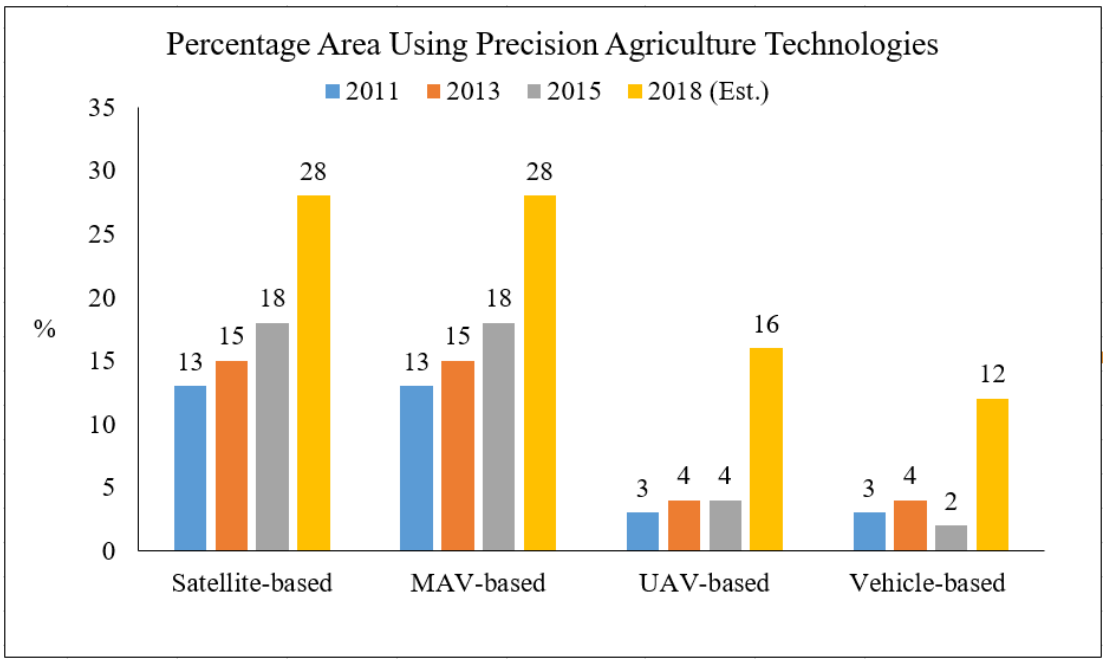

Figure 2.5 Percentage area using precision agriculture technologies (Adapted from Erickson & Widmar, 2015)

There are several barriers that prevent the growth and expanded use of PA technologies. The first one and for most producers is that farms income pressure limit the use of PA. The following barrier is that producers lack confidence in site-specific recommendation, some of them found the cost were greater than benefits. Also, Interpreting the sensor data and translate it to practical management plans can be time consuming and require highly trained expertise. Some other physical reasons can also limit the use of PA such as topography and soil types in the fields (Erickson & Widmar, 2015).

Conclusions

This review has briefly compared four remote sensing technologies mounted on four different platforms (vehicle-based, UAV-based, MAV-based, and Satellite-based) on specification, data collection efficiency and data availability; summarized the applications and limitations for each type of remote sensing tool, analyzed the total costs of each sensor type

representative to show the minimum benefit requirement for each type of sensors to get a positive ROI; and discussed the current status of adoption for each remote sensing tool.

Remote sensing based applications in PA have gone through dramatic advances in the recent years and will continue the trend. The future applications may be ascribed to the improvement of simplifying image processing, lowering hardware prices, automation of data-to-plan translation to reduce the labor cost. Although remote sensing tools can detect the field variability fairly easily, it is usually very hard to identify exact reasons that is causing the nonuniformities in the field. Multi-sensor strategy can help to improve the diagnosis accuracy. It can be a combination of different sensors on the same platforms or from different platforms. Emerging information technologies like on-the-going process & analysis, cloud computing, multi-platform communication, and data sharing also can be integrated into PA for advanced, intelligent data collection and analysis. In addition, the sensor and technologies will continue to develop, more researches will be done, more methods will be validated, and more people will adopt these PA tools to optimize the profitability and protect the environment.

References

Amaral, L. R., Molin, J. P., Portz, G., Finazzi, F. B., & Cortinove, L. (2015). Comparison of crop canopy reflectance sensors used to identify sugarcane biomass and nitrogen status. *Precision agriculture*, *16*(1), 15-28.

Aranguren, M., Castellón, A., & Aizpurua, A. TOP DRESSING NITROGEN RECOMMENDATION IN WHEAT AFTER APPLYING ORGANIC MANURES. USE OF FIELD DIAGNOSTIC TOOLS. *Efficient use of different sources of nitrogen in agriculture–from theory to practice Skara, Sweden 27 June–29 June 2016*, 414.

Arora, A., Sharma, R. K., Saharan, M. S., Venkatesh, K., Dilbaghi, N., Sharma, I., & Tiwari, R. (2013). Quantifying stripe rust reactions in wheat using a handheld NDVI remote sensor. In *Proceedings of BGRI2013 Technical Workshop* (pp. 19-22).

Bendig, J., Willkomm, M., Tilly, N., Gnyp, M. L., Bennertz, S., Qiang, C., ... & Bareth, G. (2013). Very high resolution crop surface models (CSMs) from UAV-based stereo images for rice growth monitoring in Northeast China. *Int. Arch. Photogramm. Remote Sens. Spat. Inf. Sci*, *40*, 45-50.

Bendig, J., Bolten, A., Bennertz, S., Broscheit, J., Eichfuss, S., & Bareth, G. (2014). Estimating biomass of barley using crop surface models (CSMs) derived from UAV-based RGB imaging. *Remote Sensing*, *6*(11), 10395-10412.

Berni, J. A. J., Zarco-Tejada, P. J., Suarez, L., & Fereres, E. (2009a). Thermal and narrowband multispectral remote sensing for vegetation monitoring from an unmanned aerial vehicle. IEEE Transactions on Geoscience and Remote Sensing, 47, 722–738.

Berni, J. A. J., Zarco-Tejada, P. J., Suarez, L., Gonzalez-Dugo, V., & Fereres, E. (2009b). Remote sensing of vegetation from UAV platforms using lightweight multispectral and thermal imaging sensors.Retrieved March 12, 2012 from http://www.ipi.uni-hannover.de/fileadmin/institut/pdf/isprs-Hannover2009/ Jimenez_Berni-155.pdf.

Bricklemyer, R. S., & Brown, D. J. (2010). On-the-go VisNIR: potential and limitations for mapping soil clay and organic carbon. *Computers and Electronics in Agriculture*, *70*(1), 209-216.

Chaves, A. A., La Scalea, R. A., Colturato, A. B., Kawabata, C. L. O., Furtado, E. L., & Branco, K. C. (2015). Using UAVs and digital image processing to quantify areas of soil and vegetation. In *Journal of Physics: Conference Series* (Vol. 633, No. 1, p. 012112). IOP Publishing.

Clevers, J. G., & Gitelson, A. A. (2013). Remote estimation of crop and grass chlorophyll and nitrogen content using red-edge bands on Sentinel-2 and-3. *International Journal of Applied Earth Observation and Geoinformation*, *23*, 344-351.

Cordero, E., Moretti, B., Miniotti, E., Tenni, D., Beltarre, G., Romani, M., & Sacco, D. (2016). Optimizing Topdressing Fertilization Through Ground Sensing Measurements in Rice. *Atti del XLV Convegno della Società Italiana di Agronomia Sassari*, *20*, 22.

Daughtry, C. S. (2001). Discriminating crop residues from soil by shortwave infrared reflectance. Agronomy Journal, 93(1), 125-131.

Deery, D., Jimenez-Berni, J., Jones, H., Sirault, X., & Furbank, R. (2014). Proximal remote sensing buggies and potential applications for field-based phenotyping. *Agronomy*, *4*(3), 349-379.

De Rosa, D., Rowlings, D., Biala, J., Scheer, C., Basso, B., Migliorati, M. D. A., & Grace, P. R. (2016). Monitoring the N release from organic amendments using proximal sensing.

Drones in Agriculture: An Overview of Current Capabilities and Future Directions

Duncan, J., Dash, J., & Atkinson, P. M. (2015). The potential of satellite-observed crop phenology to enhance yield gap assessments in smallholder landscapes. *Frontiers in Environmental Science*, *3*, 56.

Erdle, K., Mistele, B., & Schmidhalter, U. (2011). Comparison of active and passive spectral sensors in discriminating biomass parameters and nitrogen status in wheat cultivars. *Field Crops Research*, *124*(1), 74-84.

Erickson, B., & Widmar, D. A. (2015). Precision agricultural services dealership survey results. Sponsored By CropLife Magazine And The Center For Food And Agricultural Business. Purdue University.

Feng, W., Zhang, H. Y., Zhang, Y. S., Qi, S. L., Heng, Y. R., Guo, B. B., ... & Guo, T. C. (2016). Remote detection of canopy leaf nitrogen concentration in winter wheat by using water resistance vegetation indices from in-situ hyperspectral data. Field Crops Research, 198, 238-246.

Fitzgerald, G. J. (2010). Characterizing vegetation indices derived from active and passive sensors. International Journal of Remote Sensing, 31(16), 4335-4348.

Franke, J., & Menz, G. (2007). Multi-temporal wheat disease detection by multi-spectral remote sensing. *Precision Agriculture*, *8*(3), 161-172.

Fulton, A., Schwankl, L., Lynn, K., Lampinen, B., Edstrom, J., & Prichard, T. (2011). Using EM and VERIS technology to assess land suitability for orchard and vineyard development. *Irrigation Science*, *29*(6), 497-512.

Gago, J., Douthe, C., Coopman, R., Gallego, P., Ribas-Carbo, M., Flexas, J., ... & Medrano, H. (2015). UAVs challenge to assess water stress for sustainable agriculture. *Agricultural Water Management*, *153*, 9-19.

Garcia-Ruiz, F., Sankaran, S., Maja, J. M., Lee, W. S., Rasmussen, J., & Ehsani, R. (2013). Comparison of two aerial imaging platforms for identification of Huanglongbing-infected citrus trees. Computers and Electronics in Agriculture, 91, 106-115.

Gómez-Casero, M. T., Castillejo-González, I., García-Ferrer, A., Peña-Barragán, J. M., Jurado-Expósito, M., García-Torres, L., & López-Granados, F. (2010). Spectral discrimination of wild oat and canary grass in wheat fields for less herbicide application. Agronomy for Sustainable Development, 30(3), 689-699.

Griffin, T. W., & Lowenberg-DeBoer, J. (2005). Worldwide adoption and profitability of precision agriculture Implications for Brazil. Revista de Politica Agricola, 14(4), 20-37.

Grisso, R. D., Alley, M. M., Holshouser, D. L., & Thomason, W. E. (2005). Precision Farming Tools. Soil Electrical Conductivity.

Hruska, R., Mitchell, J., Anderson, M., and Glenn, N.F. 2012. Radiometric and geometric analysis of hyperspectral imagery acquired from an unmanned aerial vehicle. Remote Sens. 4(9): 2736–2752. doi: 10.3390/rs4092736

Hunt, E. R., Cavigelli, M., Daughtry, C. S., Mcmurtrey, J. E., & Walthall, C. L. (2005). Evaluation of digital photography from model aircraft for remote sensing of crop biomass and nitrogen status. *Precision Agriculture*, *6*(4), 359-378.

Immitzer, M., Vuolo, F., & Atzberger, C. (2016). First experience with Sentinel-2 data for crop and tree species classifications in central Europe. Remote Sensing, 8(3), 166.

Kross, A., McNairn, H., Lapen, D., Sunohara, M., & Champagne, C. (2015). Assessment of RapidEye vegetation indices for estimation of leaf area index and biomass in corn and soybean crops. *International Journal of Applied Earth Observation and Geoinformation*, *34*, 235-248.

Kolotii, A., Kussul, N., Shelestov, A., Skakun, S., Yailymov, B., Basarab, R., ... & Ostapenko, V. (2015). Comparison of biophysical and satellite predictors for wheat yield forecasting in Ukraine. *The International Archives of Photogrammetry, Remote Sensing and Spatial Information Sciences*, *40*(7), 39.

Lass, L. W., Prather, T. S., Glenn, N. F., Weber, K. T., Mundt, J. T., & Pettingill, J. (2005). A review of remote sensing of invasive weeds and example of the early detection of spotted knapweed (Centaurea maculosa) and babysbreath (Gypsophila paniculata) with a hyperspectral sensor. *Weed Science*, *53*(2), 242-251.

Maresma, Á., Ariza, M., Martínez, E., Lloveras, J., & Martínez-Casasnovas, J. A. (2016). Analysis of vegetation indices to determine nitrogen application and yield prediction in maize (Zea mays L.) from a standard UAV service. Remote Sensing, 8(12), 973.

Miller, N. J., Griffin, T., Bergtold, J., Sharda, A., & Ciampitti, I. (2017). Adoption of Precision Agriculture Technology Bundles on Kansas Farms. In *2017 Annual Meeting, February 4-7, 2017, Mobile, Alabama* (No. 252832). Southern Agricultural Economics Association.

Moran, M. S., Inoue, Y., & Barnes, E. M. (1997). Opportunities and limitations for image-based remote sensing in precision crop management. *Remote sensing of Environment*, 61(3), 319-346.

Mulla, D. J. (2013). Twenty-five years of remote sensing in precision agriculture: Key advances and remaining knowledge gaps. *Biosystems engineering*, 114(4), 358-371.

Myers, D., Ross, C. M., & Liu, B. (2015). A Review of Unmanned Aircraft System (UAS) Applications for Agriculture. In *2015 ASABE Annual International Meeting* (p. 1). American Society of Agricultural and Biological Engineers.

Olsen, R. (2017). Paperweights: FAA Regulation and the Banishment of Commercial Drones.

Osborne, S. L. (2007). Utilization of existing technology to evaluate spring wheat growth and nitrogen nutrition in South Dakota. *Communications in soil science and plant analysis*, *38*(7-8), 949-958.

Pinter Jr, P. J., Hatfield, J. L., Schepers, J. S., Barnes, E. M., Moran, M. S., Daughtry, C. S., & Upchurch, D. R. (2003). Remote sensing for crop management. *Photogrammetric Engineering & Remote Sensing*, 69(6), 647-664.

Raper, T. B., Varco, J. J., & Hubbard, K. J. (2013). Canopy-based normalized difference vegetation index sensors for monitoring cotton nitrogen status. *Agronomy Journal*, *105*(5), 1345-1354.

Shaver, T. M., Khosla, R., & Westfall, D. G. (2010). Evaluation of two ground-based active crop canopy sensors in maize: growth stage, row spacing, and sensor movement speed. Soil Science Society of America Journal, 74(6), 2101-2108.

Schimmelpfennig, D., & Ebel, R. (2016). Sequential adoption and cost savings from precision agriculture. Journal of agricultural and resource economics, 41(1), 97-115.

Shiratsuchi, L., Ferguson, R., Shanahan, J., Adamchuk, V., Rundquist, D., Marx, D., & Slater, G. (2011). Water and nitrogen effects on active canopy sensor vegetation indices. Agronomy journal, 103(6), 1815-1826.

Singh, C. B., Jayas, D. S., Paliwal, J., & White, N. D. G. (2009). Detection of insect-damaged wheat kernels using near-infrared hyperspectral imaging. *Journal of stored products research*, *45*(3), 151-158.

Sona, G., Passoni, D., Pinto, L., Pagliari, D., Masseroni, D., Ortuani, B., & Facchi, A. (2016). UAV multispectral survey to map soil and crop for precision farming applications. *INTERNATIONAL ARCHIVES OF THE PHOTOGRAMMETRY, REMOTE SENSING AND SPATIAL INFORMATION SCIENCES*, *41*, 1023-1029.

Stafford, J. V. (2000). Implementing precision agriculture in the 21st century. Journal of Agricultural Engineering Research, 76(3), 267-275.

Swain, K. C., Thomson, S. J., & Jayasuriya, H. P. (2010). Adoption of an unmanned helicopter for low-altitude remote sensing to estimate yield and total biomass of a rice crop. *Transactions of the ASABE*, *53*(1), 21-27.

Thenkabail, P. S., Smith, R. B., & De Pauw, E. (2002). Evaluation of narrowband and broadband vegetation indices for determining optimal hyperspectral wavebands for agricultural crop characterization. Photogrammetric Engineering and Remote Sensing, 68(6), 607-622.

Tremblay, N., Fallon, E., & Ziadi, N. (2011). Sensing of crop nitrogen status: Opportunities, tools, limitations, and supporting information requirements. HortTechnology, 21(3), 274-281.

Trotter, M. G., Lamb, D. W., Donald, G. E., & Schneider, D. A. (2010). Evaluating an active optical sensor for quantifying and mapping green herbage mass and growth in a perennial grass pasture. Crop and Pasture Science, 61(5), 389-398.

Whelan, B. M., McBratney, A. B., & Boydell, B. C. (1997). The impact of precision agriculture. proceedings of the ABARE outlook conference. The Future of Cropping in NW NSW, Moree, UK, 5.

Whitehead, K., & Hugenholtz, C. H. (2014). Remote sensing of the environment with small unmanned aircraft systems (UASs), part 1: a review of progress and challenges. Journal of Unmanned Vehicle Systems, 2(3), 69-85.

Wu, J., Wang, D., Rosen, C. J., & Bauer, M. E. (2007). Comparison of petiole nitrate concentrations, SPAD chlorophyll readings, and QuickBird satellite imagery in detecting nitrogen status of potato canopies. *Field Crops Research*, *101*(1), 96-103.

Zarco-Tejada, P. J., Diaz-Varela, R., Angileri, V., & Loudjani, P. (2014). Tree height quantification using very high resolution imagery acquired from an unmanned aerial vehicle (UAV) and automatic 3D photo-reconstruction methods. European journal of agronomy, 55, 89-99.

Zhang, N., Wang, M., & Wang, N. (2002). Precision agriculture—a worldwide overview. *Computers and electronics in agriculture*, 36(2), 113-132.

Chapter 3 - Comparison of Optical Sensors Based High-throughput Phenotyping for Biomass, Canopy Height Estimation and Grain Yield Prediction in Winter Wheat

Introduction

With the rapidly and steadily increasing world population crossing 7.3 billion and expected to reach 9.7 billion in 2050 (DESA, 2015), the world's food scenario is rapidly changing and global food production will need to increase by 70-110% to meet the growing demand (Alexandratos, 2009). At the same time, intensifying agricultural production can have a substantial environmental footprint and often comes at the expense of natural resources that support an agroecosystem. To meet the challenge of increasing agricultural productivity while simultaneously mitigating environmental degradation research and new technologies are needed to (1) assess crop condition quickly in a timely manner, (2) improve crop yield and quality, (3) reduce chemical and fertilizer inputs via more efficient use, (4) provide information for better in-field management decisions to increase profits, or, in other words, precision agriculture (Seelan et al. 2003).

The general components of precision agricultural practice are data collection, field variability mapping, decision mapping, and finally management practice. Remote sensing could be involved in first three of these components (Zhang & Kovacs, 2012). Although the potential of remote sensing for precision agriculture is clearly established, its adoption by farmers remains low (Seelan et al. 2003).

Remote sensing has been routinely used for decades at a larger-scale for general crop assessment such as yield prediction using satellites imagery (Idso, Jackson, & Reginato 1977; Idso, Pinter, Jackson, & Reginato, 1980; McDonald & Hall, 1980; Vossen & Meyer-Roux, 1995), but modern precision agriculture requires: short revisit times, high spatial resolution, and rapid data collection, all of which satellites rarely have. Literature indicates that remotely sensed imagery from satellites is not practical due to costs, availability, and data processing (Lamb, 2008). To monitor crops in a more timely and cost-efficient way, scientists are increasingly turning to optical sensors on the ground and aerial platforms to assess factors such as crop vigor, leaf nitrogen status

and potentials yields (Whitehead, 2014). Vehicle-based sensors mainly include active optical sensors (AOSs) such as the GeenSeeker, Crop Circle, and RapidScan, etc. Aerial-based sensors usually include passive optical sensors (POSs) such as visible cameras, CMOS (complementary metal oxide semiconductor)/CCD (charge coupled device) sensor based converted cameras, multispectral imagers, hyperspectral cameras, thermal cameras, etc. that are mounted on small unmanned aircraft systems (sUASs). The most basic assumption, as supported by empirical evidence (Ray, 1994), made about these sensors is that some algebraic combination of spectral reflectance or vegetation indices (VIs) can tell something useful about crop conditions.

Even with so many advanced sensors and platforms commercially available, farmers still prefer to adopt "embodied knowledge" technologies rather than "information intensive" technologies (Griffin et al. 2004). "Embodied knowledge" technologies do not require additional skills utilize. In contrast, "information intensive" technologies often require specialized skills and additional time to provide full benefits (Griffin et al. 2004). For example, farmers, crop consultants and extension agents often lack familiarity with different sensors, their uses, and the interpretation, the last of which, in practice, is the key to management decision making.

Thus to help farmers, crop consultants and extension agents better understand the performance of different sensors and provide guidance for sensor selection, the objectives of this study are to compare three of the most commonly used optical sensors including two POSs (Canon T4i® modified color infrared (CIR) camera and a Micasense RedEdge® multispectral imager) and one AOS (Holland Scientific® RapidScan CS-45® hand-held AOS) on: (1) In-season biomass estimation, (2) Grain yield prediction, (3) Canopy height estimation, and (4) Other factors to be considered in sensor selections.

Materials and methods

Study site descriptions

Winter wheat was planted for the 2015-2016 crop year at four locations selected on the basis of soil, precipitation, and their average productivity across the state of Kansas. One of the locations was at a Kansas State University Agronomy Ashland Bottoms research farm located to the south of Manhattan, KS and the remaining three were supplied by cooperating Kansas producers at Clifton, Victoria, and Valley Center, KS.

The following table (Table 3.1) shows the contextual information of each study site. Soil type information was obtained from the Web Soil Survey (NRCS, 2016). Cultural practice and historical average yield information were obtained from private conversations with farmers. Soil tests were done by either the authors or the farmers at the study sites.

Table 3.1 Locations, soils, cultural practices and average yields for wheat production in four environments in Kansas.

Location	Experiment Type	Latitude	Longitude	Soil Map Unit	Cultural Practice	Hybrids/Varieties
Manhattan, KS	Research plot	39.137615°	-96.640046°	Belvue Silt Loam	Conventional tillage after corn	Everest/Jagger/Karl 192/1863
Clifton, KS	On farm	39.554647°	-97.236159°	Crete Silty Clay Loam	No-till after soybean	WB grainfield
Victoria, KS	On farm	38.910426°	-99.201224°	Harney Silt Loam	No-till after wheat	TAM 111
Valley Center, KS	On farm	37.874093°	-97.244777°	Ladysmith/Rosehill Silty Clay	Conventional tillage after corn	Everest

Experimental Design

For the Manhattan, KS study site, small 3 x 5 m plots were arranged in a randomized complete block design (RCBD) with stripped block with three replications. Within each block, four wheat hybrids (Table 3.1) were planted as main treatments and four N rates were applied at the Feekes 4 growth stage as sub-treatments (0, 56, 112 and 168 kg/ha). There were 96 total plots (4 hybrids x 4 rates x 2 replications within block x 3 blocks).

Each of the on-farm study sites was a RCBD with four replications using 3 m x 12 m small plots as experimental units. At each study site, wheat varieties were selected and planted by farmers and received starter fertilizer as per their usual methods to enhance the development of emerging seedlings (Table 3.1). Also, eleven N rates were applied to the winter wheat at Feekes growth stages (4, 7, and 9). The rates varied at different sites due to different N recommendations. Each site had 44 plots (11 rates x 4 replications).

Customary field management practices (e.g.: preplant and postemergence applications of, respectively, Dicamba® and Huskie herbicides were performed as normal to remove the limiting factors of crop production. The purpose of applying different rates of N fertilizer and planting different hybrids was to generate gradients of N stress and plant growth within the field which was used later for building in-season biomass estimation and grain yield prediction models.

Sensor data collection

The commercially available RapidScan CS-45® (Holland Scientific®, Inc, Lincoln, NE, USA) was used as the AOS in this study. The RapidScan uses three modulated polychromatic

lamps as the light source and detects the reflectance of each in the Red, Red Edge and NIR spectral regions (Table 3.2). The field of view (FOV) of this device is a narrow strip of ~45° by ~10° range (Holland-Scientific, 2012), yielding a 33.5 cm x 5.2 cm strip on the canopy when the data are collected at 0.3 m above the canopy. The sensor was run crosswise to the sowing direction.

The Canon T4i DSLR (digital single-lens reflex) camera (Canon® Inc, Tokyo, Japan) was used as the CMOS sensor in this study. Like most of the CMOS and CCD sensor based commercial cameras, this camera is also sensitive to the NIR spectrum. In normal use, NIR blocking filters are installed so that cameras produce true color RGB images. Removal of this filter, however, allows the capture of NIR. Installing a blue notch filter enables measurement at NIR wavelengths to be recorded on the camera's blue channel. These modifications were done by LDP LLC, Carlstadt, NJ, USA (Table 3.2). The multispectral imager used in this study was a MicaSense RedEdge multispectral camera (MicaSense® Inc.). It is capable of measuring five discrete channels (Blue, Green, Red, Red Edge and NIR) having the specific ranges shown in Table 3.2. The Canon and MicaSense cameras were mounted side by side on a DJI s800 Evo hexacopter (DJI® Science and Technology, Co., Ltd. Shenzhen, China) with a gimbal to maintain a nadir orientation during the image collection. All pictures were recorded in RAW format, which provides the capability to do image correction before analysis. An intervalometer device (DigiSnap 2000 by Harbortronics®) was used to trigger the Canon camera with 1 frame/ 2 seconds. The MicaSense camera was triggered automatically at the defined image overlaps set by the "Auto-Capture" function built-in their WiFi web application.

In this study, both side and along-track overlap were set to 80% to get sufficient overlap. When the angle of illumination and sensor viewing angle are nearly identical and in the same plane, the bidirectional reflectance distribution function (BRDF) effects will show up and produce a hot spot in the picture. Obtaining images from multiple viewing angles and within two hours of the solar noon helped to reduce the BRDF effects. All sUAS operations were performed at 60 m above ground level (AGL) with Certificate of Authorization (COA numbers: 2015-CSA-6-COA-R for the Manhattan site, and 2014-CSA-6-COA for the Clifton, Victoria and Valley Center sites). All sensor data were collected eleven times during the growing season, at Feekes growth stages 3, 4, 6, 7, 10, 10.2, 10.5, 10.5.2, 10.5.4, 11.1, 11.3. On each date, the POSs data were collected right before AOS data to avoid the crop destruction caused by the AOS data collector who needed to

walk through the fields. Then biomass sampling was performed as described in the following section.

Table 3.2 Specification of three optical sensors used in this study.

Optical Sensor Name	RapidScan CS-45	Canon T4i modified CIR camera	MicaSense RedEdge multispectral camera
Sensor type	Active	Passive	Passive
Effective pixels (megapixels)	N/A	18	1.2
Ground Sample Distance (cm)	N/A	0.5 at 60m AGL 2.2 at 120 m AGL	3.3 at 60 m AGL 8.2 at 120 m AGL
Bandwidth (nm)	Red: 20 Red Edge: 20 NIR: 20	Green: 60 Red: 90 NIR: 60	Blue: 20 Green: 20 Red: 10 Red Edge: 10 NIR: 40
Peak wavelength (nm)	Red: 670 Red Edge: 730 NIR: 780	Green: 552 Red: 638 NIR: 833	Blue: 475 Green: 560 Red: 668 Red Edge: 717 NIR: 840

Field data collection

Biomass data were collected intensively at the nearest study site, Manhattan, during the growing season at Feekes growth stages 3, 4, 6, 7, 10, 10.2, 10.5, 10.5.2, 10.5.4, 11.1, 11.3. Twenty-four plots were selected for sampling that covered a high-to-low biomass gradient. A Japanese sickle was used to cut a 0.5 m x 0.5 m area from the east side (to avoid the middle portion that will be used for yield data collection) of each plot. The fresh biomass was put into paper bags, immediately weighed after taring, and then oven dried at 70°C to constant weight for dry biomass data.

Grain yield data were collected from all four study sites. At the Manhattan location, a 1 m x 1 m area in the middle of each plot was hand harvested at physiological maturity, oven dried at 70°C to constant weight, hand threshed, then weighed for grain yield data. The corresponding data from the Clifton, Victoria, Valley Center locations, exported from a yield monitor on the combine harvester. Grain yield data were adjusted to 12% moisture content for all study sites.

The CH measurements (from the ground surface to the top of the) were taken at the Manhattan site from 12 selected plots at four growth stages. 10 randomly chosen plants were measured with a meter stick in each plot and then averaged. A total of 48 CH measurements were taken in the growing season.

Image processing

Images from the MicaSense camera were uploaded and processed using ATLAS by MicaSense. Similar data from the Canon camera were processed at the KSU Precision Agriculture Laboratory as described in the following sections and Figure 3.1.

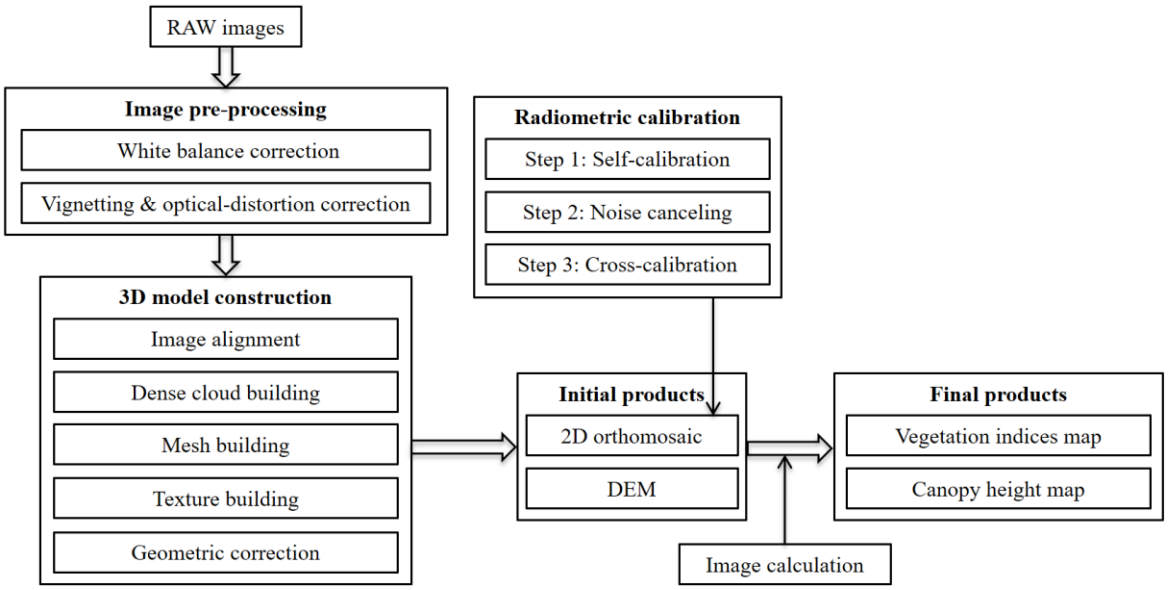

Figure 3.1 Image processing workflow for a CMOS sensor based modified Canon T4i CIR camera

Image pre-processing

POSs respond differently under variable sky conditions including clouds, changing solar zenith angle, pollution, and dust (Fitzgerald, 2010). Most of the CMOS sensor based commercial cameras are also prone to the vignetting effect, which reduces image brightness at the periphery (Lebourgeois et al. 2008; Hakala et al. 2010; Kelcey and Lucieer 2012). Lens distortion is another common problem within imaging systems (Hruska et al. 2012). To improve the results, each original image was corrected for white balance, vignetting, and optical distortion using the Adobe Photoshop Camera Raw 9.1.1.461 (Adobe Systems Inc, Mountain View, CA, USA) and

manufacture-provided lens profile data (Bowers 2002). As mentioned above, the lossless RAW file format was chosen to make this possible.

Orthomosaic and DSM (digital surface model) generation

Flight instability can introduce significant artifacts into the image illumination and geometry (Rango et al. 2009). Thus images are usually orthorectified to remove perspective and relief distortion and then stitched together to form a large orthomosaic that covers the whole area of interest. Agisoft PhotoScan Pro 1.2.6 (Agisoft LLC, St. Petersburg, Russia) was used to do the stitching with redundant images first being removed to ensure an even distribution of pictures across the field. Such evenness often yields a better orthomosaic (De Lussy 2005; Blaha 2013).

In addition, PhotoScan also generates DSMs. The first step in this process is aerial triangulation during which the true positions and orientations of the images are established. This entails automatically identifying a large number of tie points that are conjugate across multiple images. To optimize the photo positions and orientations, 36 ground control points (GCPs) were used for geometric correction (Hugenholtz et al. 2013). These GCPs were evenly distributed in the field and surveyed with a Topcon Hiper Lite + RTK (real time kinematic) GPS (global positioning system) unit (Topcon Co., Tokyo, Japan) with a map accuracy of 2 cm. After processing PhotoScan Pro exported the DSM in TIFF format.

Radiometric calibration method

POSs normally need radiometric calibration before quantitative analysis due to their lack of direct spectral reflectance measurements, which is the basis for most remote sensing applications in agriculture (Seelan 2003). If a sensor was uncalibrated and suffered from an unknown bias, it may be good for detecting the relative difference in crop condition but not good for quantifying the differences (Whitehead 2014). In fact, POSs data can be utilized as for quantitative analysis as long as an effective calibration procedure is performed on the imagery (Blockley et al. 2016). This section shows the newly developed “3-step radiometrically calibrate method” for POSs.

Step one: Self-calibration using a calibration panel

The purpose of step one is to provide cross-time and space comparison ability. A gray gradient calibration panel with nine shades of gray (5%, 20%, 30%, 40%, 50%, 60%, 70%, 80% and 90%) was generated by mixing flat black and white as described by Wang et al. (2015). True spectral reflectance for each gray level was measured by averaging 10 readings taken from different viewing angles using an ASD FieldSpec 3 spectroradiometer (Analytical Spectral Devices, Inc., Boulder, CO, USA). To build the calibration model, the mean Brightness Values (BVs) of the nine shades of gray were extracted and plotted against the spectral reflectance measurements mentioned above. Figure 3.2 shows an example of such calibration models for the Green, Red and NIR bands, respectively. After step one, POSs data from different locations and time can be compared.

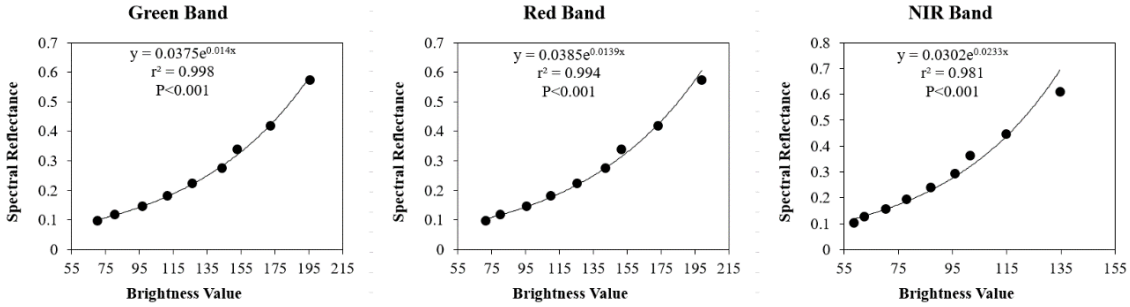

Figure 3.2 The relationship between CMOS sensor camera brightness values and spectral reflectance measurements for Green, Red and NIR bands.

Step Two: Noise canceling

Compared with the multispectral imager, the wavebands for CMOS sensor tend to be broader, with considerable overlap between all bands (Lebourgeois et al. 2008; Rump et al. 2011). The following plots (Figure 3.3) demonstrate three mixed bands for Canon T4i CIR camera (a.) and five discrete bands for MiceSense RedEdge multispectral camera (c.). For imaging sensors, the measured light radiation for each channel can be described as the integration of the camera's sensitivity over the spectral range (Blockley et al. 2016). This concept was used to do noise canceling by subtracting the noise from improper channels and then adding to the proper channel. For example, to correct the green channel for noise generated by the NIR light, a calibrated fraction of the latter's reading is subtracted from the former and then added to the NIR channel. Similar procedure was performed on the red channel. Figure 3.b. shows the Canon T4i CIR camera transmissivity after noise canceling.

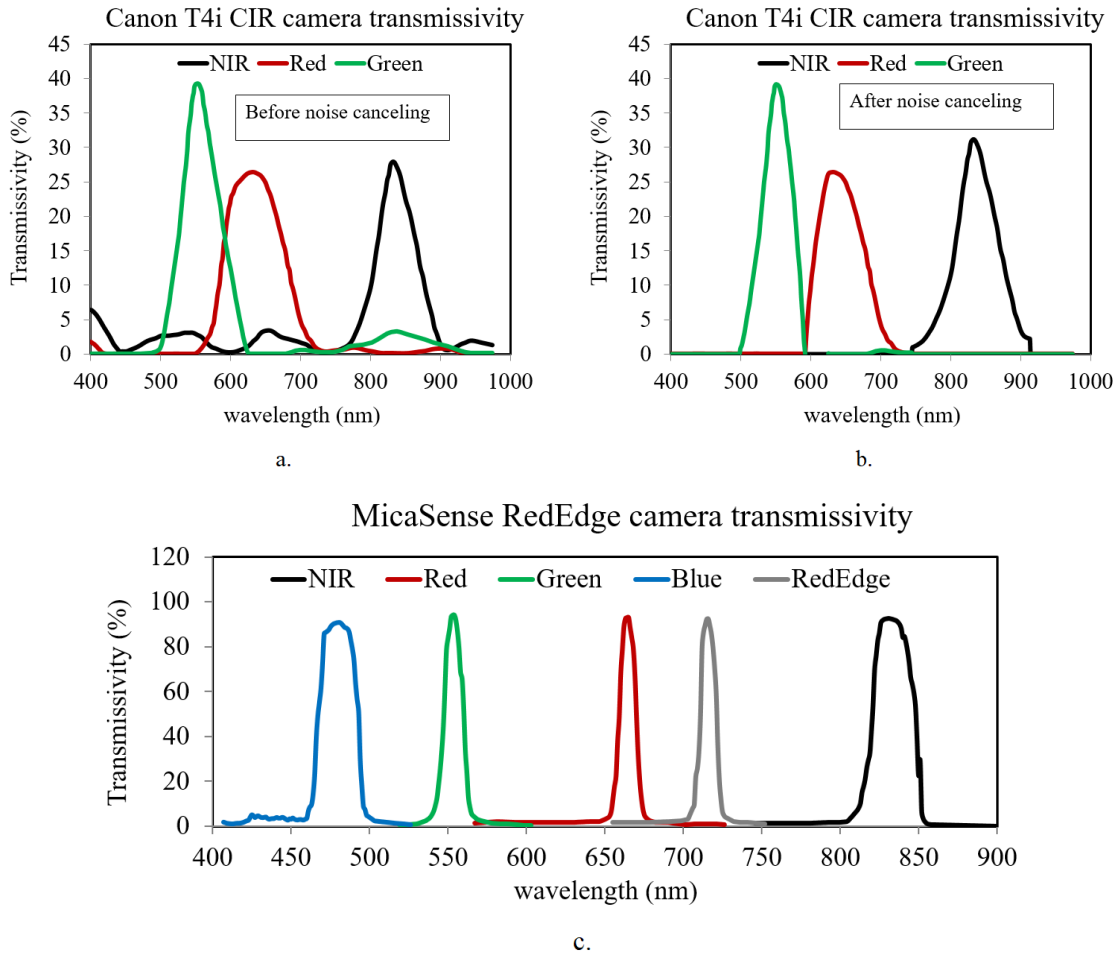

Figure 3.3 Spectral response of: a. Canon T4i CIR camera and b. MicaSense RedEdge multispectral imager (adopted from LDP LLC. and MicaSense Inc.). This is also an illustration for contaminated vs. clean bands.

Step Three: Cross-calibration

Imaging system differences in spectral sensitivities can have a significant impact on the vegetation index values, even with satellite systems (Trishchenko et al. 2002). The purpose of step three is to provide cross-sensor comparison ability.

To build the calibration model, a large set of AOS data were collected from 14 site-dates during the growing season covering high-to-low NDVI values. Only three data points from each site-date were used (the minimum, the mean, and the maximum). A total of 42 points were selected and regressed against corresponding data collected from the Canon camera that had been calibrated as described in step one and step two. Figure 3.4 demonstrates the highly correlated relationship

between AOS NDVI and POS NDVI, the linear regression model shown in the figure was then used to do the cross-calibration.

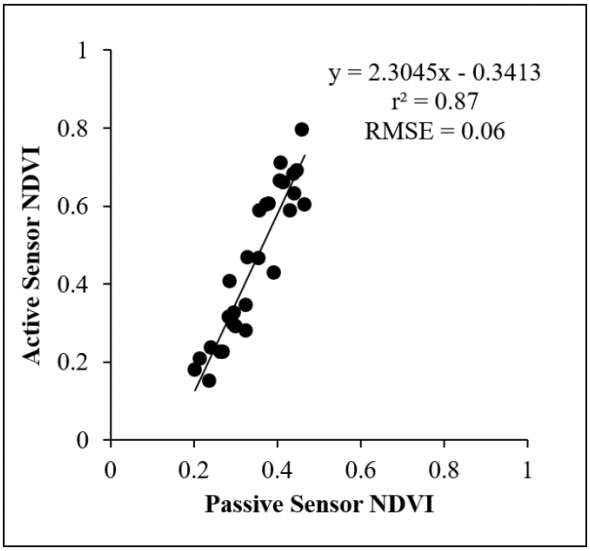

Figure 3.4 Scatter plots and regression of active and passive sensor produced NDVI.

Statistical analysis

The correlation and regression analyses were carried out in Microsoft® Excel® 2010 (Microsoft Co. Redmond, Washington, USA) and SAS® 9.3 PROC GLIMMIX procedure (SAS Institute Inc., Cary, North Carolina, USA). The plot mean NDVI obtained from the POSs and the AOS was evaluated against each other. The canopy height estimated by the DSM was evaluated against the ground truth measurement. These results are presented in scatter plots with linear regression equations. In-season biomass and grain yield were estimated or predicted using sensor VIs by building linear regression models. The model accuracy was measured with root mean square error (RMSE) and relative error (RE).

Results and discussion

Comparison of vegetation index from three different sensors

All three sensors have red and NIR bands, therefore, the NDVI was selected to be the VI during the comparison. As shown below, the NDVI map (Figure 3.5.a) generated from the Canon

T4i CIR images illustrates the huge variation in the field and within each plot. The NDVI map (Figure 3.5.b) generated from the MicaSense RedEdge images also shows a lot of variation in the field and within each plot. Although this imager has a lower spatial resolution compared to the Canon T4i (3.3 cm/pixel compared to 0.5 cm/pixel), there is, even more, variation showing on its NDVI map if one watches closely. The MicaSense RedEdge imager has five individual lenses so that it generates cleaner data at each waveband and thus provide wider dynamic range compared to the Canon camera. An NDVI table was exported from the RapidScan and converted into a colorized NDVI map (Figure 3.5.c) for better visual comparisons. The NDVI map from the RapidScan shows the same pattern of variation at the field level as the two POSs did, but does not show the difference within each plot. Because there was only one averaged NDVI value being assigned to the whole area of each plot. When taking either human-based or vehicle-based AOS data, the sensor passes the top of the canopy in a fraction of a second. Only a small portion of the canopy was sampled, the remaining area that did not get sampled may pose a challenge for calculating representative VI for the whole plot. However, this may not be an issue for real world crop production because the sensor sampling resolution is good enough to match the size of a management unit. The main issue is that there is still a good number of data points need to be taken to get a good and representative assessment of the whole field, which can be time-consuming.

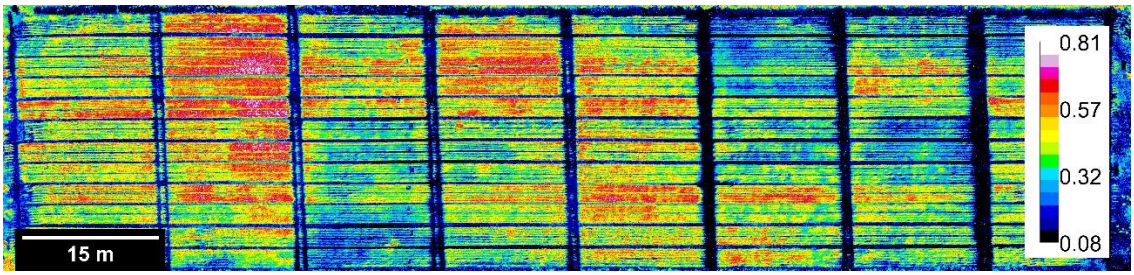

a.

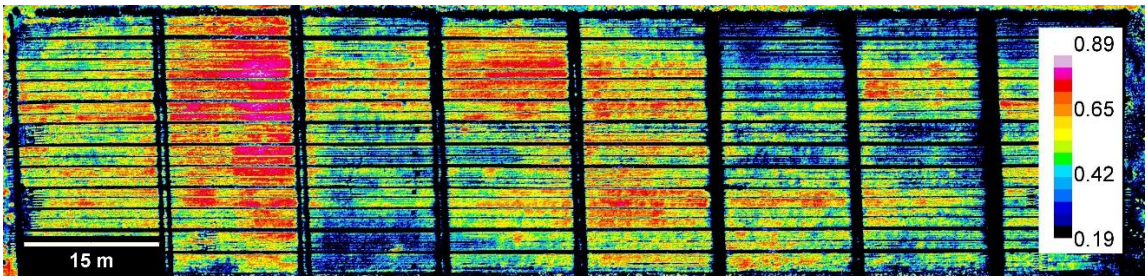

b.

0.43	0.65	0.4	0.47	0.4	0.33	0.33	0.32
0.45	0.65	0.5	0.61	0.53	0.38	0.44	0.34
0.47	0.71	0.5	0.6	0.55	0.4	0.53	0.38
0.49	0.68	0.52	0.64	0.57	0.37	0.57	0.41
0.58	0.69	0.46	0.53	0.56	0.44	0.4	0.51
0.5	0.59	0.42	0.45	0.58	0.45	0.39	0.44
0.45	0.62	0.34	0.38	0.44	0.35	0.34	0.45
0.5	0.59	0.42	0.46	0.53	0.46	0.45	0.56
0.47	0.62	0.4	0.5	0.6	0.61	0.54	0.5
0.47	0.52	0.37	0.48	0.62	0.48	0.48	0.48
0.4	0.5	0.3	0.39	0.45	0.51	0.41	0.41
0.46	0.52	0.33	0.41	0.56	0.55	0.46	0.47

c.

Figure 3.5 NDVI maps produced from three optical sensors: a. Canon T4i CIR camera b. MicaSense RedEdge multispectral imager and c. RapidScan CS-45 active optical sensor.

To get a better idea of the three sensors' relationships statistically, NDVI values from the Canon T4i and the MicaSense RedEdge were regressed against each other and then compared with RapidScan's NDVI. As shown below on the left in Figure 3.6, NDVI values from Canon T4i and RedEdge are highly correlated with a coefficient of determination (r^2) of 0.80 ($p<0.001$). These data points were collected from four key growth stages (F4, F7, F10, and F10.5) to cover high-to-low values. When the comparison was done at the individual stage, the r^2 value was even higher and could get high up to 0.98 at Feekes 10.5 ($p<0.001$). As shown on the right in Figure 3.6, the RapidScan NDVI values were highly correlated with Canon's and MicaSense RedEdge's NDVI values. In general, over 82% of the total variance in AOS data can be explained by the POS data. This suggested Canon T4i CIR and MicaSense RedEdge have the potentials to be used for crop assessment, just like AOS did, such as in-season biomass estimation and grain yield prediction (Hunt et al. 2010; Hunt et al, 2011; Laliberte et al. 2011).

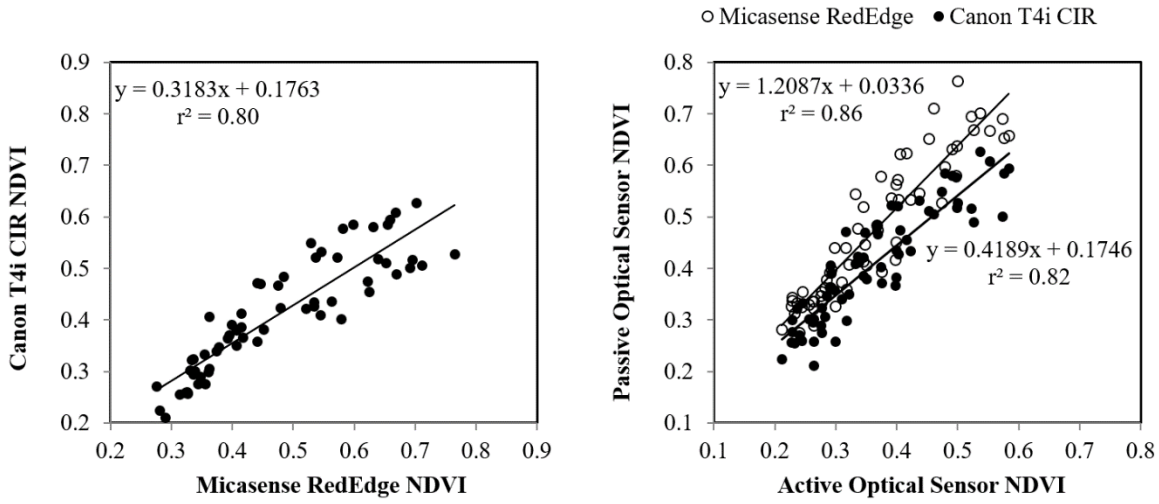

Figure 3.6 Winter wheat NDVI maps at Feekes 10 generated using three optical sensors. a. Canon T4i converted CIR camera. b. MicaSense RedEdge multispectral camera and c. RapidScan CS-45.

In-season biomass estimation and validation

One of the goals of this study is to estimate in-season biomass using sensor VIs and determine when the most accurate estimation is. Figure 3.7.a demonstrates the changes of correlations between sensor VIs and dry biomass across the growing season. From Feekes 3 (tiller formed) to Feekes 11.1 (milky ripe), VIs from both the Canon and the RedEdge consistently have a high correlation ($0.72<r^2<0.96$, all $p<0.001$) with the dry biomass in the same pattern. The correlations between the AOS VIs and the biomass were weak before Feekes 6 (first node) ($0.26<r^2<0.37$). At the earlier growing season, the soil was the dominate reflector (Tits 2013), and the sensor readings could be easily affected by the placement or the direction of the AOS (Barker 2013) (e.g.: AOS between the rows or on the row have different output, AOS parallel or crosswise with the rows have different output). The correlations had a huge jump after Feekes 6. As the plant grown taller and wider, the crop became the dominate reflector so the results suffered less impact from the soil and had higher correlations with the biomass(from Feekes 7 to 11.1, $0.47<r^2<0.75$, all $p<0.001$). After Feekes 11.1, all three sensors began picking up noises from structural components, such as spikes and some newly emerged weeds, which strongly influence spectral reflectance and impact the sensitivity of the VIs. This decreased the estimation accuracy at later growing season (Aparicio et al. 2002). Correlation between AOS VIs and biomass had a sudden decrease at Feekes 10.2 (heading), then came back up at flowering stage. This low point was

caused by the data collector instead of the sensor itself. During this data collection, the AOS was held incorrectly going parallel instead of crosswise with the sowing direction.

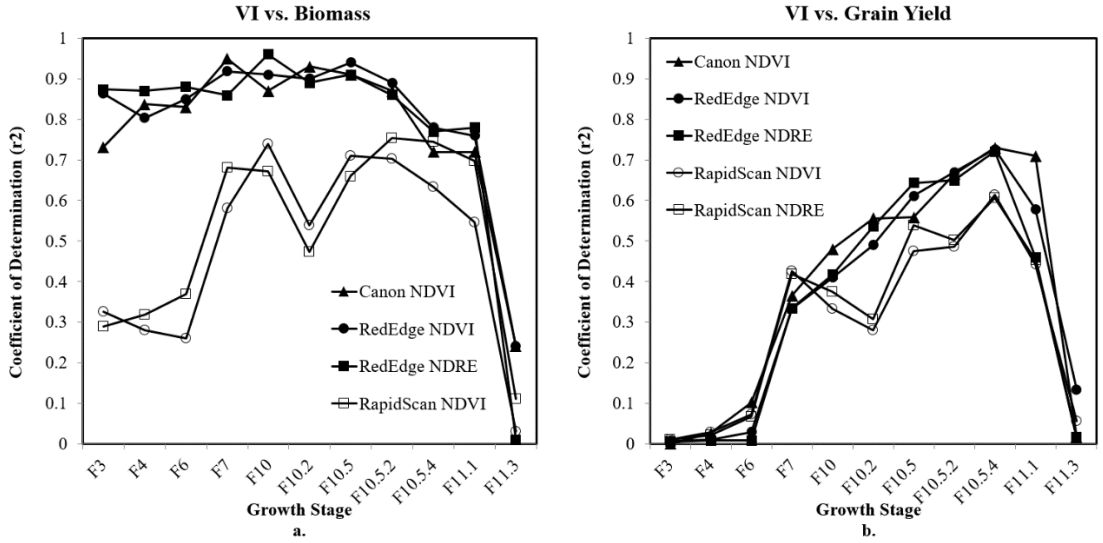

Figure 3.7 The change of relationships (in terms of coefficient of determination or r^2) between spectral indices and dry biomass and grain yield for winter wheat across the growing season 2015-2016.

Validations for in-season biomass estimation were conducted using half of the data points collected from Manhattan site (Table 3.3). In general, the two POSs outperformed the AOS at every growth stage (or had higher r^2 and smaller RMSE and RE values). Feekes 3 and Feekes 7 are the earliest stages for reliable biomass estimation using POSs VIs and AOS VIs, respectively. The most accurate estimation for all sensors is either at Feekes 10 or the stages immediately before/after it. At this growth stage, the head of winter wheat is visible but still in the leaf sheath below the flag leaf and winter wheat has the greenest and expanded leaves, thus has the most photosynthesis activities.

Table 3.3 Coefficients of determination (r^2) for the relationships between winter wheat dry biomass and spectral indices obtained from one active optical sensor (RapidScan) and two passive sensors (Canon T4i CIR camera, MicaSense RedEdge) at key growing stages.

Sensor / VI	Regression Model	n	r^2	RMSE (kg/m^2)	RE (%)
	Feekes 4				
Canon T4i CIR / NDVI	Biom=192.27*VI-18.221	12	0.84**	0.62	14.97
MicaSense RedEdge / NDVI	Biom=219.15*VI-39.679	12	0.80**	0.77	17.49
MicaSense RedEdge / NDRE	Biom=445.71*VI-43.965	12	0.87**	0.62	16.14
RapidScan CS-45 / NDVI	Biom=283.34*VI-34.017	12	0.32*	1.43	32.15
RapidScan CS-45 / NDRE	Biom=672.84*VI-36.605	12	0.28*	1.48	36.68
	Feekes 7				
Canon T4i CIR / NDVI	Biom=442.06*VI-81.21	12	0.95**	1.00	15.72
MicaSense RedEdge / NDVI	Biom=540.68*VI-145.31	12	0.92**	1.33	13.77
MicaSense RedEdge / NDRE	Biom=1064.2*VI-140.47	12	0.86**	1.75	12.41
RapidScan CS-45 / NDVI	Biom=698.36*VI-123.95	12	0.68**	2.64	33.71
RapidScan CS-45 / NDRE	Biom=1472.8*VI-91.79	12	0.58**	3.02	37.98
	Feekes 10				
Canon T4i CIR / NDVI	Biom=806.01*VI-205.37	12	0.87**	3.45	9.63
MicaSense RedEdge / NDVI	Biom=730.59*VI-250.01	12	0.91**	2.66	15.33
MicaSense RedEdge / NDRE	Biom=1085.7*VI-164.24	12	0.96**	1.73	17.52
RapidScan CS-45 / NDVI	Biom=1068.7*VI-220.92	12	0.67**	5.06	32.87
RapidScan CS-45 / NDRE	Biom=2881.4*VI-287.77	12	0.74**	4.51	33.78
	Feekes 10.5				
Canon T4i CIR / NDVI	Biom=1878.5*VI-732.38	12	0.91**	5.14	16.57
MicaSense RedEdge / NDVI	Biom=1299.3*VI-351.17	12	0.94**	3.40	12.83
MicaSense RedEdge / NDRE	Biom=1948.7*VI-239.22	12	0.91**	4.41	8.25
RapidScan CS-45 / NDVI	Biom=1294*VI-124.15	12	0.66**	9.52	20.55
RapidScan CS-45 / NDRE	Biom=3048*VI-122.33	12	0.71**	9.14	19.31
	Feekes 10.5.4				
Canon T4i CIR / NDVI	Biom=1831.8*VI-361.4	12	0.72**	11.32	11.28
MicaSense RedEdge / NDVI	Biom=1831*VI-436.41	12	0.78**	9.95	7.06
MicaSense RedEdge / NDRE	Biom=3104.8*VI-258.99	12	0.77**	10.02	9.88
RapidScan CS-45 / NDVI	Biom=3197.3*VI-745.6	12	0.75**	10.62	21.20
RapidScan CS-45 / NDRE	Biom=7416.6*VI-585.37	12	0.63**	12.74	19.59

*$p<0.01$,**$p<0.001$.

Another goal of this study is to predict grain yield using sensor VIs and determine how early grain yield can be accurately predicted. Figure 3.7.b demonstrates the changes of correlations between sensor VIs and grain yield across the growing season. Before Feekes 7, the three sensors performed similarly and were weakly correlated with grain yield. Because at the earlier growing season, yield factors had not been determined: tillers had not completely formed, tiller abortions might still occur due to N deficiency, head size and seed number had not been determined. At Feekes 7, all sensor VIs started to pick up a significant amount ($0.33<r^2<0.43$, all $p<0.01$) of variation in grain yield, which benefited from rapid vegetative growth and stem elongation at this phase. After Feekes 7, most of the yield factors had been determined. More and more variation in grain yield could be explained by sensor VIs. This makes sense because the closer to the end of the growing season the less uncertainty the grain yield will be if proper field practices were performed and the weather stayed normal. The highest r^2 values for all sensor VIs were obtained at Feekes 10.5.4 (kernels watery ripe, $0.61<r^2<0.73$, all $p<0.0001$). After Feekes 10.5.4, wheat started to ripe and water content decreased. Less green plant materials made the photosynthesis rate lower, which resulted in lower correlations between all sensor VIs and grain yield. The low correlation point at Feekes 10.2 was caused by the data collector who held the AOS incorrectly as described previously.

Validation for in-season grain yield prediction was conducted using half of the data points collected from all four study sites (Table 3.4). In general, all sensor VIs can be used as good predictors for grain yield as early as Feekes 7. The accuracy of prediction became more and more reliable towards the end of the growing season until Feekes 10.5.4. During this period, POS consistently outperformed AOS except at growth stage Feekes 7 where AOS performed slightly better than POSs. The most accurate yield prediction was made at the kernels ripe stage, however, there is not much value at this late stage for making effective management decisions.

Table 3.4 Coefficients of determination (r^2) for the relationships between winter wheat grain yield and spectral indices obtained from one active optical sensor (RapidScan) and two passive sensors (Canon T4i CIR camera, MicaSense RedEdge) at key growth stages.

Sensor / VI	Regression Model	n	r^2	RMSE (kg/m^2)	RE (%)
	Feekes 4				
Canon T4i CIR / NDVI	Yield=7.1464*VI+1.1068	114	0.03	0.82	27.13
MicaSense RedEdge / NDVI	Yield=1.8641*VI+2.4214	114	0.01	0.83	27.46
MicaSense RedEdge / NDRE	Yield=2.7867*VI+2.5356	114	0.01	0.83	27.51
RapidScan CS-45 / NDVI	Yield=4.8845*VI+1.7915	114	0.03	0.82	27.36
RapidScan CS-45 / NDRE	Yield=9.0801*VI+1.9937	114	0.02	0.82	27.54
	Feekes 7				
Canon T4i CIR / NDVI	Yield=16.019*VI-1.8291	114	0.37*	0.66	18.99
MicaSense RedEdge / NDVI	Yield=3.9257*VI+1.5175	114	0.33*	0.68	20.92
MicaSense RedEdge / NDRE	Yield=6.8109*VI+1.5724	114	0.33*	0.68	20.92
RapidScan CS-45 / NDVI	Yield=6.5479*VI+1.0512	114	0.43**	0.62	18.48
RapidScan CS-45 / NDRE	Yield=14.217*VI+1.2644	114	0.42**	0.63	18.58
	Feekes 10				
Canon T4i CIR / NDVI	Yield=19.701*VI-3.7549	114	0.41**	0.64	18.41
MicaSense RedEdge / NDVI	Yield=4.6298*VI+0.3139	114	0.35*	0.67	19.28
MicaSense RedEdge / NDRE	Yield=8.1034*VI+0.3133	114	0.42**	0.63	18.53
RapidScan CS-45 / NDVI	Yield=5.5391*VI+0.7194	114	0.33*	0.68	20.95
RapidScan CS-45 / NDRE	Yield=13.009*VI+0.5957	114	0.37*	0.66	20.09
	Feekes 10.5				
Canon T4i CIR / NDVI	Yield=19.787*VI-4.4103	114	0.57**	0.55	15.22
MicaSense RedEdge / NDVI	Yield=6.0034*VI-0.2665	114	0.61**	0.52	13.48
MicaSense RedEdge / NDRE	Yield=9.6869*VI-0.1037	114	0.64**	0.50	13.71
RapidScan CS-45 / NDVI	Yield=6.5394*VI+0.4755	114	0.48**	0.60	18.65
RapidScan CS-45 / NDRE	Yield=15.562*VI+0.053	114	0.54**	0.56	16.90
	Feekes 10.5.4				
Canon T4i CIR / NDVI	Yield=27.112*VI-6.4058	114	0.73**	0.43	13.07
MicaSense RedEdge / NDVI	Yield=8.944*VI-1.9999	114	0.73**	0.43	11.70
MicaSense RedEdge / NDRE	Yield=13.466*VI-0.7903	114	0.72**	0.44	12.20
RapidScan CS-45 / NDVI	Yield=9.0282*VI-0.9472	114	0.61**	0.52	14.48
RapidScan CS-45 / NDRE	Yield=20.077*VI-0.475	114	0.61**	0.52	14.78

*p<0.01,**p<0.001.

Compared to the AOS VIs, the POS VIs almost always had higher correlations with the biomass and grain yield during the growing season. The reasons are: (1) It is easy to take samples from an image simply by drawing a polygon at the region of interest (ROI) and easy to modify the ROI as one wants. On the contrary, the sampling area of an AOS can never be modified after the data collection; (2) It is hard to consistently place the AOS on the top of a crop row while passing through a wheat field; (3) In addition, it is important to keep the same distance between the AOS and the canopy, the irradiance at the photo-detector of the AOS is governed by the inverse square law which will cause a significant change in signal magnitude when the relative distance between sensor and target varies (Holland et al. 2012).

Literature suggested that suggested VIs using red edge wavelengths, such as NDRE, are more efficient than NDVI in identifying N variability in crops (Shiratsuchi et al., 2011; Feng et al. 2016; Rosa et al. 2016) and can be used for vegetation stress studies (Hruska et al. 2012). But in this wheat study, NDVI and NDRE, either from the MicaSense or the RapidScan, showed similar performance on biomass estimation and grain yield prediction. Another hypothesis raised was that NDRE may be more sensitive to varieties compared to NDVI. To test it, the NDVI and NDRE data from the Manhattan site were divided into four groups based on varieties, averaged, and their coefficient of variation (CV), also known as relative standard deviation (RSD), were calculated to measure the data dispersion. The results showed the CV or RSD from the NDVI data and the NDRE data are statistically same. This is true for both the RapidScan CS-45 and the MicaSense RedEdge multispectral imager.

Therefore, at least in this wheat study, under relative low LAI (leaf area index) conditions, there was no evidence to show that NDRE is more useful for crop assessment and more sensitive to varieties. This may not be true on other crops with higher LAI such as corn and grain sorghum. It is well known that NDVI often loses sensitivity after plants accumulate a critical level of leaf cover or chlorophyll content while NDRE does not. This is because the red-edge light is more translucent to leaves than red light and so it is less likely to be completely absorbed by a canopy. To get a better idea of the pros and cons for NDRE, more studies have to be conducted on other crops and applications to prove these inferences.

Canopy height (CH) estimation and validation

DSMs were generated using high-resolution images taken from the Canon T4i and the MicaSense RedEdge. Then the CH was estimated by subtracting the base DSM from the DSM at the specific growth stage. Figure 3.8 shows an example of CH map at Feekes 10 estimated with Canon T4i imagery. Since ground truth height measurements were only taken at the Manhattan site on four dates, only these four dates' CHs were estimated.

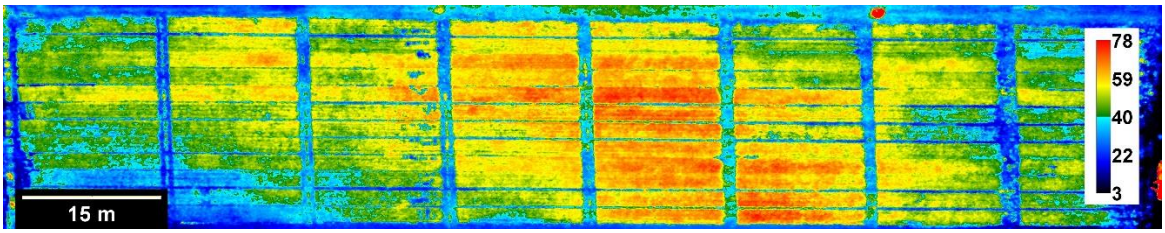

Figure 3.8 A canopy height map of winter wheat at Feekes 10 generated by subtracting base DSM from Feekes 10 DSM.

CH maps were then imported to ImageJ software for sampling and analysis. To avoid the edge effect, each plot was reduced by ~0.3 m on each end. Also, the areas where the destructive biomass sampling was performed were excluded. A total of 48 estimated CH values were extracted from the Canon CH maps and the MicaSense CH maps, respectively. They were then plotted against the observed CH as shown below in Figure 3.9.

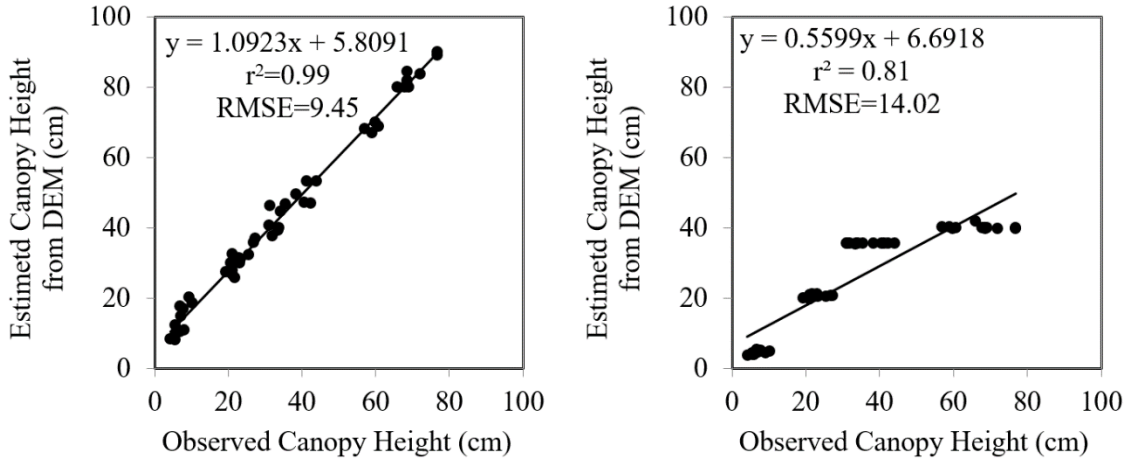

Figure 3.9 Comparisons between observed and estimated wheat canopy height generated from DEM derived from a. Canon T4i CIR camera and b. MicaSense RedEdge multispectral imager. Data were collected from Feekes growth stages: 4, 7, 10 and 10.5.

The results show that both Canon and MicaSense estimated CH were highly correlated with the observed CH (r^2=0.99 and 0.81, respectively), but the Canon has the higher correlation and more accurate estimation (RMSE=9.45 and 14.02 cm, respectively). This is mainly due to the smaller sensor on the MicaSense RedEdge and its coarse spatial resolution, which has less power to detect the height sub-difference compared to the Canon. Also, the RedEdge DSMs were downloaded from the imagery service ATLAS by MicaSense. The methodologies they employed to generate the DSM is unknown.

Although Canon provided more accurate CH estimation than RedEdge estimation, the accuracy (RMSE=9.45 cm) was still not good enough for winter wheat crop production and breeding programs where rapid and accurate phenotyping is required. In this study, the Canon DSMs were built without inertial measurement unit (IMU) data which can be used to optimize the position of point cloud during DSM construction and to improve the accuracy to ~3 cm (Nagai et al., 2004). Another way to improve the DSM accuracy is by integrating onboard RTK GPS to raw imagery data through the controlling computer on the sUAS. This method can offer centimeter level accuracy (Carbonneau & Dietrich, 2017).

In this study, the estimated CH represents the average CH of all pixels in the sampling area. Literature indicated that as a result, not only the top of the plant, for example, the head, was measured, but also the lower parts (Dendig et al.,2014), such as the leaves and even the soil, especially at the earlier growing season when the canopy is still not closed up and at the later growing season when most leaves shrank or dropped and the soil became more visible. Therefore, the CH would be over-estimated by using DSMs. Our estimated CHfrom Canon DSM (Figure 3.9. on the left) agreed with this statement.

Factors to be considered during sensor selection

Because the applications of sUAS have seen tremendous growth in recent years (Whitehead and Hugenholtz, 2014), more and more farmers and crop consultants have started to consider adopting this new technology as a decision-making tool for crop assessment and management. Among many questions they may ask, the first one is what platform and sensor I should use since there are so many options commercially available. To answer this question, this section will have complete comparisons of three types of sensors used in this study which can

provide some guidance for the sensor selection. The platform selection is not a goal for this study so it will not be discussed.

CMOS sensor cameras usually have excellent spatial resolution and affordable prices. Accurate 2D orthomosaics and DSMs can be generated with additional contextual information, such as ground control points. While CMOS sensors have a number of advantages, they lack direct spectral reflectance measurements from where the remotes sensing analysis starts. This is also a shortage for multispectral imager since both of them are passive sensors. Also, the dynamic range of such cameras is also limited for spectral analysis (Hardin and Jensen 2011). However, as effective radiometric calibration methods are being developed like the one described in this study, the brightness values from the passive sensors can be converted to reflectance and can be compared crossing time, space and sensors. Also, the trade-off between spatial resolution and processing time should be noted. The image processing time increases dramatically with image resolution, but too low of a resolution limits the ability to differentiate details such as texture. It is important for the data collectors to optimizing path planning and sensing strategies to minimize data redundancy and processing time.

The advantage of the multispectral imagers is the quality of the spectral measurements. While CMOS sensors have broadband and mixed spectral response, multispectral imagers are capable of measuring discrete spectrum at the specific range like the one used in this study, MicaSense RedEdge. Although the effective pixel number for multispectral imager is far less than CMOS cameras, it is still good enough for crop production and also good for research if the altitude is set properly. DSMs generated from multispectral imager are also useful to some extent. In the past, payload capacity has been a restriction for sUAS to carry heavier cameras like multispectral or hyperspectral sensors, but the newly released high-end sensor systems are getting lighter, more compact and more user-friendly, which provides more opportunities in sUAS-based remote sensing applications compared to CMOS based cameras. The price for multispectral cameras, however, are normally higher than CMOS sensor based cameras that normally including camera body, lens and modification costs) (e.g.: MicaSense RedEdge, $5900; Canon T4i NIR/Red/Green, $1325).

There are plenty of advantages of the use of POSs, however, two of the major requirements for POSs are 1) radiometric calibration and 2) image processing. Since AOSs are using the internal light source, no additional calibration is needed and can be used under any weather condition and

anytime during the day while POSs data need to be collected within two hours of the solar noon for optimum performance. Image processing is also not required for AOSs since they output spectral reflectance and VI directly and usually can be exported to a spreadsheet. POSs require highly skilled experts or imagery service companies to do image processing and analysis, which can be time-consuming (e.g.: MicaSense RedEdge, 24 h (using ATLAS imagery service); Canon T4i CIR, 4 h (less than 300 RAW images)). However, POSs saves time during data collection while AOSs takes a good time to get a representative assessment of the whole field, whether the sensor is human-based or vehicle-based. At the same time, use of sUAS mounted POSs are nondestructive to the field while the use of AOSs can be destructive at the middle-late growing season for wheat and may cause soil compaction if the AOSs are mounted on vehicles.

Conclusions

Comparing one active optical sensor and two passive optical sensors, the winter wheat in-season biomass could be estimated by CMOS sensor based camera and Multispectral imager from Feekes 3 (tiller formed) to Feekes 11.1 (milky ripe), and by the active optical sensor from Feekes 7 to Feekes 11.1. The VIs based estimations provided by CMOS sensor camera and multispectral imager were more powerful and more temporally stable than the active optical sensor. The most accurate estimations were obtained at booting stage for all three sensors.

The winter wheat grain yield could be predicted from Feekes 7 to Feekes 11.1 by all three optical sensors. Consequently, Feekes 7 was the earliest time for reliable grain yield prediction. This is because that most of the yield components had been determined such as head size and seed number and the only thing left in the growing season is the grain filling. The VIs based grain yield predictions using the CMOS sensor based camera and the multispectral imager were more powerful and more temporally stable than the active optical sensor except Feekes 7 where AOS outperformed POSs slightly.

There was no significant difference between CMOS sensor based camera and multispectral imager on in-season biomass estimation and grain yield prediction. No evidence of any advantage or difference of NDRE was found compared to NDVI when they were used for biomass estimation and yield prediction in winter wheat.

The canopy height could be estimated by the CMOS sensor camera and the multispectral imager when high precision GCPs were used. The CMOS sensor based camera generated better

DSMs mainly due to the higher sensor resolution. DSMs accuracy could be improved by feeding the raw imagery data with IMU data and onboard RTK GPS data.

Active optical sensors can be used more freely with the change of light conditions and time of day, and use of AOS does not require radiometric calibration and data processing that passive sensors need. However, passive optical sensors are more efficient for large scale data collection like in crop production and breeding program and the data require no interpolation, which is usually performed in AOS data during analysis. Also, passive sensors currently have more bands which provides possibilities for different applications in precision agriculture. It is always good to be clear about the purpose of the application and the budget situation before selecting sensors.

Future work is needed to conducted on other crops to validate the estimation and prediction methods. The three-step radiometric calibration for CMOS sensors cameras is sensor specific so it needs to be tested on other sensors to test the cross-sensor comparison ability. Also, lack of standardized processing procedures including data collection protocol, image calibration, and processing methods can limit information exchange in the community and slow down the development of optical sensor based crop assessment in precision agriculture. We believe, with more effort put by farmers, researchers and industry together, precision agriculture today will be normal agriculture tomorrow.

Acknowledgements

This work was supported by the Kansas State University, Department of Agronomy and did not receive any other specific grant from funding agencies in the public, commercial, or not-for-profit sectors.

References

Alexandratos, N. (2009). World food and agriculture to 2030/50. Highlights and views from mid.

Aparicio, N., Villegas, D., Araus, J.L., Casadesus, J., Royo, C., 2002. Relationship between growth traits and spectral vegetation indices in durum wheat. Crop Sci. 42, 1547–1555

Barker, D. W., & Sawyer, J. E. (2013). Factors affecting active canopy sensor performance and reflectance measurements. Soil Science Society of America Journal, 77(5), 1673-1683.

Bendig, J., Bolten, A., Bennertz, S., Broscheit, J., Eichfuss, S., & Bareth, G. (2014). Estimating biomass of barley using crop surface models (CSMs) derived from UAV-based RGB imaging. Remote Sensing, 6(11), 10395-10412.

Bláha, M., Eisenbeiss, H., Sauerbier, M., & Grün, A. (2013). Photogrammetric Modeling of Drapham Dzong (Buthan).

Blockley, R., & Shyy, W. (2016). Unmanned Aircraft Systems. E. Atkins, A. Ollero, & A. Tsourdos (Eds.). John Wiley & Sons.

Bowers, C. M., & Johansen, R. J. (2002). Photographic evidence protocol: the use of digital imaging methods to rectify angular distortion and create life size reproductions of bite mark evidence. Journal of Forensic Science, 47(1), 178-185.

Campbell, J. B., & Wynne, R. H. (2011). Introduction to remote sensing. Guilford Press.

Carbonneau, P. E., & Dietrich, J. T. (2017). Cost-effective non-metric photogrammetry from consumer-grade sUAS: implications for direct georeferencing of structure from motion photogrammetry. Earth Surface Processes and Landforms, 42(3), 473-486.

De Lussy, F., Kubik, P., Greslou, D., Pascal, V., Gigord, P., & Cantou, J. P. (2005, May). PLEIADES-HR image system products and quality-PLEIADES-HR image system products and geometric accuracy. In Proceedings of the international society for photogrammetry and remote sensing workshop.

De Rosa, D., Rowlings, D., Biala, J., Scheer, C., Basso, B., Migliorati, M. D. A., & Grace, P. R. (2016). Monitoring the N release from organic amendments using proximal sensing.

DESA, U. (2015). World population prospects: The 2015 revision, key findings and advance tables. Working PaperNo.

Feng, W., Zhang, H. Y., Zhang, Y. S., Qi, S. L., Heng, Y. R., Guo, B. B., ... & Guo, T. C. (2016). Remote detection of canopy leaf nitrogen concentration in winter wheat by using water resistance vegetation indices from in-situ hyperspectral data. Field Crops Research, 198, 238-246.

Fitzgerald, G. J. (2010). Characterizing vegetation indices derived from active and passive sensors. International Journal of Remote Sensing, 31(16), 4335-4348.

Harrell, D. L., Tubana, B. S., Walker, T. W., & Phillips, S. B. (2011). Estimating rice grain yield potential using normalized difference vegetation index. Agronomy Journal, 103(6), 1717-1723.

Hardin, P.J., and Jensen, R.R. 2011. Small-scale unmanned aerial vehicles in environmental remote sensing: challenges and opportunities. GIScience & Remote Sensing. 48(1): 99–111

Hugenholtz, C.H., Whitehead, K., Barchyn, T.E., Brown, O.W., Moorman, B.J., LeClair, A., Hamilton, T., and Riddell, K. 2013. Geomor- phological mapping with a small unmanned aircraft system (sUAS): feature detection and accuracy assessment of a photogram-metrically-derived digital terrain model. Geomorphology. 194:16–24. doi: 10.1016/j.geomorph.2013.03.023

Holland, K.H., Lamb, D. W.,& Schepers, J.S., 2012. Radiometry of Proximal Active Optical Sensors (AOS) for Agricultural Sensing. IEEE Journal of Selected Topics in Applied Earth Observations and Remote Sensing,Vol 5, No. 6

Hruska, R., Mitchell, J., Anderson, M., and Glenn, N.F. 2012. Radiometric and geometric analysis of hyperspectral imagery acquired from an unmanned aerial vehicle. Remote Sens. 4(9): 2736–2752. doi: 10.3390/rs4092736

Hunt, E. R., Hively, W. D., Fujikawa, S. J., Linden, D. S., Daughtry, C. S., & McCarty, G. W. (2010). Acquisition of NIR-green-blue digital photographs from unmanned aircraft for crop monitoring. Remote Sensing, 2(1), 290-305.

Hunt, E. R., Hively, W. D., McCarty, G. W., Daughtry, C. S. T., Forrestal, P. J., Kratochvil, R. J., ... & Miller, C. D. (2011). NIR-green-blue high-resolution digital images for assessment of winter cover crop biomass. GIScience & remote sensing, 48(1), 86-98.

Idso, S. B., Jackson, R. D., & Reginato, R. J. (1977). Remote-sensing of crop yields. Science, 196(4285), 19-25.

Idso, S. B., Pinter, P. J., Jackson, R. D., & Reginato, R. J. (1980). Estimation of grain yields by remote sensing of crop senescence rates. Remote sensing of Environment, 9(1), 87-91.

Laliberte, A. S., & Rango, A. (2011). Image processing and classification procedures for analysis of sub-decimeter imagery acquired with an unmanned aircraft over arid rangelands. GIScience & Remote Sensing, 48(1), 4-23.

Laliberte, A. S., Winters, C., & Rango, A. (2011). UAS remote sensing missions for rangeland applications. Geocarto International, 26(2), 141-156.

Lamb, D. W., Frazier, P., & Adams, P. (2008). Improving pathways to adoption: Putting the right P's in precision agriculture. Computers and Electronics in Agriculture, 61(1), 4-9.

Lamb, D. W., Steyn-Ross, M., Schaare, P., Hanna, M. M., Silvester, W., & Steyn-Ross, A. (2002). Estimating leaf nitrogen concentration in ryegrass (Lolium spp.) pasture using the

chlorophyll red-edge: theoretical modelling and experimental observations. International Journal of Remote Sensing, 23(18), 3619-3648.

Lebourgeois, V., Bégué, A., Labbé, S., Mallavan, B., Prévot, L., and Roux, B. 2008. Can commercial digital cameras be used as multi- spectral sensors? A crop monitoring test. Sensors. 8(11): 7300–7322. doi: 10.3390/s8117300

MacDonald, R. B., & Hall, F. G. (1980). Global crop forecasting. Science, 208(4445), 670-679.

Miller, N., Griffin, T., Bergtold, J., Sharda, A., & Ciampitti, I. (2017). Adoption of Precision Agriculture Technology Bundles on Kansas Farms.

Nagai, M., Shibasaki, R., Manandhar, D., & Zhao, H. (2004, July). Development of digital surface model and feature extraction by integrating laser scanner and CCD sensor with IMU. In Proceedings of the ISPRS Congress, Geo-Imagery Bridging Continents.

Rango, A.; Laliberte, A.; Herrick, J.E.; Winters, C.; Havstad, K.; Steele, C.; Browning, D. Unmanned aerial vehicle-based remote sensing for rangeland assessment, monitoring, and management. J. Appl. Remote Sens. 2009, 3, 033542

Ray, T. W. (1994). A FAQ on vegetation in remote sensing. California: Div. of Geological and Planetary Sciences California Institute of Technology.

Rump, M., Zinke, A., and Klein, R. 2011. Practical spectral characterization of trichromatic cameras. ACM Transactions on Graphics (TOG) – Proceedings of ACM SIGGRAPH Asia 2011. doi: 10.1145/2070781.2024204.

Seelan, S. K., Laguette, S., Casady, G. M., & Seielstad, G. A. (2003). Remote sensing applications for precision agriculture: A learning community approach. Remote Sensing of Environment, 88(1), 157-169.

Tits, L., Somers, B., Stuckens, J., Farifteh, J., & Coppin, P. (2013). Integration of in situ measured soil status and remotely sensed hyperspectral data to improve plant production system monitoring: Concept, perspectives and limitations. Remote Sensing of Environment, 128, 197-211.

Trishchenko, A. P., Cihlar, J., & Li, Z. (2002). Effects of spectral response function on surface reflectance and NDVI measured with moderate resolution satellite sensors. Remote Sensing of Environment, 81(1), 1-18.

Vossen, P., & Meyer-Roux, J. (1995). 1.1. CROP MONITORING AND YIELD FORECASTING ACTIVITIES OF THE MARS PROJECT. INSTITUTE FOR REMOTE SENSING APPLICATIONS.

Wang, Chuyuan, et al. "A simplified empirical line calibration method for sUAS-based remote sensing." Red 590 (2015): 680.

Zhang, C., & Kovacs, J. M. (2012). The application of small unmanned aerial systems for precision agriculture: a review. Precision agriculture, 13(6), 693-712.

Zhang, N., Wang, M., & Wang, N. (2002). Precision agriculture—a worldwide overview. Computers and electronics in agriculture, 36(2), 113-132.

Chapter 4 - Integrating Phenology Model into Hi-res Imagery Based Wheat Biomass Estimation

Introduction

Nitrogen is well documented as a limiting nutrient in crop production and is considered one of the best producer inputs to increase profitability under an appropriate management system (Teal et al., 2006). However, according to Raun & Johnson (1999), Nitrogen use efficiency (NUE) has been relatively low throughout the world. On average, only 33% of the total N fertilizer applied for cereal production in the world is taken up and used by the crop. Low NUE can result in increased fertilizer cost, lower profits, and increased environmental impact (Asebedo, 2015). Improved N management is essential to maintain producers' income and diminish environmental degradation (Teal et al., 2006).

"Right Time" and "Right Rate" are two of the fundamental pieces of the 4-R N management principles and emphasizes the synchrony between amount of N demand and the time of N application is essential for improving NUE (Robert, 2007).

In order to figure out when is the "Right Time", we should first understand the four components to determine winter wheat grain yield (Miller, 1992). The first component is number of heads per plant, which is determined by seeding rate and tiller formation. Tillering occurs from Feekes 2 through 4 and N applications during these stages can have a positive impact on the number of tillers formed, thus generating more heads per plant and a larger grain yield potential. N stress during Feekes 2 through 4 can result in a reduction in head numbers, which cannot be corrected with an N application after Feekes 4 (Asebedo, 2015). The second component, the size of each head, is determined at Feekes 5. Preventing N stress at this growth

stage will maximize head size and seed number and will increase potential grain yield capacity. Once Feekes 5 has passed head size will be fixed, N applications after this stage will not have an impact on head size, therefore permanent reductions in grain yield capacity may occur. The third and fourth components are number of seeds per head and the size of each seed which is determined from Feekes 10 through 11. By maintaining N sufficiency during these growth stages, a greater number of seed will be set and filled if given good growing conditions. With an understanding of the four components determining winter wheat grain yield, it is clear that preventing N stress during the Feekes growth stages previously described is important. According to Waldren & Flowerday (1979), winter wheat' N uptake is most rapid from tillering through booting stages, with 80% of the total accumulation occurring before grain fill. Therefore, winter wheat will acquire most of its N from Feekes 3 through Feekes 9 (Asebedo, 2015).

Applying different rates of N according to the N and productivity levels has been a popular way of nitrogen management (Raun et al., 2002). The above ground biomass can be considered as an indicator of productivity and can be estimated using Normalized Difference Vegetation Index (NDVI) in a nondestructive way by taking spectral measurements remotely (Raun et al., 2002). Currently, there are several methods available to identify in-field productivity variability. Using a vehicle-based active sensor is often labor intensive, inefficient, and destructive to the crop (Wang et al., 2017). Remotely sensed imagery can also provide important information about N and productivity in crop (Goel et al., 2003; Cho et al., 2007; Huang et al., 2007). Although very promising, imagery acquired by aircraft or satellite has some limitations such as the low spatial resolution, low temporal resolution, and the cloud influence (Myers et al., 2015). To fill this gap, the use of unmanned aircraft system (UAS) for various agricultural applications has soared over the last decade because of their potential to be a low-

cost, accessible, and practical substitute for satellite and civil aircraft for high resolution and remotely sensed data (Myers et al., 2016). Although UAS provide the flexibility to select the date for data collection, it is not feasible to fly it too frequently such as on a weekly basis on a median/large size farm. It would be ideal to scout the field only at the key growth stages to save the unnecessary field trips. Thus the ultimate question will be how to optimize the date for imagery collection, get on-time biomass variability scouting, and get ready for a N application at the key growth stage.

Therefore, the objectives of this study are: (1) to develop high frequent in-season biomass estimation models using UAS imagery; (2) to develop a wheat phenology model to predict the starting date of three key growth stages (F4, F7, and F9); (3) to combine the results from (1) and (2) to predict biomass variability on new data.

Materials and Methods

Biomass Estimation

Site Description

Winter wheat was planted for the 2014-2015, 2015-2016 crop year at the Kansas State University Agronomy Ashland Bottoms research farm located to the south of Manhattan, KS. An experiment was established on a lowland flat soil position (39.137615 ° Lat, -96.640046 ° Lon). The soil is classified as a Belvue silt loam with a sudden increase in sand content within the first 25 cm of the soil surface (Web Soil Survey, 2017). This high sand subsoil results in the field having good drainage ability and low available water holding capacity, which can make some winter wheat vulnerable to drought stress under dry conditions.

Experiment Design

Small plots with size of 3 m x 15 m were arranged in a randomized complete block design (RCBD) with stripped block with three replications. Within each block four hybrids (Everest, Jagger, Karl 192, and 1863) of wheat were planted as main treatments and four rates of N were applied at growth stage of Feekes 4 as sub-treatments (0, 56, 112 and 168 kg/). The total number of plots is 96 (4 hybrids x 4 rates x 2 replications within block x 3 blocks).

Image Data

The imagery was collected by a converted Canon T4i DSLR camera (Canon® Inc, Tokyo, Japan). The modification was done by removing the infrared filter to record NIR (modification was done by LDP LLC, Carlstadt, NJ, USA). A blue notch filter was then installed to block only visible blue on the blue channel while still allowing the NIR wavelength to be measured. After modification, this camera can record Red, Green, and Blue lights. The detailed specification was summarized in the Table 4.1. The camera was flown at solar noon at 60 m above ground level by a DJI s800 evo hexacopter (DJI® Science and Technology, Co., Ltd. Shengzhen, China) with a gimbal to maintain nadir camera position during the flights. All imagery data was recorded in RAW format which provides capability to do image corrections before analysis. The camera was triggered every two seconds with an intervalometer device (DigiSnap 2000 by Harbortronics®). The flight path was programmed with 80% overlap (side and forward) and was repeatedly used for all imagery collections at different growth stages: 3, 4, 6, 7, 9, 10.2, 10.5, 10.5.2, 10.5.4, 11.1, 11.3. All UAV operations was performed under the Certificate of Authorization (COA number: 2015-CSA-6-COA-R).

Table 4.1 Specifications of the converted Canon T4i CIR camera used in this study.

Effective pixels (megapixels)	Ground Sample Distance (cm/pixel)	Bandwidth (nm)	Peak wavelength (nm)
18	0.5	Green: 60 Red: 90 NIR: 60	Green: 552 Red: 638 NIR: 833

Images exported from the camera were uploaded to the computer and processed using the workflow described by Wang et al. (2017) as shown in Figure 4.1. Normalized Difference Vegetation Index (NDVI) maps were generated which was then used to extract NDVI values and build empirical model for wheat biomass estimation.

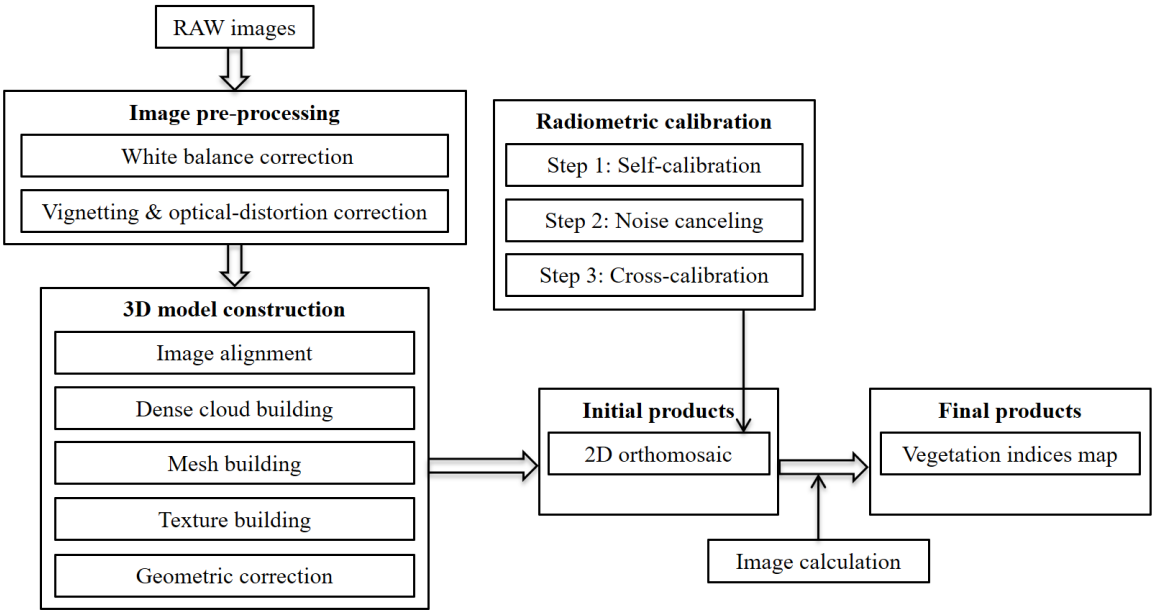

Figure 4.1 Image processing workflow for a CMOS sensor based converted Canon T4i CIR camera

Biomass Data

For biomass data collection, twenty-four plots covering the biomass gradient from high to low were selected as sampling plots. A Japanese sickle was used to cut a 0.5 m x 0.5 m area from

each sampling plot. The fresh biomass was put into paper bags, immediately weighed after taring, and oven dried at 70°C to constant weight for dry biomass data.

Biomass Estimation

For biomass estimation, the multi-temporal NDVI and biomass data from 2014-2015 season were divided into training and validation datasets. Linear regression models were derived for NDVI vs. dry biomass using the training data and evaluated by their coefficient of determination (r^2). The resulting regression models were applied to the validation datasets and analyzed by linear correlation between prediction and observed biomass measurement. The results are compared based on the root mean square error (RMSE) and relative error (RE).

Wheat Phenology Model:

There are many crop simulation models that can predict the phenological stages of winter wheat such as the wheat model in model systems: APES, CROPSYST, DAISY, DSSAT, FASSET, HERMES, STICS and WOFOST with different accuracies. The details of these models can be obtained from the references gathered by Palosuo et al. (2011). These mechanistic models typically consider the processes of plant development and describe instantaneous rates of plant processes that change rapidly over short time scale. However, a relative large amount of input information is required to run such a model. For example, the wheat model in DSAAT requires a series of soil data such as water holding capacity, depth to bottoms layer, bulk density, pH value, etc. and a series of management data such as emergence date, plant population at emergence, etc., which are not easy to gather in crop production. Thus, building a phenology model with minimum amount of input is our goal.

This wheat phenology model is based on weather data and some field contextual information that can be easily obtained. The goal is to predict the starting date of a certain

growth stage without going to the field and taking any additional field measurements. To be specific, the target growth stages are F4, F7, and F9 whose importance on determining crop yield and quality have been discussed in the introduction. Once the F4/F7/F9 dates were determined, the UAV imagery collection can be performed accordingly and the right model coefficients can be plugged to estimate the wheat biomass. The data source and the process for this phenology model was described below:

Site Description

The data used for the wheat phenology model were from 21 site-year of wheat experiments including research plot experiments and on-farm experiments. All the study sites and their contextual information were summarized in Table 4.2.

Table 4.2 Study sites and their contextual information.

Year	Site	Lat	Long	Variety/Hybrids	Soil Type	Sowing Date	F4 Starting Date	F7 Starting Date	F9 Starting Date
2017	AshlandBottoms	39.145486	-96.633281	1863	Belve Silt Loam	20161101	20170308	20170410	20170420
2017	Belleville	39.815155	-97.673867	Everest	Crete Silt Loam	20161003	20170301	20170414	20170421
2017	NorthFarm	39.213613	-96.593230	1863	Reading Silt Loam	20161104	2017317	20170407	20170420
2017	Salina	38.740553	-97.611120	Everest	Roxbury Silt Loam	20160926	20170302	20170405	20170415
2017	Solomon	38.871475	-97.434555	WB 4458	McCook Silt Loam	20160922	20170308	20170409	20170420
2016	Ashland Bottoms	39.137615	-96.640046	Everest	Belvue Silt Loam	20151103	20160316	20160405	20160415
2016	Clifton	39.554647	-97.236159	WB grainfield	Crete Silty Clay Loam	20151013	20160313	20160414	20160424
2016	ValleyCenter	37.874093	-97.244777	Everest	Gossel Silty Clay Loam	20151013	20160225	20160401	N/A
2016	Victoria	38.910426	-99.201224	TAM 111	Harney Silt Loam	20150930	20160312	20160407	N/A
2016	SmithCenter	39.771420	-98.906700	Everest	Holdrege Silt Loam	20151105	20160304	20160407	20160423
2016	Gypsum	38.710340	-97.439077	Everest	Hord Silt Loam	20151006	20160305	20160410	20160423
2016	Minneapolis	39.183623	-97.727988	Everest	Solomon Silt Clay	20151006	20160305	20160411	20160425
2015	Ashland Bottoms	39.137615	-96.640046	Everest	Belvue Silt Loam	20151112	20150421	20150427	20150505
2014	Manhattan	39.211828	-96.596908	Everest	Reading Silt Loam	20131017	20140306	20140401	20140501
2013	Solomon	38.833269	-97.355152	Armour	McCook Silt Loam	20121024	20130319	20130421	20130504
2013	Manhattan	39.212153	-96.598840	Everest	Reading Silt Loam	20121023	20130328	20130424	20130505
2013	Partridge	37.961222	-98.123249	Everest	Trver Loam	20120108	20130315	20130419	20130506
2013	Pittsburg	37.394278	-95.015905	Pioneer 25R78	Parson Silt Loam	20121025	20130221	20130416	20130505
2013	McCun	37.368732	-95.047313	Pioneer 25R30	Cherokee Silt Loam	20121013	20130220	20130416	20130505
2012	Gypsum	38.704400	-97.445073	Armour	Hord Silt Loam	20111014	20120318	20120402	20120409
2012	Manhattan	39.211828	-96.596908	Everest	Reading Silt Loam	20111015	20120307	20120324	20120405

Weather Data

The daily maximum air temperature (Tmax), minimum air temperature (Tmin), precipitation (PPT) for the 21 site-years were obtained from the nearest agrometeorological stations that can be retrieved from the Kansas Mesonet site at http://mesonet.k-

state.edu/weather/historical/ and www.mesonet.org. The weather data for the sites that are far away from weather stations were interpolated using inverse distance weighting (IDW) method, by weighting longitude and latitude. There are some other weather variables that are important to crop growth such as solar radiation, relative humidity, but they were not included due to the unavailability at some of the study sites.

Ground Truth Data

The ground truth data included the planting date and the starting dates of the key phenological growth stages (F4, F7, and F9). The data were summarized in the Table 3. The ground truth data will be used to calibrate and validate the phenology model.

Model presentation

The phenology model workflow from input through output is shown in Figure 4.2. The key components are described in detail in the following sections.

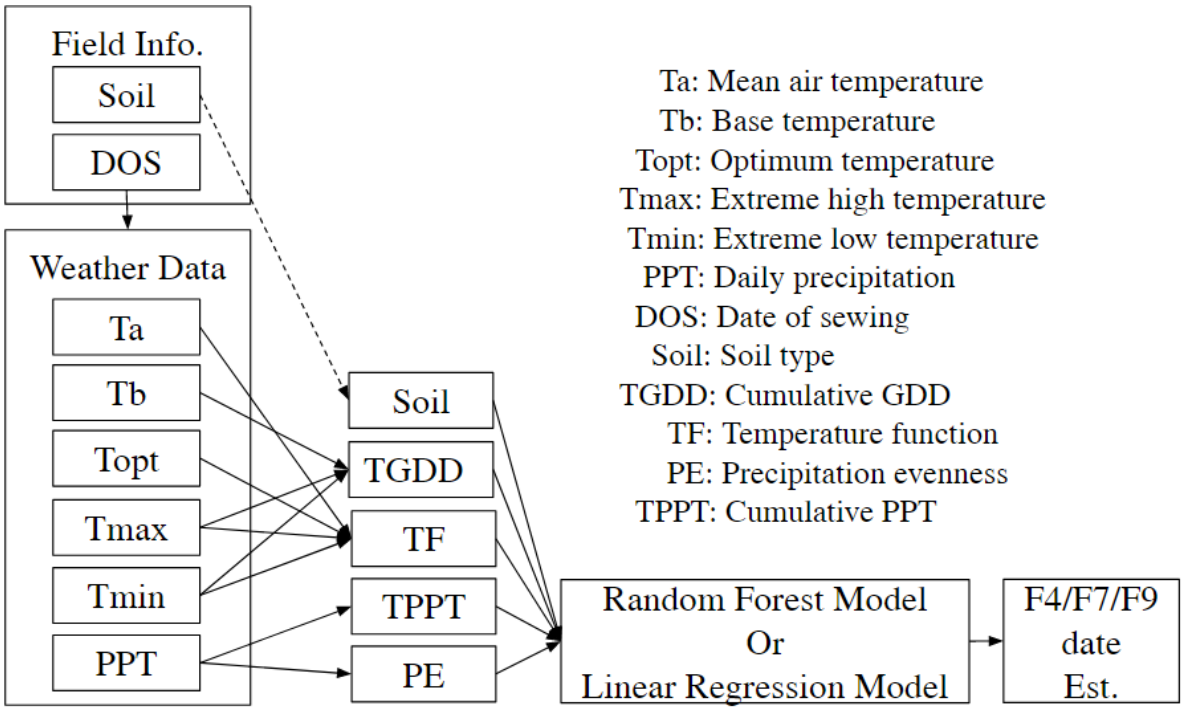

Figure 4.2 Workflow for a wheat phenology model for F4 starting date estimation

TGDD (Cumulative Grow Degree Day):

Temperature or heat units are called growing degree days (GDD) and are calculated by subtracting the lower threshold temperature from the average daily air temperature as shown in Eq. 4.1. Although the lower growth limit for wheat is about 42 °F, Bauer et al., 1984 found better correlation in the GDD predictions by defining the lower threshold temperature as 32 °F (0 °C). One additional constraints on Ta is: if the daily mean temperature is less than the base temperature, it is set equal to the base temperature.

$$GDD = Ta - Tb \qquad Eq.4.1$$

$$TGDD = sum(GDD) \qquad Eq.4.2$$

where,

GDD = Growing degree day (°C)

TGDD = Cumulative GDD (°C)

Ta = Daily mean air temperature (°C)

Tb = base temperature, 0 °C for winter wheat

The GDD assumes a linear relationship between plant development and all temperatures above the based temperature. This simplicity leads to inaccuracies in the GDD predictions (Barger 1969).

TF (Temperature function):

Both extreme high and extreme low temperature decrease the rate of crop growth and development. This effect is accounted for by introducing the air temperature (Ta) in 2nd-degree polynomials determined by an optimal temperature for cop functioning (Topt, 20 °C for wheat)

and two extreme values (Tmax and Tmin, 0 and 37 °C, respectively) beyond which the plant growth stops (Brisson et al., 2003; Duchemin et al., 2008). This leads to:

$$TF = 1 - [(Topt - Ta) / (Topt - Tmin)]^2 \quad if\ Tmin < Ta < Topt \qquad Eq.4.3$$
$$= 1 - [(Ta - Topt) / (Tmax - Topt)]^2 \quad if\ Tmax > Ta > Topt$$
$$= 0 \quad if\ Ta < Tmin\ or\ Ta > Tmax$$

where,

TF = Temperature function

Topt = Optimal temperature for crop functioning, 20 °C for winter wheat

Tmax = Extreme high temperature, 47 °C for winter wheat

Tmin = Extreme low temperature, 0 °C for winter wheat

TPPT (cumulative precipitation):

$$TPPT = sum(PPT) \qquad Eq.4.4$$

where,

TPPT = Cumulative precipitation (mm)

PPT = Daily precipitation (mm)

PE (precipitation evenness):

The Shannon's equitability (E_H) was used to represent the precipitation evenness during a given period, which can impact crop growth (Tremblay et al., 2012).

$$\boldsymbol{E_H} = \frac{H}{lnS} \qquad Eq.4.5$$

$$H = -\sum_{k=0}^{n} Pi * lnPi \qquad Eq.4.6$$

where,

E_H = Shannon's equitability. Value from 0 and 1 with 1 being completely evenness

H = Shannon diversity index

Pi = The proportion of precipitation in day i relative to the cumulative precipitation in n days

Field contextual information:

Field contextual information are valuable and can vary at different site-years. We included DOS (date of sowing) and Soil (soil type) as input in the model. Some other field contextual data were available to this study but not included in the model. For example, winter wheat hybrids used by the farmers may impact the phenology model, but since some of the hybrids did not have enough replication, they were excluded from the model.

Weather Data Date Range:

To specify the time frame of weather data, we use sowing date as the starting point and the "stop date" as the ending point. Instead of using a random date for the "stop date", we proposed some dates options that can be used as "stop date" for phenology model targeting different wheat growth stages (Table 4.3). This will make the model calibration/validation work easier and make it usable to other people.

Table 4.3 The "stop date" setup options for different stage phenology model

	F4	F7	F9
Option 1	20-Feb	20-Mar	10-Apr
Option 2	1-Mar	30-Mar	20-Apr
Option 3	10-Mar	10-Apr	30-Apr
Option 4	20-Mar	n/a	10-May

Model:

Random Forest Model:

We trained and applied Random Forest (RF), a binary tree based machine-learning method, to predict the starting date of F4/F7/F9 stage based on all inputs from weather data and field contextual information. RF can be used for both classification and regression purpose, and the scope of our study is to use it as a regression tool. Compared to traditional linear regression, RF model is relatively insensitive to outliers in training data and allows for non-linear regression (Svetnik et al., 2003). Furthermore, RF models can also be used to rank the importance of variables in a regression problem. Therefore, RF model is adopted here to predict the stage date and help us to understand the importance of those weather variables.

Linear Regression Model:

Multiple linear regression models (MLR) were constructed to test all combinations of weather and field information variables for benchmarking the performance of RF predictions. Eq. 4.7 illustrates the MLR used in this study:

$$Date\ Est. = a_1 * TGDD + a_2 * TF + a_3 * TPPT + a_4 * PE + a_5 * Soil + b \qquad Eq.\ 4.7$$

where,

$a_1, a_2, a_3, a_4, a_5, = Regression\ coefficients$

$b = Intercept$

Results and Discussion

In-season Wheat Biomass Estimation using high-definition UAV based imagery

In order to use the phenology model to optimize the imagery data collection date and estimate biomass, we firstly built a series of in-season biomass estimation models at different growth stages using the 2014-2015 season data including imagery and ground biomass measurements. Figure 4.3 shows the example of color infrared orthomosaics for some growth stages (not all stages were included in Figure 4.3) generated using imagery data taken with the modified camera mounted on a UAS. The color is blueish because the blue band was used to record the NIR light which were mostly reflected by the plants.

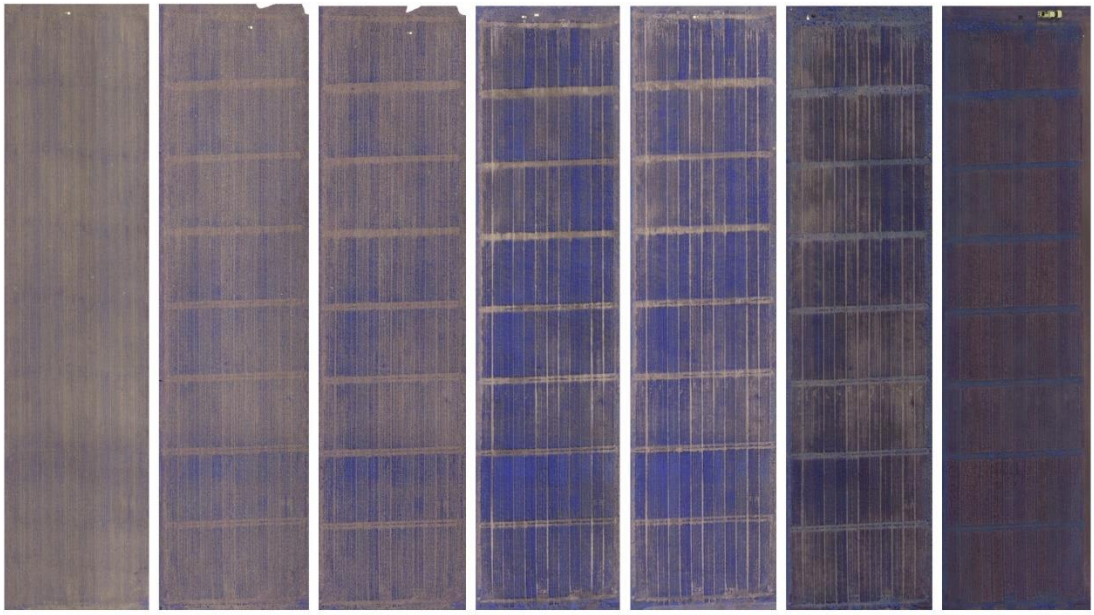

Figure 4.3 Orthomosaics of a wheat field at different growth stages. The plant materials are in blueish color because the camera is using the blue band to record NIR light which is mostly reflected by the plants.

Table 4.4 Demonstrates the biomass estimation model at different growth stages from F3 through F11.1 and their estimation accuracy that were evaluated by root mean square error (RMSE) and relative error (RE).

Table 4.4 UAV imagery based biomass estimation model and validation at different growth stage.

Stage	Model				R^2	RMSE (ton/ha)	RE
F4	Biomass =	2.6759	× NDVI	-0.3438	0.63	0.15	34%
F7	Biomass =	4.6479	× NDVI	-0.9290	0.79	0.26	26%
F10	Biomass =	8.3220	× NDVI	-2.3698	0.88	0.39	20%
F10.2	Biomass =	12.6553	× NDVI	-3.0690	0.94	0.40	14%
F10.5	Biomass =	14.7580	× NDVI	-4.0011	0.93	0.51	15%
F10.5.2	Biomass =	21.5811	× NDVI	-6.0531	0.83	1.18	25%
F10.5.4	Biomass =	24.5857	× NDVI	-6.8464	0.70	1.59	31%
F11.1	Biomass =	39.3072	× NDVI	-10.0896	0.57	2.03	37%
F11.2	Biomass =	51.2012	× NDVI	-13.3008	0.45	2.41	43%

All $p < 0.001$

From Feekes 3 (tiller formed) to Feekes 11.1 (milky ripe), NDVI from the Canon camera have a consistent and high correlation ($0.72<r2<0.95$, all $p<0.001$) with the dry biomass. The most accurate estimation was observed at F10 and F10.2 which is the booting stage. At this stage, the head of winter wheat is visible but still in the leaf sheath below the flag leaf and winter wheat has the greenest and expanded leaves, thus has the most photosynthesis activities. After this stage, wheat turned into reproductive stages and the correlation decreased. As shown in Figure 4.4. the slope and intercept of the model were constantly changing in the season. This is suggesting that growth stage has a big impact on the crop remote sensing results. At earlier growth stage, the slope is low because there are not much green materials out there and the absolute biomass difference over unit NDVI is small. As the wheat putting more leaves on itself and growing taller, the ratio between the biomass difference and unit NDVI gets bigger.

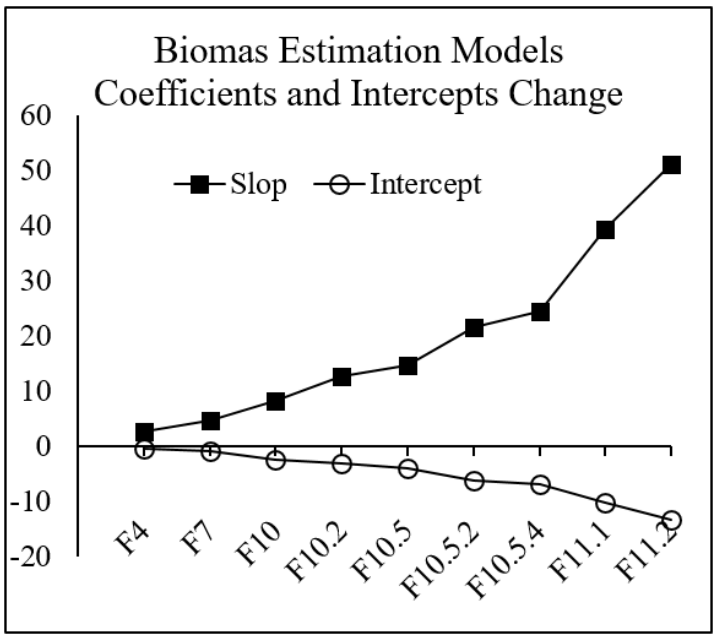

Figure 4.4 Biomass estimation model slopes and intercepts seasonal change.

Wheat F4/F7/F9 phenology model using weather data and field contextual information

In order to predict the F4/F7/F9 date without going to the field and taking any in-situ measurements. 21 site-years of weather data and contextual data were used to train and test the phenology models. For each targeted stage, there were three or four "stop date" options to choose from. The validations of the models are summarized in Table 4.5 by stages by "stop date". The RMSE is the average RMSE of 200 iterations. For each iteration, the data was divided into 75% training set and 25% testing set after randomization.

Table 4.5 Validation of wheat phenology model targeting F4/F7/F9 starting dates.

Stage	Stop Date	Averaged RMSE	
		RF Model	MLR Model
F4	Feb_20	19 days	7 days
	Mar_01	19 days	7 days
	Mar_10	19 days	8 days
	Mar_20	19 days	7 days
	Avg.	**19 days**	**7 days**
F7	Mar_20	16 days	7 days
	Mar_30	16 days	8 days
	Apr_10	17 days	8 days
	Avg.	**16 days**	**8 days**
F9	Apr_10	15 days	11 days
	Apr_20	16 days	9 days
	Apr_30	15 days	6 days
	May_10	15 days	7 days
	Avg.	**15 days**	**8 days**

As shown above in Table 4.5, the phenology model error (RMSE) is about a week for F4, F7, and F9 using linear regression model, which significantly outperform RF model whose error are 2-3 weeks. This is probably due to the fact that by throwing all the available variables into RF model, instead of improving the model performance, it increases the noise level in the data. Considering the fact that RF model is more computational expensive than linear regression model, the latter is recommended in future phenology model development. A week sounds like a huge error, but in real world crop production, it is totally acceptable due to the complexity and difficulties of collecting data at a large scale and coordinating it under favorable weather conditions.

Table 4.6 Properties of positive and negative of coefficients in linear regression models

Coef. Symbol	a_1	a_2	a_3	a_4	a_5	b
Variable	TGDD	TF	TPPT	PE	Soil Type	Intercept
02-20_for_F4	0.1165	-1.3427	-0.0197	54.1176	4.6641	82.9762
03-01_for_F4	0.0515	-0.1827	-0.0214	35.7869	5.1628	86.9652
03-10_for_F4	0.0776	-0.7292	-0.0173	40.7549	3.7935	102.0491
03-20_for_F4	0.1265	-1.4395	-0.0363	56.7731	7.0656	101.6422
03-20_for_F7	0.0872	-0.9400	-0.0364	32.6559	8.0055	116.9884
03-30_for_F7	0.1010	-1.1591	-0.0294	35.5588	7.6181	122.8731
04-10_for_F7	0.0469	-0.3039	-0.0220	22.2562	6.7653	131.1985
04-10_for_F9	0.0185	0.1886	-0.0069	41.6047	4.6866	112.7745
04-20_for_F9	0.0490	-0.3348	-0.0148	31.6951	5.3292	130.8943
04-30_for_F9	0.0087	0.3043	-0.0225	68.8448	3.4768	114.4713
05-10_for_F9	0.0182	0.2164	-0.0110	39.1447	1.3304	130.5264
Positive Or Negative	Positive	Negative	Negative	Positive	Positive	Positive

To get a better idea of the phenology model developed using linear regression, the model coefficients was summarized in Table 4.6 as well as their properties of positive/negative. For each stop date option and each stage, only the best model was selected (after 200 iterations). As shown in the table, the coefficient for the temperature function is negative, which mean this stress function indeed provides a penalty to the crop growth. Likewise, the precipitation evenness has a positive impact on the crop growth.

As the side product of RF models, the features fed into the models were evaluated for their importance when they were used for predictions.

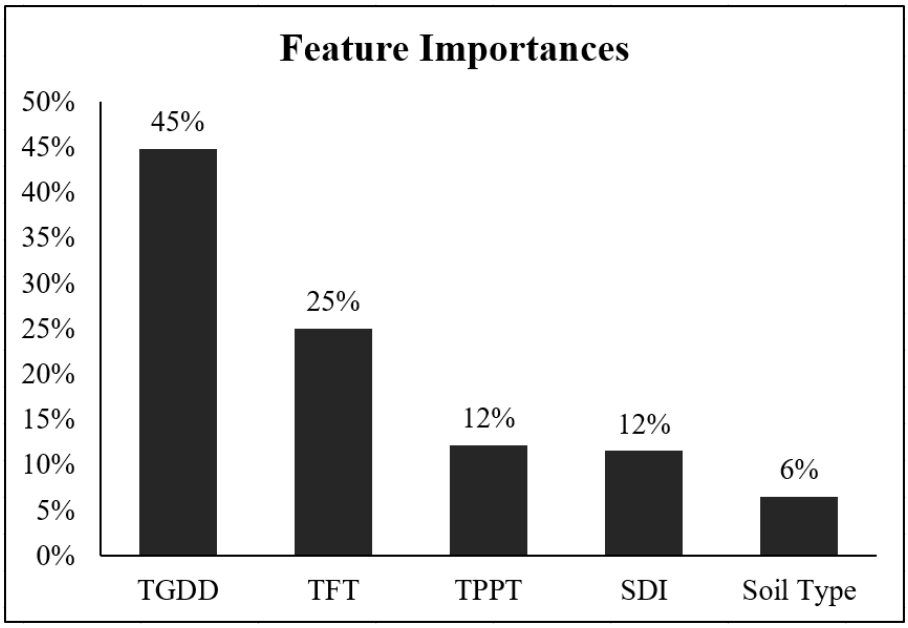

Figure 4.5 Feature importance generated from Random Forest Model

As shown in Figure 4.5, among all the variation (less than 100%) explained by TGDD, TFT, TPPT, SDI, and Soil type, TGDD explained the most variation (45%) while Soil type explained the least (6%) compared to other features. This is suggesting that, for phenology prediction, the TGDD is the most important feature and temperature based stress are also important (25%). In terms of precipitation, the cumulative amount and the precipitation temporal distribution are equally important.

Integrating phenology model into imagery based wheat biomass

To do the integration, we firstly estimated the F4, F7, and F9 starting dates for winter wheat grown in 2015-2016 season using the phenology models evaluated in Table 6 (The actual model were not listed in the table due to the insufficient space). The predicted dates for different growth stages were summarized in Table 4.6. The prediction error for F4/F7/F9 were 8 days, 3

days, and 10 days, respectively. This accuracy agreed with the model accuracy in the past section.

Table 4.7 Predicted starting dates for F4/F7/F9 for a wheat field grown in 2015-2016.

Stage	Present Date	Predicted Date	Observed date
F4	10-Mar	8-Mar	16-Mar
F7	10-Apr	5-Apr	8-Apr
F9	20-Apr	15-Apr	25-Apr

Once the dates determined, imagery data collection were planned and performed on those dates accordingly. Next, from all the biomass models developed using 2014-2015 wheat data, the models specifically built for F4/F7/F9 were selected to plug into the imagery based NDVI data collected from 2015-2016 season. Figure 6. shows the examples of wheat NDVI maps at different growth stages.

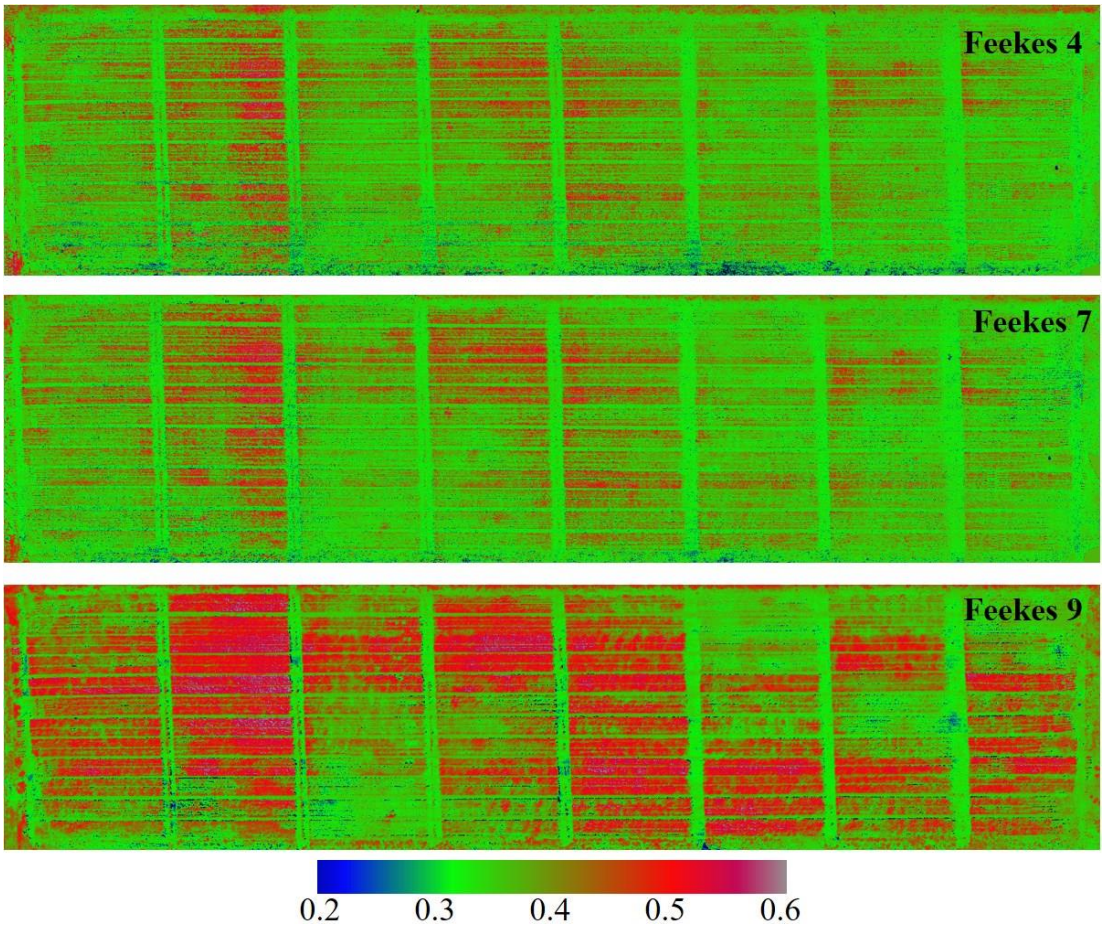

Figure 4.6 NDVI maps for a wheat field at F4, F7, and F9.

Biomass at specific stages were then predicted and compared to the observed measurements as shown in Figure 4.7.

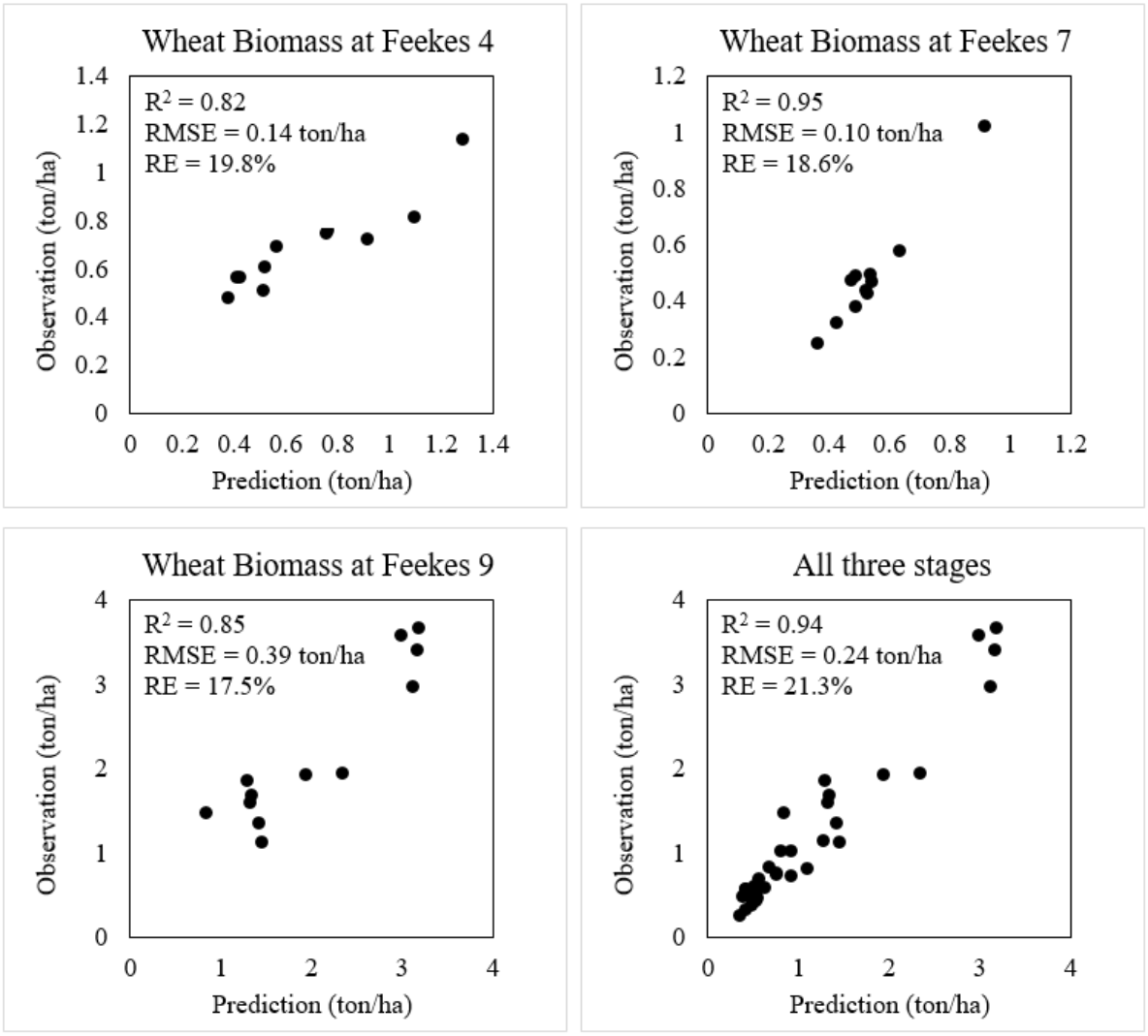

Figure 4.7 Comparison of predicted and observed wheat biomass at F4/F7/F9 growth stage in 2015-2016 season.

Wheat biomass was accurately estimated using previously year's models. At F4 and F7, the RMSE were about 0.14 and 0.10 ton/ha, respectively. As the plant growing bigger and taller, more dry matter was accumulated therefore the RMSE at F9 was relative greater (0.39 ton/ha). The relative error of biomass estimation at all three interested stages (F4/F7/F9) were less than 20%.

Conclusions

In the study, we firstly estimated in-season winter wheat biomass using CIR imagery collected with a UAS. From F4 though F11.1, the biomass was highly correlated with NDVI with $0.57 < r2 < 0.94$ and could be estimated with different degree of accuracy. The estimation accuracy increased as the wheat growing and developing and then decreased after the wheat turning into the reproductive phase. The most accurate estimations were observed at booting and heading stages (F10, 11.2, 10.5) with REs less than 20%. These frequent in-season models were then used as models banks for new years' data to select from.

Secondly, a wheat phenology model targeting the key growth stages for N management including F4, 7, and 9 was built to optimize the imagery collection time without the pre-requirements for any field measurements because the model was based on the weather data which can be easily retrieved from the nearest agrometeorological stations and the field contextual information that was acquired prior to the growing season. The starting dates of F4 and F7 can be predicted within about a week while the error for F9 date prediction was more than a week but less than 11 days.

Finally, a new site-year's data (2015-2016, Ashland Bottoms) was used to test the integration of the phenology model and biomass model. The F4, 7, and 9 starting dates were predicted within 8,3,10 days, respectively. They were then used to schedule the imagery collection. NDVI values derived from these images were plugged into the biomass models that were built in previous year and accurately predict the biomass at F4, 7, and 9 with the RE less than 20%.

References

Asebedo, A. R. (2015). *Development of sensor-based nitrogen recommendation algorithms for cereal crops*. Kansas State University.

Bauer, A., Frank, A. B., & Black, A. L. (1984). Estimation of spring wheat leaf growth rates and anthesis from air temperature. *Agronomy Journal*, 76(5), 829-835.

Bregaglio, S., Frasso, N., Pagani, V., Stella, T., Francone, C., Cappelli, G., ... & Confalonieri, R. (2015). New multi-model approach gives good estimations of wheat yield under semi-arid climate in Morocco. Agronomy for sustainable development, 35(1), 157-167.

Brisson, N., Gary, C., Justes, E., Roche, R., Mary, B., Ripoche, D., ... & Bussière, F. (2003). An overview of the crop model STICS. *European Journal of agronomy*, *18*(3), 309-332.

Cho, M. A., Skidmore, A., Corsi, F., Van Wieren, S. E., & Sobhan, I. (2007). Estimation of green grass/herb biomass from airborne hyperspectral imagery using spectral indices and partial least squares regression. *International Journal of Applied Earth Observation and Geoinformation*, *9*(4), 414-424.

Duchemin, B., Maisongrande, P., Boulet, G., & Benhadj, I. (2008). A simple algorithm for yield estimates: Evaluation for semi-arid irrigated winter wheat monitored with green leaf area index. *Environmental Modelling & Software*, *23*(7), 876-892.

Goel, P. K., Prasher, S. O., Landry, J. A., Patel, R. M., Bonnell, R. B., Viau, A. A., & Miller, J. R. (2003). Potential of airborne hyperspectral remote sensing to detect nitrogen deficiency and weed infestation in corn. *Computers and electronics in agriculture*, *38*(2), 99-124.

Huang, W., Lamb, D. W., Niu, Z., Zhang, Y., Liu, L., & Wang, J. (2007). Identification of yellow rust in wheat using in-situ spectral reflectance measurements and airborne hyperspectral imaging. *Precision Agriculture*, *8*(4-5), 187-197.

Miller, T. D. (1992). Growth stages of wheat. *Better crops with plant food. Potash & Phosphate Institute*, *76*, 12.

Myers, D., Ross, C. M., & Liu, B. (2015). A Review of Unmanned Aircraft System (UAS) Applications for Agriculture. In *2015 ASABE Annual International Meeting* (p. 1). American Society of Agricultural and Biological Engineers.

Palosuo, T., Kersebaum, K. C., Angulo, C., Hlavinka, P., Moriondo, M., Olesen, J. E., ... & Trnka, M. (2011). Simulation of winter wheat yield and its variability in different climates of Europe: a comparison of eight crop growth models. European Journal of Agronomy, 35(3), 103-114.

Raun, W. R., Solie, J. B., Johnson, G. V., Stone, M. L., Mullen, R. W., Freeman, K. W., ... & Lukina, E. V. (2002). Improving nitrogen use efficiency in cereal grain production with optical sensing and variable rate application. *Agronomy Journal*, *94*(4), 815-820.

Roberts, T. L. (2007). Right product, right rate, right time and right place… the foundation of best management practices for fertilizer. *Fertilizer Best Management Practices*, *29*.

Svetnik, V., Liaw, A., Tong, C., Culberson, J. C., Sheridan, R. P., & Feuston, B. P. (2003). Random forest: a classification and regression tool for compound classification and QSAR modeling. Journal of chemical information and computer sciences, 43(6), 1947-1958.

Teal, R. K., Tubana, B., Girma, K., Freeman, K. W., Arnall, D. B., Walsh, O., & Raun, W. R. (2006). In-season prediction of corn grain yield potential using normalized difference vegetation index. *Agronomy Journal*, *98*(6), 1488-1494.

Tremblay, N., Bouroubi, Y. M., Bélec, C., Mullen, R. W., Kitchen, N. R., Thomason, W. E., ... & Vories, E. D. (2012). Corn response to nitrogen is influenced by soil texture and weather. *Agronomy Journal*, *104*(6), 1658-1671.

Waldren, R. P., & Flowerday, A. D. (1979). Growth stages and distribution of dry matter, N, P, and K in winter wheat. *Agronomy Journal*, *71*(3), 391-397.

Zhang, C., & Kovacs, J. M. (2012). The application of small unmanned aerial systems for precision agriculture: a review. Precision agriculture, 13(6), 693-712.

Chapter 5 - Summary

Accurate and timely assessment of crop condition across a field is a key objective of many agronomists and farmers during precision farm management, and of many researchers during phenotyping in the breeding programs. Traditional remote sensed measurements acquired by earth orbiting satellites have been used for decades with varying degrees of success for classifying crop types and predicting yields but their limitations are associated with low spatial resolution and unfavorable revisit time in precision agriculture; Traditional phenotyping methods involve destructive sampling and manual measurements were time consuming and labor intensive.

High spatial resolution images taken by passive optical sensors (POSs) mounted on low altitude remote sensing platforms such as UAV and MAV could fill this gap. Also, vehicle-based active optical sensors (AOSs) have been used to compute Normalized Difference Vegetation Index (NDVI)-type vegetation indices (VIs) to assess factors such as crop vigor, leaf nitrogen status, and potential yields.

AOSs can be used more freely under changing light conditions and times of the day. AOSs do not require the radiometric calibration and data processing that passive sensors need. However, passive optical sensors are more efficient for large-scale data collection in crop production and breeding programs and the data require no interpolation, which is usually performed in AOS data during analysis. Also, passive sensors currently have more bands, thus providing broader possibilities for application in precision agriculture.

After reviewing the current status of different optical sensors used in precision crop production including satellite-based, MAV-based, UAS-based, and vehicle-based active or passive optical sensors. We found that MAV- and UAS-based optical sensors have more potential in precision crop production due to their high spatial and temporal resolutions. Compared to UAS, MAV-based remote sensing deserves more attentions than it already has due to its flexibility on sensor selection and high efficiency on data collection. It provides reasonable high resolution (20 cm) data at a relative low prices and has the most return on investment (Table 2.11) compared to vehicle-, UAS-, satellite-based optical sensors.

For crop assessment at plot level such as the high-throughput phenotyping in wheat breeding programs, UAS- and vehicle-based optical sensors are more useful. Based on the results presented in this study, CMOS sensor modified camera and multispectral imager mounted on a UAS were more powerful and temporally stable on in-season biomass estimation and grain yield prediction than the vehicle-based active sensor. The canopy height could be estimated by the CMOS sensor camera and the multispectral imager when high precision GCPs were used. This estimation accuracy could be potentially improved by feeding the raw imagery data with IMU data and onboard RTK GPS data. When dealing with imagery data, radiometric calibration and image processing must be considered and standardized for better results.

Based on the results presented in this study, in-season biomass can be consistently estimated using UAS imagery based VIs, which can be furtherly used to determine the intra-field variability of productivity for downstream applications such as fertilization recommendations. The method provided in this study can also be used in forage production to assess how much to cut for hay and to adjust the forage management practices based on the biomass estimation to get better marking prices. To be able to use these pre-built models over time, growth stage

information is needed so that the correspondent model can be selected to be plugged in. The proposed phenology model based on weather data and field contextual information is helpful to predict the starting dates of the key stages of wheat growth. The prediction error is about a week, which is good enough in real world crop production. As described in the introduction section in Chapter 4, N management is growth stage sensitive. When we can accurately predict what is the yield potential and what is the growth stage at the same time, we can start better improving the N recommendation algorithms utilizing the remote sensing spectral data, which make sense for both soil fertility and crop physiology. For example, we put more N under low biomass situation at Feekes 4 because it still can recover yield potential by impacting the primary yield determine factors, the tillering and head size. In middle season, we put less N under low biomass situation at Feeks 7 because it cannot impact tillering and head size at this stage, which leads to a permanent yield loss. It is not profitable by applying more N. This is the reverse logic of the way people doing their N recommendation algorithms for VRA applications. They usually think they need to apply more under low biomass situation, which turns out to be a waste of money.

When using machine learning method, we throw all the data to the model and hope it can sort it out correctly. The reality is the performance may not be as good as expected or comparable to other methods such as linear regression model. We still need to have a good knowledge of the crop, environment, and their interactions to incorporate the biological factors into the models for better decision making.

Optical sensor based crop assessment in precision agriculture and high-throughput phenotyping have gone through dramatic advances in the recent years and will continue the trend. The future applications may be ascribed to the improvement of simplifying image processing, lowering hardware prices, automation of data-to-plan translation to reduce the labor

cost. Although remote sensing tools can detect the field variability fairly easily, it is usually very hard to identify exact reasons that is causing the nonuniformities in the field. Multi-sensor strategy and expert based models can help to improve the diagnosis accuracy. Emerging information technologies like on-the-going process & analysis, cloud computing, multi-platform communication, and data sharing also can be integrated into PA for advanced, intelligent data collection and analysis. In addition, the sensor and technologies will continue to develop, more researches will be done, more methods will be validated, and hopefully, more people will adopt these PA tools to optimize the profitability on their farms and reduce the environmental impact for a sustainable future.

(The End)